TECHNICAL REPORTS OF THE METEOROLOGICAL RESEARCH INSTITUTE No. 68

International Symposium on Aerosol Studies Explored by Electron Microscopy

BY

Yasuhito Igarashi, Weijun Li, Peter. R. Buseck, Kikuo Okada, Daizhou Zhang, Kouji Adachi, Yuji Fujitani, Hikari Shimadera, Daisuke Goto, Chizu Mitsui, Masashi Nojima, Naga Oshima, Hitoshi Matsui, Hiroshi Ishimoto, Atsushi Matsuki, Pradeep Khatri, Tomoki Nakayama, Shohei Mukai, Kenji Ohishi, Norihito Mayama, Tetsuo Sakamoto, Hiroaki Naoe, Yuji Zaizen, Hiroki Shiozuru, Taichu Y. Tanaka and Mizuo Kajino

気象研究所技術報告

第 68 号

国際シンポジウム 電子顕微鏡を用いたエアロゾル研究

五十嵐康人、Weijun Li, Peter.R.Buseck, 岡田菊雄、
張代洲、足立光司、藤谷雄二、嶋寺光、
五藤大輔、三井千珠、野島雅、大島長、
松井仁志、石元裕史、松木篤、Pradeep Khatri,
中山智喜、向井将平、大石乾詞、間山憲仁、
坂本哲夫、直江寛明、財前祐二、塩流水洋樹、
田中泰宙、梶野瑞王

気 象 研 究 所

METEOROLOGICAL RESEARCH INSTITUTE, JAPAN

International Symposium on Aerosol Studies Explored by Electron Microscopy

by

Yasuhito Igarashi, Kikuo Okada, Kouji Adachi, Naga Oshima, Hiroshi Ishimoto, Yuji Zaizen, Taichu Y. Tanaka and Mizuo Kajino
Meteorological Research Institute, Japan Meteorological Agency

Weijun Li
Shandong University, China

Peter. R. Buseck
Arizona State University, United States

Daizhou Zhang
Pref. University of Kumamoto

Yuji Fujitani
National Institute for Environmental Studies

Hikari Shimadera
Central Research Institute of Electric Power Industry

Daisuke Goto and Hitoshi Matsui
The University of Tokyo

Chizu Mitsui
Oxford Instruments,United State

Masashi Nojima
Tokyo University of Science

Atushi Matsuki
Kanazawa University

Pradeep Khatri
Chiba University

Tomoki Nakayama
Nagoya University

Shohei Mukai
Kobe University

Kenji Ohishi and Tetsuo Sakamoto
Kogakuin University

Norihito Mayama
Tokyo Institute of Technology AND Kogakuin University

Hiroaki Naoe and Hiroki Shiozuru
Japan Meteorological Agency

Contents

序

大気エアロゾルは、大気放射過程や雲形成及び降雨生成過程などを通して、気候及び気象に大きな影響を与える．近年、気候・気象モデルは急速に進歩しており、大気エアロゾル諸過程のモデルも高度化している。これらのモデルの開発・検証のためにも個別粒子の微細構造を含めたエアロゾル観測データの必要性が高まっている。電子顕微鏡は、個別エアロゾル粒子の微細構造（例えば形態・組成・混合状態）を詳細に調べることができる強力なツールである。しかし、そのデータをモデル研究に活用するためには、時間分解能、空間代表性などクリアすべき課題は多い。

気象研究所では、２０１２年２月１６－１７日に、「International symposium on aerosol studies explored by electron microscopy　(電子顕微鏡を用いたエアロゾル研究-モデル研究とのリンクをどう進めるか)」と題した公開シンポジウムを開催した。このシンポジウムでは、電子顕微鏡等を用いた大気エアロゾルの研究と微物理モデルを用いた研究の双方の分野から、海外を含む多数の研究者が参加し、電子顕微鏡とモデルのリンクの意義、現在の試み、将来の可能性について意見交換を行なった。討論の中で、モデルが必要とするのはサイズ分布、化学組成、形態学情報等の高精度で時空間代表性のあるデータであること、そのような測定データを得るためには、サンプル採取と分析方法の規格化が必要で、また高効率の分析方法が求められること、さらに、それらを用いてグローバルなデータベースの構築を目標とすべきであることなど、将来に向けた展望が議論された。

このシンポジウムにより、電子顕微鏡とモデル研究者相互の理解を深めることができたことは、大気科学、気象学のさらなる発展にとって非常に有意義であった。本技術報告はこの国際シンポジウムにおける発表や議論をとりまとめた資料であり、関連する研究の進展の一助となれば幸いである。

なお、海外招待講演者（Peter R. Buseck 教授および Weijun Li 博士）の招聘費用は、環境省の平成 23 年度環境研究総合推進費（課題番号 A-1101）「地球温暖化対策としてのブラックカーボン削減の有効性の評価」による。この招聘によりブラックカーボンに関する最先端の知見が当該研究の研究メンバーに共有されました。ここに記して謝意を表します。

2013 年 1 月　　環境・応用気象研究部長

三上　正男

International symposium on aerosol studies explored by electron microscopy: How can electron microscopy improve atmospheric models?

Foreword

Yasuhito Igarashi*

[1]Atmospheric Environment and Applied Meteorology Research Department, Meteorological Research Institute, 1-1 Nagamine, Tsukuba, Ibaraki 305-0052, Japan

*Corresponding author. Tel.: +81 29 853 8621; Fax: +81 29 855 7240; Email address: yigarash@mri-jma.go.jp (Y. Igarashi)

The Meteorological Research Institute (MRI) of the Japan Meteorological Agency held an international symposium regarding the use of electron microscopy in aerosol studies and atmospheric simulation models on 16 and 17 February 2012. To our knowledge, this was the first symposium of its kind anywhere in the world. The purpose of the symposium was to discuss (1) current atmospheric aerosol research making use of electron microscopy and (2) the use of the results of such studies in aerosol model simulations. Two keynote speakers and 18 invited speakers addressed the symposium, and there were 16 poster presentations. In total, we had close to 80 participants, who engaged in two days of intense discussion. The papers in this MRI technical report present the contents of the keynote lectures, the invited presentations, posters, and discussions.

Keywords: Electron microscopy, Aerosol, Observation, Atmospheric model

Background and scope

The primary motivation of this international symposium was the first replace of a transmission electron microscope (TEM) at the Meteorological Research Institute (MRI) in the 30 years since the MRI relocated from Tokyo to its present location in Tsukuba. This new TEM makes available state-of-the-art TEM technologies, such as automated analysis of the aerosols with energy dispersive X-rays and 3-D tomography.

Recent research trends in atmospheric aerosol sciences include the rapid development of computer models for projecting air quality, weather forecasting, and climate research. It is essential to incorporate into these models aerosol physics and chemistry. With these trends in mind, we, the aerosol researchers at the MRI, recognized that electron microscopy should play a crucial role in atmospheric aerosol research. For electron microscopy to fulfill this role, however, improved communication between electron microscopists and aerosol modelers is key.

Another motivation was to recognize the 30-year history of research on aerosols conducted at the MRI making use of TEM and scanning electron microscopy (SEM). This research was led by the former section head of our laboratory, Dr. Kikuo Okada, who has carried out pioneering aerosol research since the 1980s, when atmospheric aerosol morphology and mixing states were largely unknown. Electron microscopy is a set of versatile technologies that can be used to investigate the morphology and mixing state (elemental composition) of individual aerosol particles. To clarify the climatic and meteorological impacts of aerosols and related processes, Dr. Okada used electron microscopy to examine sea salt, mineral dust (Asian dust), soot, sulfate, nitrate, and mixtures of these. His research targets included samples retrieved from the poles to the tropics, and from the boundary layer to the stratosphere, and his work has contributed greatly to our understanding of the basic roles of atmospheric aerosols in climate and meteorology (see Dr. Okada's paper in this volume).

Therefore, we decided to organize an international symposium to review the research traditions at the MRI and the cutting-edge research that has been carried out there, to set forth current knowledge and state-of-the-art technologies, and finally to promote the integration of observational, experimental, and model studies by encouraging mutual un-

derstanding among researchers.

Keynote speakers

Two distinguished keynote speakers addressed the symposium: Prof. Peter R. Buseck, Arizona State University (ASU), U.S.A., and Dr. Weijun Li, Shandon University, China. Prof. Buseck is a well-known electron microscopist whose scientific endeavors cover vast areas of geology, mineralogy, crystallography, electron microscopy, and atmospheric aerosols. Dr. Li is a promising young Chinese scientist who has used electron microscopy to conduct aerosol research at ASU under the supervision of Prof. Buseck.

The audience listened with rapt attention to Prof. Buseck's outstanding and technically sophisticated lecture on the use of electron microscopy in aerosol research. Dr. Li focused on recent TEM investigations of haze, an important air quality problem in China. His electron micrographs of aggregates of fly ash spherules were particularly impressive.

Invited speakers

The invited speakers included Dr. Kikuo Okada, formerly of the MRI (and currently a guest researcher there) and Prof. Yasunobu Iwasaka, Kanazawa University. These two leading Japanese scientists presented thought-provoking reviews in which they shared their great expertise and long research experience in the field of atmospheric and aerosol sciences.

Dr. Kouji Adachi (MRI), Dr. Yuji Fujitani (National Institute for Environmental Studies), Prof. Masahiko Hayashi (Fukuoka University), Dr. Tomoko Kojima (Kumamoto University), and Dr. Masahi Nojima (Tokyo University of Science) spoke on state-of-the-art electron microscopy techniques: 3-D tomography (Dr. Adachi), focused ion beam secondary ion mass spectrometry (FIB-SIMS) (Dr. Fujitani), environmental scanning electron microscope (ESEM) (Prof. Hayashi), 2-D elemental mapping by scanning transmission electron microscopy (STEM) (Dr. Kojima), and secondary ion mass spectrometry (SIMS) (Dr. Nojima).

Prof. Daizhuo Zhang (Prefectural University of Kumamoto), Dr. Keiichiro Hara (Fukuoka University), Prof. Kazuhiko Miura (Tokyo University of Science), and Dr. Atsushi Matsuki (Kanazawa University) described aerosol observations conducted in western Japan (Prof. Zhang), the Antarctic (Dr. Hara), the Pacific and Mt. Fuji (Prof. Miura), and the Arctic (Dr. Matsuki).

Dr. Hikari Shimadera (Central Research Institute of the Electric Power Industry), Dr. Daisuke Goto (University of Tokyo), and Drs. Naga Oshima and Hiroshi Ishimoto (MRI) described recent simulation experiments with different kinds of models: a regional chemical transport model (Dr. Shimadera), a global chemical transport model (Dr. Goto), a microphysics model (Dr. Oshima), and a shape model (Dr. Ishimoto).

In addition, the novel features of the new TEM system installed at the MRI were briefly presented by representatives of the manufacturers (Ms. Chizu Mitsui, Oxford Instruments, and Mr. Hiromitsu Furukawa, System in Frontier Inc.).

Poster presentations

In the poster sessions, a total of 16 posters were presented, covering topics such as aerosol observations, including morphology, composition, and optical properties; state-of-the-art technologies; and novel approaches to aerosol modeling, and their mixtures.

Discussion session

During the discussion session, Dr. Igarashi, Prof. Buseck, Dr. Oshima and Dr. Matsuki presented comments and suggestions. All of them emphasized the urgent need to build bridges between microscopists and modelers to further advance our understanding of atmospheric aerosols and improve atmospheric models. Endeavors such as this symposium were concluded to be necessary to promote active collaboration among scientists.

Acknowledgments

On behalf of the local organizing committee of the international symposium, I would like to express my sincere gratitude to all speakers and participants. I also hope that this MRI technical report volume will inspire and inform its readers. Thanks are also extended to the Environment Research and Technology Development Fund "Assessment of the Effects of Reductions of Black Carbon Aerosols as a Measure of Slowing down Global Warming" (Fund #A-1101; PI: Prof. Yutaka Kondo, Univ. of Tokyo), whose support made the invitation of the keynote speakers possible.

Finally, I would like to add my thanks to our laboratory staff for their support in organizing the present symposium. Ms. K. Yanagida helped the editing this volume to which my thanks are also due.

Table 1: Final agenda of the International Symposium on Aerosol Studies Explored by Electron Microscopy

Thursday, 16 February 2012

Opening (welcoming remarks, purpose of the workshop)	Y. Igarashi (MRI)
Keynote lectures	
Individual aerosol particles in hazes of North China	W. J. Li (Shandong U.)
Identification and Analysis of Atmospheric Aerosol Particles (& Climate Implications)	P. R. Buseck (Arizona State U.)
Invited oral presentations	
Welcome speech by the Director General	Y. Kano (MRI)
Studies of aerosol particles performed with the MRI electron microscopes during the last three decades	K. Okada (MRI)
Modification of dust particles by sea salt adherence and surface chemical reactions in the marine atmosphere	D. Zhang (Pref. U. of Kumamoto)
Aerosol particle shape revealed by transmission electron microscopy and the implications for its optical properties	K. Adachi (MRI)
Internal mixtures of diesel nanoparticles investigated by FIB-SIMS microscopy	Y. Fujitani (NIES)
Modeling atmospheric transport of fine particulate matter with WRF/CMAQ in the Kanto region in summer 2007	H. Shimadera (CRIEPI)
Treatment of black carbon by a global climate model and the potential contribution of electron microscopy	D. Goto (U. of Tokyo)
Aerosol particle analysis with INCAFeature TEM	C. Mitsui (Oxford Instruments)

Friday, 17 February 2012

Invited oral presentations	
Observation of fine ice crystals on ice nucleus at -70 °C using ESEM	M. Hayashi (Fukuoka U.)
Vertical distributions of aerosol constituents and their mixing states in Antarctic troposphere during the summer	K. Hara (Fukuoka U.)
Aerosol isotope analysis by secondary ion mass spectrometry	M. Nojima (Tokyo U. of Sci.)
Two-dimensional elemental mapping using a scanning transmission electron microscope	T. Kojima (Kumamoto U.)
Aging of black carbon and its impact on aerosol optical properties and cloud condensation nuclei activities using a mixing state resolved model	N. Oshima (MRI)
Formation and variations of aerosols around Beijing using the WRF-chem model	H. Matsui (U. of Tokyo)
Shape modeling of dust and soot particles for remote sensing applications by considering the geometrical features of sampled aerosols	H. Ishimoto (MRI)
Importance of structural diversity in atmospheric aerosols from viewpoint of environmental effects	Y. Iwasaka (Kanazawa U.)
Modification of individual sea salt particles	K. Miura (Tokyo U. of Sci.)
Single particle analysis of aerosols and cloud residues in the Arctic troposphere	A. Matsuki (Kanazawa U.)
The latest application software for electron tomography	H. Furukawa (JEOL)

Posters

Determination of the aerosol direct effect over the East China Sea using ground-based remote sensing and aircraft observation data	P. Khatri (Chiba U.)
Particle effective density measurement using a DMA-APM- CPC system in Nagoya, Japan: Estimation of mixing state and shape	T. Nakayama (Nagoya U.)
Measurements of light absorption enhancement of black carbon using a photoacoustic spectrometer in Nagoya, Japan	T. Nakayama (Nagoya U.)
Some measurements of mixing state of soot-containing particles at urban and non-urban sites	S. Hasegawa (Center for Environ. Sci. in Saitama)
Changes in chemical compositions of sea-salt particles collected at Mt. Rokko, Kobe, Japan	S. Mukai (Kobe U.)
Laser post-ionization mass spectrometry of PAHs on diesel soot particles	K. Ohishi (Kogakuin U.)
Analysis of black carbon particles by high-resolution TOF-SIMS	N. Mayama (Tokyo Inst. Tech./Kogakuin U.)
Analysis of source apportionment and chemical transformation of particles in trans-boundary air pollution using high lateral resolution imaging SIMS	T. Sakamoto (Kogakuin U.)
Mixing state of atmospheric black carbon particles and its effect on light absorption	H. Naoe (MRI)
Fine mineral aerosols collected in Japan during two Asian dust events: Size distributions and mixing properties	Y. Zaizen (MRI)
Aerosol-related services of the Japan Meteorological Agency	H. Shiozuru (JMA)
Climatic effect of black carbon in the MRI global climate model	Y. T. Tanaka (MRI)
Model formulation and predictability of atmospheric aerosol properties and processes	M. Kajino (MRI)
Transmission electron microscope for atmospheric aerosol analysis	JEOL
The latest application software for electron tomography	JEOL
Particle analysis of aerosol with INCA Feature TEM	Oxford Instruments

Individual aerosol particles in hazes of North China

Weijun Li[1], Longyi Shao[2], Peter R. Buseck[3], Daizhou Zhang[4], Xiaoye Zhang[5], Peiren Li[6] and Wenxing Wang[1]

[1]Environment Research Institute, Shandong University, Jinan, Shandong 250100, China
[2]State Key Laboratory of Coal Resources and Safe Mining, China University of Mining and Technology, Beijing 100083, China
[3]School of Earth and Space Exploration & Department of Chemistry and Biochemistry, Arizona State University, Tempe, AZ 85287-1404, USA
[4]Faculty of Environmental and Symbiotic Sciences, Prefectural University of Kumamoto, Kumamoto 862-8502, Japan
[5]Centre for Atmospheric Watch and Services, Chinese Academy of Meteorological Sciences, China Meteorological Administration, Beijing, China
[6]Weather Modification Office of Shanxi Province, Taiyuan 030032, China

Corresponding author. Email address: liweijun@sdu.edu.cn (W. J. Li)

Brown hazes have far-reaching effects at both regional and global scales, influencing both climate change and human health. In recent decades, brown hazes have caused the atmospheric air quality to deteriorate all over eastern China, where regional haze layers over both large cities and rural areas exhibit surprisingly high loadings of atmospheric pollutants. To evaluate regional brown hazes in northern China, transmission electron microscopy was employed to study individual haze particles produced by different kinds of haze episodes. We classified brown hazes into three types: smoke-urban-haze, industrial-urban haze, and coal-burning haze.

Keywords: Aerosol particles; Elemental composition; Mixing properties of aerosols; Single particle analysis; Electron microscopy; Aircraft

1. Smoke-urban haze

Emissions from agricultural biomass burning (ABB) in northern China have a significant impact on the regional and global climate. In northern China in June 2007, the monthly average aerosol optical depth (AOD) at 550 nm reached a maximum of 0.7. The AOD measurements are consistent with the occurrence of regional brown hazes and observations of severe aerosol pollution at that time. Aerosol particles were collected in urban Beijing from 12 to 30 June 2007 during a period of high haze and studied by transmission electron microscopy (TEM) and energy-dispersive X-ray spectrometry. The dominant particle types collected in the fine fraction (diameter < 1 μm) were ammonium sulfate, soot, K_2SO_4, KNO_3, and organic matter, although the K salts were minor between 21 and 30 June (Figure 1). The K-rich particles, which can be used as tracers of biomass burning, together with wildfire maps show that intense regional ABB in northern China contributed significantly to the regional haze observed between 12 and 20 June. We therefore classified the haze into two episodes: a type 1 (smoke-urban) haze between 12 and 20 June and a type 2 (industrial-urban) haze between 21 and 30 June. During the first haze episode, soot particles were mixed with the other particle types. Abundant organic matter and soluble salts emitted by ABB increased the particle sizes during transport and resulted in more hygroscopic aerosol particles in downwind areas, where they became cloud condensation nuclei. The high AOD (average 2.2) in Beijing during 12 to 20 June can be partly explained by the hygroscopic growth of fine aerosol particles and by the strong absorption of internally mixed soot particles, both coming from regional ABB emissions. These findings show that it is important to consider the origins of a haze, because different origins lead to different types of particles [1].

2. Industrial-urban haze

To evaluate a wintertime regional brown haze in northern China (Figure 2), trace gases and aerosols were measured at an urban site between 9 and 20 November 2009. Ion chromatography and TEM were used to investigate soluble ions in $PM_{2.5}$ and the mixing state of individual particles. The contrasts between clear and hazy days were examined in detail. Concentrations of the primary gases, including NO (55.62 ppbv), NO_2 (54.86 ppbv), SO_2 (83.03 ppbv), and CO (2.07 ppmv), on hazy days were two to six times their levels on clear days. In contrast, concentrations of O_3 remained low (5.71 ppbv) on hazy days. Mass concentrations of $PM_{2.5}$ (135.90 μg m^{-3}) and black carbon (7.85 μg m^{-3}) were three times higher on hazy days than on clear days. By TEM analysis, it was estimated that fractions of both ammoniated

sulfate (AS)-soot (20%) and AS-soot/organic matter/fly ash (20%) were larger on hazy days than on clear days (13% and 12%), implying that coagulation is an important mixing process in polluted air.

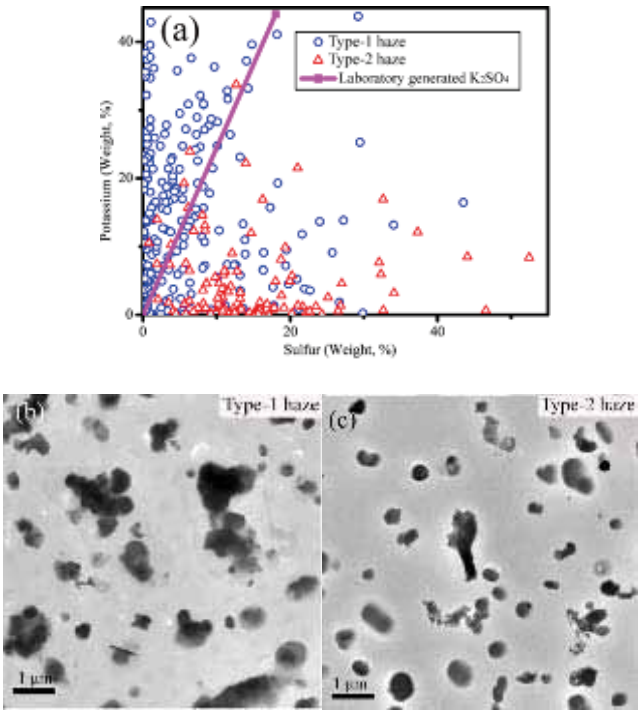

Figure 1 Potassium and sulfur contents of individual particles of type 1 and type 2 hazes.

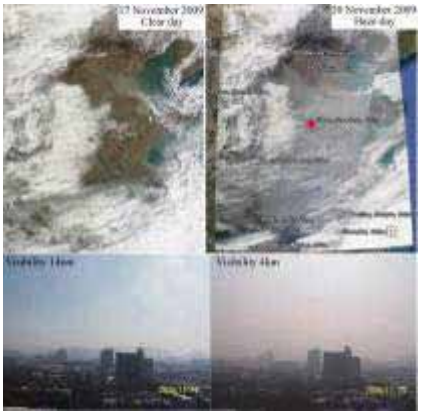

Figure 2 Reduction of visibility caused by a regional winter haze in northern China.

Emissions from coal combustion for power generation, industrial activities, and household heating led to the high SO_2 concentrations. Also, significantly high concentrations of secondary sulfates formed in the haze. Therefore, high concentrations of acidic gases contributed to the increased mass and number concentrations of secondary aerosols. Our study results indicate that metal-catalyzed oxidation in the aqueous phase is a major pathway of sulfate formation. The mixtures of aerosol particles, together with MODIS images, suggested that this haze covered not only the industrial cities but also extended into the neighboring rural regions [2].

3. Coal-burning haze

Heavy haze occurs frequently in winter over the Taiyuan Basin, northwestern China, a coal-burning region. During a research flight on 17–18 December 2010, aerosol particles were collected and the SO_2 concentration was monitored in a haze that occupied the atmosphere from the ground (780 m a.s.l) up to 4110 m altitude. Meteorological records revealed that the haze was stable and that it could be subdivided into three layers by chemical shifts at altitudes of about 1500 and 3000 m. From the surface to 1500 m (layer 1), the SO_2 concentration was 16–116 ppb (average, 58 ppb); from 1500 to 3000 m (layer 2), it was 2–45 ppb (average, 9 ppb); and above 3000 m (layer 3), it was 2–10 ppb (average, 4 ppb). The accumulation of SO_2 in layer 1 was attributable to the stable meteorological conditions and strong anthropogenic emissions as well as to the basin topography. Analyses of the collected particles by TEM revealed that organic particles and fly ash dominated in layers 1 and 2 and sulfate particles in layer 3. The organic aerosols frequently contained Si and Cl. Fly ash particles consisted of O and Si with minor Fe, Mn, Zn, Ti, Pb, As, Co, and Cr. These two types of aerosol particles are typically emitted during coal burning. Therefore, this haze is characterized primarily by aerosols produced as primary coal-burning emissions, in contrast to the hazes produced over the North China Plain, where secondary sulfate particles are dominant.

4. Conclusion

Although regional hazes occur frequently in China, the aerosol sources differ depending on the region and on the season, and various anthropogenic sources have resulted from economic development and the implementation of reforms throughout China. These regional hazes not only cause diverse health problems in continental China but also influence the regional and global climate. Compared with other areas in the world, many different atmospheric chemical mechanisms contribute to haze formation in this heavily polluted region because of the extremely high fine-particle loading in the atmosphere. Because how these haze aerosols influence cloud formation and precipitation is still unknown, haze aerosol particles from the upper atmosphere should be examined in future studies.

1 Li, W. J., L. Y. Shao, P. R. Buseck, 2010: Haze types in Beijing and the influence of agricultural biomass burning. *Atmos. Chem. Phys.*, **10**, (17), 8,119-8,130.

2 Li, W. J., S. Z. Zhou, X. F. Wang, Z. Xu, C. Yuan, Y. C. Yu, Q. Z. Zhang and W. X. Wang, 2011: Integrated evaluation of aerosols from regional brown hazes over northern China in winter: Concentrations, sources, transformation, and mixing states. *J. Geophys. Res.*, **116,** (D9), doi: 10.1029/2010JD015099.

Identification and analysis of atmospheric aerosol particles (& climate implications)

Peter R. Buseck[1], Kouji Adachi[2], Evelyn Freney[3], Tomoko Kojima[4], Weijun Li[5], Mihaly Posfai[6]

[1]School of Earth and Space Exploration & Department of Chemistry and Biochemistry, Arizona State University, Tempe, Arizona, 85287, USA
[2]Meteorological Research Institute, 1-1 Nagamine, Tsukuba, Ibaraki 305-0052, Japan
[3]Laboratoire de Météorologie Physique, CNRS, Université Blaise Pascal, Clermont Ferrand, France
[4]Kumamoto University, 2-39-1, Kurokami, Kumamoto 860-8555, Japan
[5]Environment Research Institute, Shandong University, Jinan, Shandong 250100, China
[6]University of Pannonia, Veszprém, POB 158, H-8200 Hungary

**Corresponding author. Tel.: +1 480 965 3945; Email address: pbuseck@asu.edu (P. Buseck)*

Aerosol particles are ubiquitous in the atmosphere and exert major influences on visibility, human health, and climate. The latter has received great attention in recent years and provides the primary justification for the research described in this talk. When solid, many aerosol particles are extremely small and yet have irregular shapes and, in many cases, form in complex mixtures. These variables control their interaction with solar radiation and thus determine whether they produce net heating or cooling effects.

Knowledge of their identities and physical characteristics is important for understanding reaction dynamics, source attribution and remediation, atmospheric modeling, and determining optical properties, important for climate effects. Desired parameters include size, composition, crystallographic structure, aspect ratio, and mixing state (single- or polyphase, coated or aggregated).

Many methods are available for determining sizes of individual particles, fewer for determining composition, but transmission electron microscopy (TEM) is unique for determination of structure (e.g., polymorphs or allotropes) and mixing states. Indeed, TEM is the only way to determine all of the above parameters, and it covers sizes from <1 nanometer to 10 or more micrometers. They represent a far richer and more complex world than is commonly assumed, and they contain more information than is commonly being recovered. Examples will be provided of imaging and analysis of particles from a range of environments, including discussions of their climate implications.

1

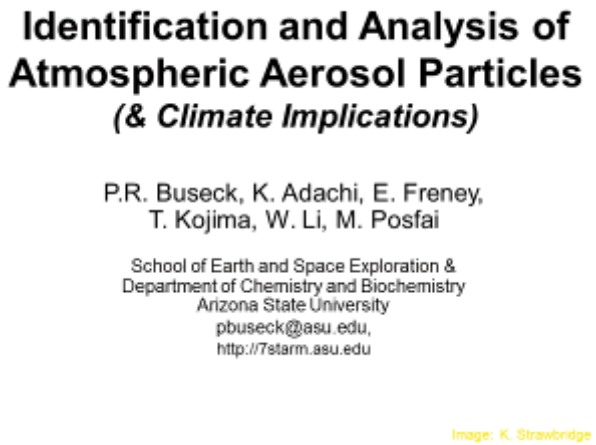

2

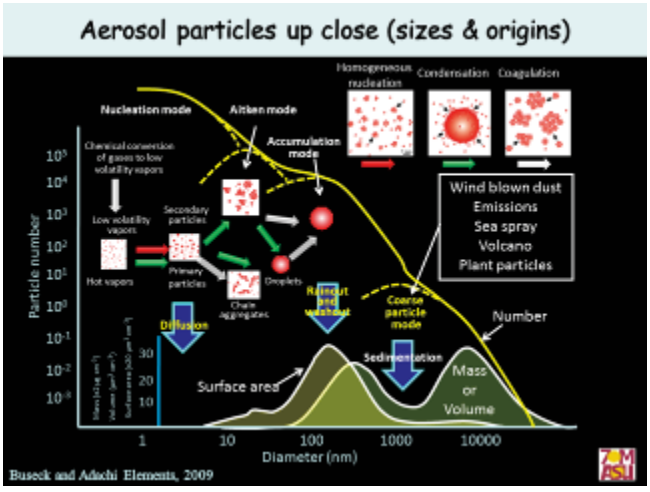

3

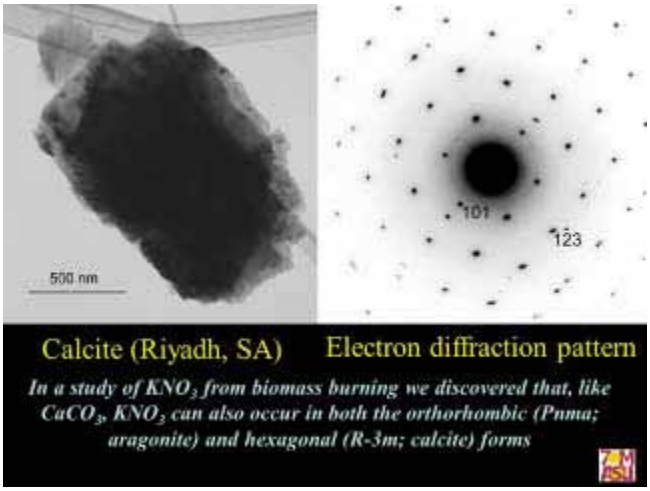
500 nm
101
123
Calcite (Riyadh, SA)
Electron diffraction pattern
In a study of KNO_3 from biomass burning we discovered that, like $CaCO_3$, KNO_3 can also occur in both the orthorhombic (Pnma; aragonite) and hexagonal (R-3m; calcite) forms

4

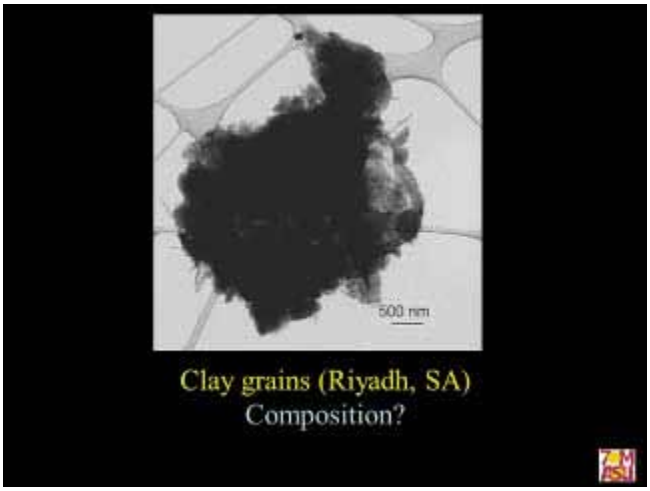
500 nm
Clay grains (Riyadh, SA)
Composition?

5

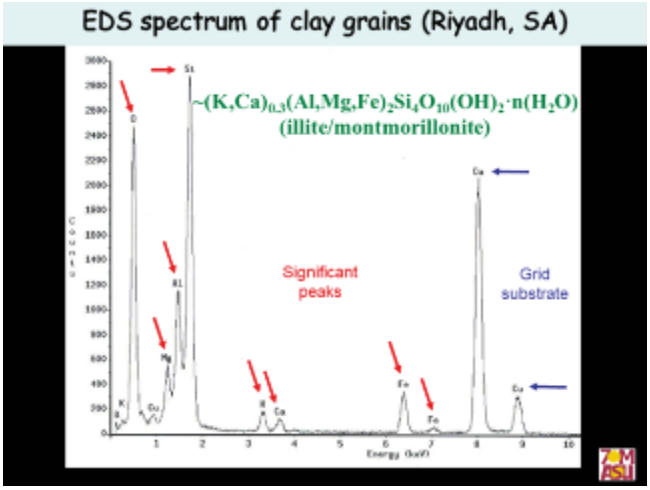
EDS spectrum of clay grains (Riyadh, SA)
~(K,Ca)0.3(Al,Mg,Fe)2Si4O10(OH)2·n(H2O)
(illite/montmorillonite)
Significant peaks
Grid substrate

6

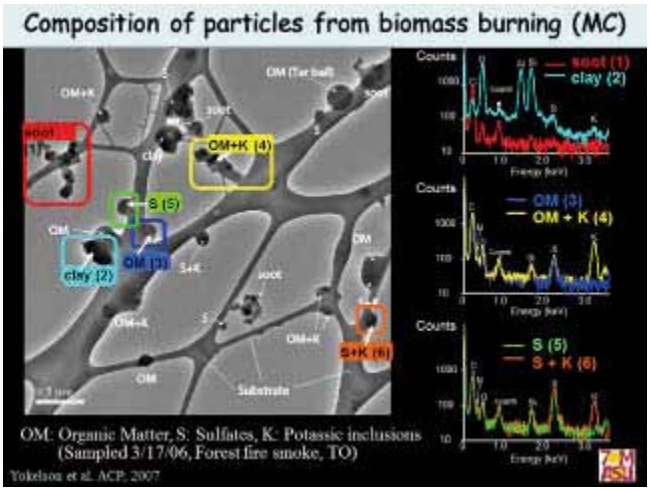
Composition of particles from biomass burning (MC)
soot (1)
clay (2)
OM (3)
OM + K (4)
S (5)
S + K (6)
OM: Organic Matter, S: Sulfates, K: Potassic inclusions
(Sampled 3/17/06, Forest fire smoke, TO)
Yokelson et al. ACP, 2007

7

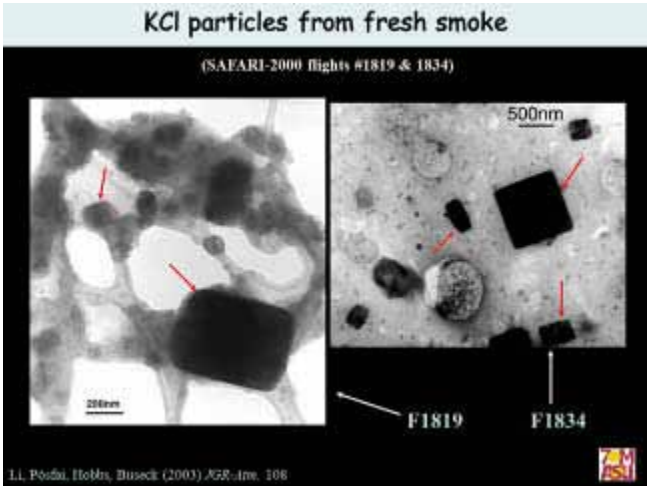
KCl particles from fresh smoke
(SAFARI-2000 flights #1819 & 1834)
500nm
F1819
F1834
Li, Posfai, Hobbs, Buseck (2003) ACP, 108

8

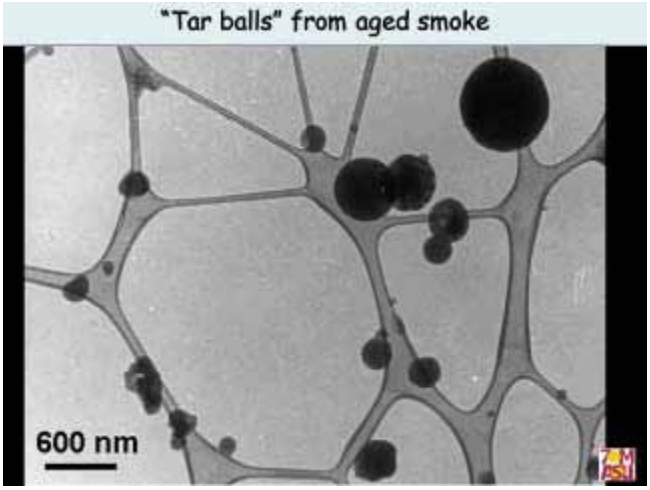
"Tar balls" from aged smoke
600 nm

9

10

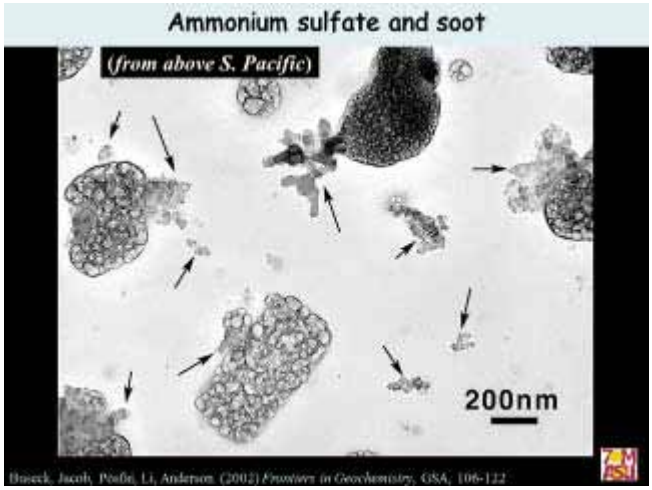

11

12

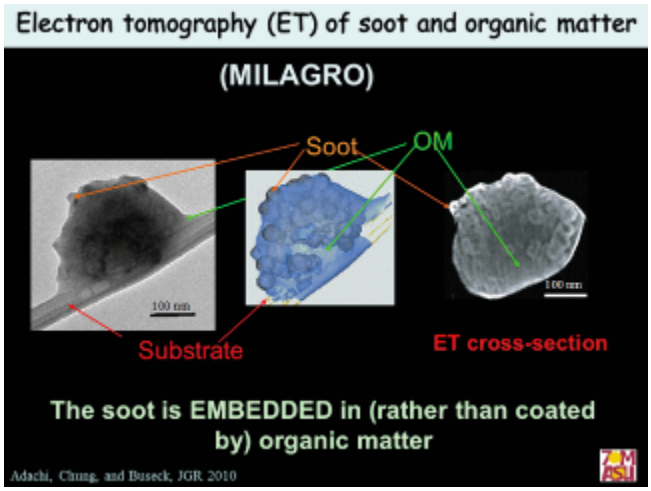

13

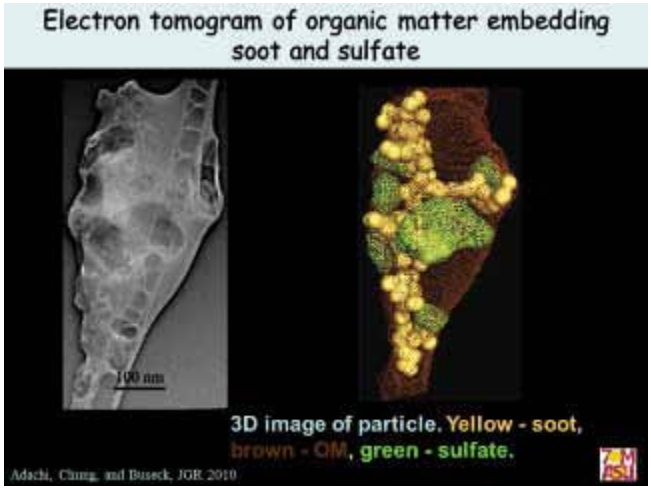

14

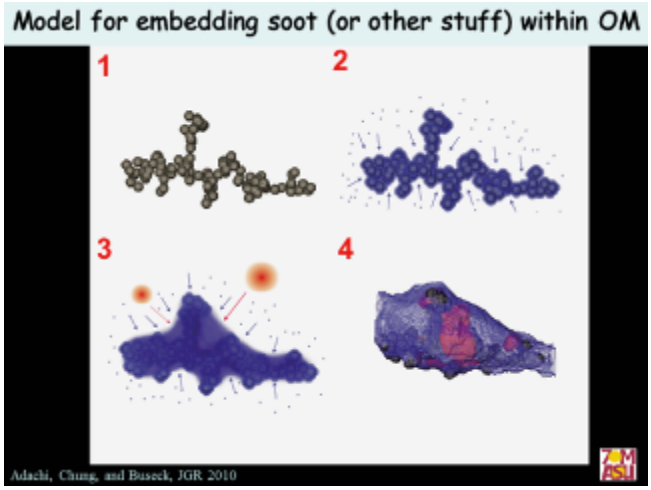

15

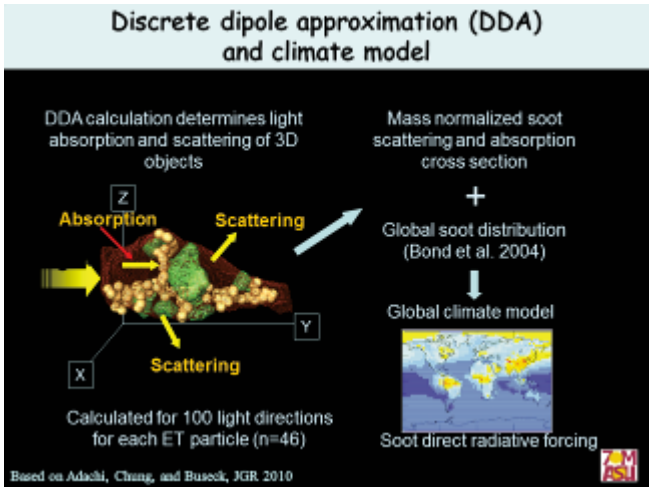

Thoughts & goals for the future

Use accurate and appropriate particle data in climate models

For example, produce models of "black carbon" that match the shapes and configurations that are actually observed

Reconcile measurements of individual particles with those from remote sources such as aircraft and satellites

The people and facilities at MRI seem to make this an ideal place for such research advances

* * * * * * * * * * * * *

Thank you very much for inviting me to this very interesting and promising symposium!

16

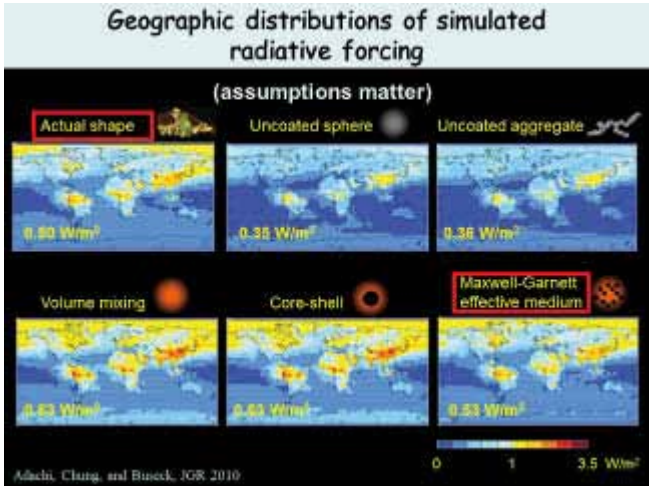

17

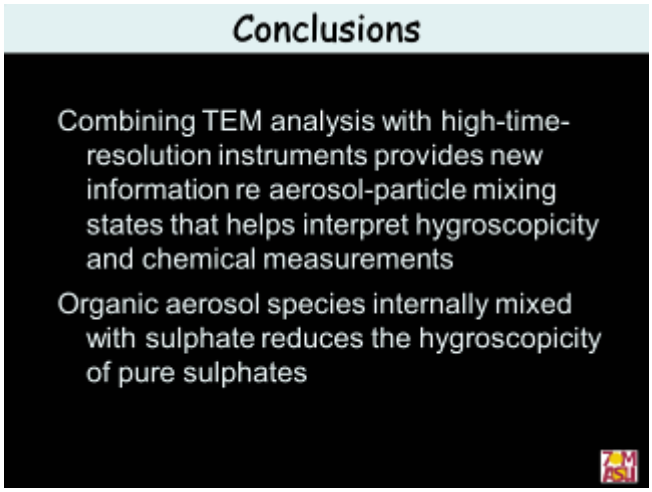

Studies of aerosol particles performed with the MRI electron microscopes during the last three decades

Kikuo Okada[1, *]

[1] Atmospheric Environment and Applied Meteorology Research Department, Meteorological Research Institute, 1-1 Nagamine, Tsukuba, Ibaraki 305-0052, Japan

**Corresponding author. Tel.: +81 29 853 8621; Fax: +81 29 855 7240, Email address: kokada@mri-jma.go.jp (K. Okada)*

During the last three decades, single-particle analyses have been carried out in the MRI by using a transmission electron microscope (Hitachi H-600 and H-6010) equipped with an energy-dispersive X-ray analyzer, and sometimes with a scanning electron microscope (Hitachi S-2150) as well. This report briefly describes the results obtained by these electron microscope studies.

Keywords: Aerosol particles; Elemental composition; Mixing properties of aerosols; Single particle analysis; Electron microscopy; Aircraft observation

1. Introduction

To evaluate the effect of aerosols on meteorological phenomena such as cloud formation and radiative transfer, it is important to study the composition and mixture state of individual aerosol particles. Many single-particle analyses have been carried out during the last three decades with the MRI electron microscope systems.

Here, the results obtained by using the MRI electron microscopes are briefly described.

2. Basic methods

Individual aerosol particles are usually collected on a carbon-coated nitrocellulose (collodion) film with aerosol samplers. Those collected on carbon film are usually coated with Pt/Pd alloy at a shadowing angle of 26.6° (arctan 0.5) and examined by a transmission electron microscope (TEM; Hitachi H-600 and H-6010) to assess their shape and volume.

The elemental composition of the collected particles is investigated by using the TEM equipped with an energy-dispersive X-ray (EDX) analyzer. The electron beams usually irradiate the central part of a particle with an accelerating voltage of 50 kV, and the X-ray spectrum is obtained through a Kevex UTW (ultra thin window) detector. Individual particles are quantitatively analyzed by the thin film method using Kevex Quantex^{TM} software for energy-dispersive microanalysis.

3. Results and discussion

3.1. Modification of sea-salt particles

Sea-salt particles are one of the dominant types of particles originating from natural sources. In the atmosphere, sea-salt particles are modified by chemical reactions with acidic materials that result in emission of HCl from the particles.

The weight ratio of Cl to Na in seawater is mainly fixed at about 1.8. Therefore, examination of the Cl/Na weight ratio reveals whether the atmospheric sea-salt particles have been modified. Sea-salt particles with Cl/Na < 1 are regarded as having an apparent Cl deficiency (apparent modification). In the atmosphere over coastal regions, where sea-salt particles encounter anthropogenically polluted air, the composition of sea-salt particles is distinctively modified by chemical reactions with sulfuric acid and nitric acid [1-3].

The number percentages of sea-salt particles with Cl/Na < 1 in the radius range of 0.1–1 μm change spatially. For example, the number percentage at Shengshan Island, which is about 150 km east of Shanghai, was 18% [3], whereas the percentages at Marcus Island (24.3°N, 154.0°E) in the northwestern Pacific ranged from 6% to 36% [4]. The high percentage (36%) was associated with outflow from the Asian continent. In sea-salt particle samples collected by research ships during cruises [1, 5-8], the highest percentage (98%) was observed in the tropics near Borneo in association with biomass burning [1]. Thus, the number percentage of such particles changes depending on the trajectory of the air mass, and values were generally less than 10% in remote oceanic areas.

One study examined sea-salt particles collected at Syowa Station, Antarctica [9]. In the samples collected in austral summer, when the production of marine organosulfur is enhanced, the number fractions of sulfur-rich particles and modified sea-salt particles were high. In the samples collected in austral winter, when severe storms enhance the production of sea-salt particles, the number fraction of unmodified sea-salt particles was high. Another study investigated the concentration, number-size distribution, and

morphological features of aerosol particles (although not sea-salt particles) at Barrow, Alaska, in April 1997 [10]. That study found that new particle formation from the gas phase occurred in spite of the very low concentrations of gaseous materials, especially in air masses from the lower latitudes, and the accumulation mode included particles composed of sulfuric acid and ammonium sulfate.

A sample collected on 4 February 1991 near the sea surface in the South Pacific (10°S, 175°W) contained a very low percentage (4%) of sea-salt particles with Cl/Na < 1 [5]. Aircraft (Gulfstream 2) observations carried out nearby on 3 March 1990 at 11.2 km altitude by the International Strato/Tropospheric Air Chemistry (INSTAC-II) program [11] observed high aerosol concentrations in the upper part of cumulonimbus clouds with an optical particle counter (OPC). Both cloud-active and -inactive particles were transported vertically in the cumulonimbus clouds, and in these samples the number percentages of sea-salt particles in samples were large: 42% for particles with radii of 0.05–0.1 μm and 64% for particles with radii of 0.1–1 μm. This high abundance of sea salt in the smaller particles (radius < 0.1 μm) suggests that sea-salt particles play an important role in the cloudy marine atmosphere. EDX analysis showed that Cl/Na weight ratio in the sea-salt particles tended to decrease as excess sulfur increased. The number percentage of sea-salt particles with Cl/Na < 1 was 34% in the radius range of 0.1–1 μm, or about one order of magnitude higher than the percentage in the near-surface sample [5]. Thus, the sea-salt particles were modified during their vertical transport in cumulonimbus clouds. Other studies have also observed the vertical transport of sea-salt particles by convective clouds in the middle troposphere [12-14].

3.2. Elemental composition and shape of mineral particles (Asian dust) collected in three arid regions of China

In spring 1991, mineral particles (Asian dust) were collected with a battery-operated single-stage impactor in three arid regions of China (Hohhot, Inner Mongolia Autonomous Region; Zhangye, near the southern border of the Badain-Jaran Desert; and Qira, in the Taklamakan Desert) [15-17]. Compared with samples collected in Japan [18], the particles collected in these three locations usually showed that the edge of the particles were a distinct outline on the collection film.

Type classification of all particles with radii of 0.1–6 μm based on EDX analysis indicated that the number percentages of mineral particles were very high: 98.2% at Hohhot, 99.5% at Zhangye, and 99.1% at Qira). At Hohhot, fly ash particles (classified as mineral particles) accounted for 4.4% of aerosol particles.

The shape of 6998 mineral particles with radii between 0.1 and 6 μm at the three sites was examined by TEM [19]. In all three regions, the mineral particle shapes were irregular, with a median aspect ratio *b/a* (ratio of the longest dimension *b* to the orthogonal dimension *a*) of 1.4. Although the aspect ratio exhibited no clear size dependence, the circularity factor ($4\pi S/l^2$; where S is surface area and l is periphery length) tended to decrease as the radius increased, suggesting that the larger sized particles included aggregated mineral particles. The particle height-to-width ratio *h/a* was also evaluated by measuring the length of a particle's shadow on the collection surface. The median *h/a* was 0.49 at Hohhot, 0.29 at Zhangye, and 0.23 at Qira. Analytical functions were fitted to the grand total of the frequency distributions of aspect ratios, height-to-width ratios, and circularity factors to allow parametric calculations of radiative effects and of the optical and sedimentation behavior of the mineral particles.

In another study, the influence of particle nonsphericity on the size distribution of submicrometer mineral particles as measured with an OPC was examined by comparison with TEM analysis obtained in a laboratory experiment and theoretical computations of light scattering by nonspherical particles [20]. When the size distribution of monodispersed mineral particles was compared between measurements made with the OPC and by TEM, the volume equivalent mode radii obtained with the OPC were 0.06–0.09 μm larger than those obtained by TEM.

The backscattering linear depolarization ratios of Asian and Saharan mineral dust, sea-salt, and ammonium sulfate particles were measured in a laboratory chamber to aid in the interpretation of polarization lidar measurements of tropospheric aerosols [21]. TEM results were also used in the study.

Electron micrographs of Asian dust particles in aerosols collected at Fukuoka, Japan, in March 2009 were used to produce a shape model for mineral dust particles for light scattering calculations [22]. In addition, local wind-blown mineral particles collected at Tsukuba were examined by TEM [23].

3.3. Modification of Asian dust-storm particles during long-range transport

Sea salt can modify mineral particles during long-range transport [24-26]. The abundance of dust-storm particles with radii > 1 μm internally mixed with sea salt were compared in samples from two dust-storm events observed in both Beijing, China, and Nagasaki, Japan, in spring 1991. In samples from the first event, 2% of Asian dust particles collected in Beijing on 30 April and 72% of those collected on 1 May in Nagasaki contained sea salt. In samples from the second event, 2% of dust particles collected on 7 and 9 May in Beijing and 16% of those collected in Nagasaki on 10 May included sea salt. The large abundance of Asian dust particles containing sea salt at Nagasaki during the first event was attributed to clouds encountered in the marine atmosphere during transport, which suggests that the mixed dust particles formed by cloud processes.

As previous research had suggested that sulfur accumulates on Asian dust particles [27], mineral particles from the

same dust episode were collected in April 1993 at both Beijing and Fukuoka [28]. Examination of individual dust particles by TEM showed that the dust particles collected in China had distinctly irregular shapes and contained low amounts of sulfur, whereas the dust particles collected over Japan after transport had been modified by the addition of sea salt and/or anthropogenic sulfur.

Asian dust particles were collected on a thin nitron ($C_{20}H_{16}N_4$) film in Nagoya, Japan, to detect nitrate ions [29]. TEM examination indicated that nitrate was present on the surface of dust particles collected during the dust-storm event. Nitrate and sulfate formation through heterogeneous reactions on the dust particles are one of the mechanisms of nitrogen oxides and sulfur dioxide removal from the atmosphere.

The presence of high fractions of mixed dust particles may enhance the cloud nucleating capability, as well as modulate its optical properties. As a result, the removal rate of Asian dust particles from the atmosphere might increase.

In addition to mineral particles, water-insoluble particles in rainwater at Shizuoka and Tsukuba, Japan, which were deposited directly onto electron microscope grids by ultracentrifugation [30], were found to consist of bacteria and leaf debris, and most of them were aggregated with mineral particles.

3.4. Mixing state of aerosol particles in the urban atmosphere

The composition and mixing properties of individual aerosol particles in the urban atmosphere must be known to evaluate the effect of anthropogenic aerosol particles on cloud formation and atmospheric radiation.

Aerosol particles were collected in 1989 in Katowice, Poland [31]. TEM results showed significant differences in the hygroscopic properties of aerosol particles that depended on the wind direction at the time of collection, which suggested that the aerosol particles were not well mixed and were influenced by the distribution of anthropogenic sources in Katowice and the surrounding area.

The mixing properties of individual aerosol particles with radii between 0.1 and 1 μm collected in 1991 in the urban atmosphere of Vienna, Austria [32], were studied by using water dialysis to extract water-soluble material. The averaged results showed that more than 85% of particles with radii between 0.1 and 0.7 μm were hygroscopic, and more than 50% of those with radii larger than 0.2 μm were mixed particles (hygroscopic particles with water-insoluble inclusions); mixed particles were dominant (80%) in the radius range of 0.5–0.7 μm. Moreover, the number proportion of mixed particles increased with increasing radius, and their abundance also increased as the particle mass loading in the atmosphere increased. The volume fraction of water-soluble material (ε) in mixed particles tended to decrease with increasing radius, implying that the mixed particles formed by heterogeneous processes such as condensation and surface reactions.

The mixing properties of individual aerosol particles with radii of 0.02–0.2 μm collected with an electrostatic aerosol sampler in June 2000 at Tsukuba [33] were studied by using water dialysis. The proportions of particles with water-soluble material (hygroscopic particles) ranged from 20% to 80% in the whole radius range and tended to increase with increasing radius. Moreover, morphological examination revealed two types of soot-containing particles: externally mixed (pure) and internally mixed soot particles. The number fractions of internally mixed soot particles increased with increasing radius. A sample collected in "polluted" air showed that internally mixed soot particles were dominant (number fraction, 75%) in the larger radius range of 0.1–0.2 μm.

At Tsukuba, aerosol particles in ambient air downstream of a differential mobility analyzer (DMA) were measured with an impactor at the electrical mobility radii of 0.1, 0.15, and 0.2 μm in dry conditions (relative humidity < 3%) [34-36]. The particles were collected on a film covered with silicone oil and examined by TEM to determine their diameters, shapes, and morphological changes caused by electron-beam bombardment. Measurements with an OPC were carried out in parallel to assess the abundance of externally mixed soot particles. Most of the number frequency distributions obtained by TEM peaked at the DMA diameters (mobility diameters). Circularity factors of pure soot particles decreased as the particle radius increased, and their irregular shapes produced broad size-frequency distributions. Comparison of soot particle abundance between the OPC and TEM results showed good agreement.

With regard to cloud formation, the efficiency of nucleation scavenging of aerosol particles with radii between 0.028 and 0.28 μm was measured at Tsukuba by using two thermal gradient diffusion chambers, one with and one without a water vapor source [37]. The efficiencies were measured as a function of the supersaturation of water vapor (S). The mean efficiency by aerosol volume was high (0.75–0.93) at S of 0.25–1.04%. The efficiencies were closely related to the hygroscopic properties of the aerosol particles as determined by electron microscopy. Electron microscope studies of aerosol particles in clouds and fog were also performed [38-42].

The light absorption property of carbonaceous particles was investigated at Tsukuba in relation to the mixing state [43]. The volume fraction of water-soluble material (ε) in soot-containing particles was evaluated by comparing electron micrographs before and after water dialysis. The mass absorption coefficient (unit; $m^2\ g^{-1}$) tended to increase with the average ε in soot-containing particles with radii of 0.05–0.5 μm. Thus, coatings of water-soluble material around soot particles enhance the absorption of solar radiation.

Internal mixtures of nitrate with sulfate in urban aerosol particles were examined by using the vapor-deposited thin nitron film method and EDX analysis [44].

3.5. Free tropospheric aerosol particles

Aircraft observations are used to study aerosols in the free troposphere. The INSTAC program, mentioned in section 3.1, is one example. Another is a series of the Pacific Atmospheric Chemistry Experiment (PACE) campaigns, jointly carried out by the MRI and the Australian Commonwealth Scientific and Industrial Research Organisation (CSIRO).

In the PACE I campaign, individual aerosol particles were collected at 5–6 km altitude in the middle troposphere over the western Pacific Ocean between Melbourne (38°S) and Sendai (38°N) in January 1994 [14]. By EDX analysis and morphological identification, particles were classified into various types, including sea salt, mineral, sulfate, and sulfuric acid. Sulfuric acid and ammonium sulfate, which were commonly found in particles of 0.1–1 μm radius across most of the observed region, were considered important background aerosols. Sea-salt particles were also often abundant in the tropical regions (present at up to 67%), owing to vertical transport by convective clouds. North of 20°N, mineral particles were dominant, suggesting transport of Asian dust particles in the westerly air stream. Abundant Asian dust particles covered with sulfuric acid indicated that modification of Asian dust particles had occurred.

A local flight over Saipan, a subtropical area, carried out during the PACE I campaign [45] showed that the number concentration of condensation nuclei (CN) increased with altitude in contrast to large particle concentrations, which decreased with altitude. Most particles collected at 6 km altitude were composed of sulfuric acid, suggesting that new particle formation is favored in the upper troposphere.

In the PACE III campaign, individual aerosol particles were collected at 5–6 km altitude in the middle troposphere between Melbourne and Sendai, as in the PACE I campaign, but in July 1995 [46]. The PACE III campaign results were similar to the PACE I results, except that mineral particles were absent in the northern mid-latitudes and spatial shifts in particle composition and concentrations were observed. Comparison of the results of the two campaigns suggested that seasonal shifts in the locations of the intertropical convergence zone and wind belts contributed to the seasonal differences in the spatial distributions of particles in the middle troposphere over the western Pacific.

During the PACE V campaign over Kalimantan, Indonesia, in October 1997, individual particles were collected from a very dense haze caused by Indonesian forest fires [47, 48]. Although 60–90% of the particles collected at altitudes of 1–5 km contained K, the S/K weight ratio was high, with median values of 9–18, independent of particle size. These ratios were much larger than those (median values of 2–4) measured in haze from biomass burning in northern Australia. The high weight ratios over Kalimantan were attributed to the heterogeneous growth of particles through the oxidation of SO_2. In addition to SO_2 from the combustion of forest biomass, SO_2 originating from the combustion of buried peat was believed to have also contributed to the high S/K ratios. The samples were also examined by electron microscopy after using water dialysis to extract water-soluble material, and benzene dialysis to extract organic material. Individual aerosol particles with radii of 0.1–2 μm were mainly present as an internal mixture of water-soluble organic material and inorganic salt (mainly ammonium sulfate). Chain aggregations of electron-opaque spherules (elemental carbon) were also found, but their proportion was small.

In the PACE VII campaign in February 2000 [49], the number-size distributions of aerosols with radii between 0.05 and 5 μm were observed in the free troposphere up to 11 km altitude in different air masses over the western and northwestern Pacific Ocean. The results showed that over the northern mid-latitudes, Asian outflow contained many anthropogenic particles.

During the PACE II campaign (October 1994), soot particles originating from biomass burning were collected in the middle troposphere over Australia [50]. The abundance of internally mixed soot particles tended to increase with particle radius, and internally mixed soot particles composed 88% of particles with radii of 0.1–0.35 μm.

Soot particles emitted from several hundred oil-well fires in Kuwait from February 1991 were collected by aircraft on 27 April 1991 at 7.5 km altitude over Tsukuba [51, 52]. The number percentage of soot-containing particles was high (53%) in the radius range of 0.15–1 μm. Moreover, about 90% of the soot particles were covered with water-soluble material. From the backward- and forward-trajectory analyses of air parcels, the soot particles over Japan would be supplied to the upper troposphere in the first half of April and those have circled the globe before arrival at sampling point.

Aerosol particles collected by aircraft in January 1983 in the upper troposphere (7.2 km altitude) over Showa Station, Antarctica, were examined by EDX analysis [53]. The number percentage of mineral particles was high (74%) for particles with radii between 0.1 and 1.6 μm. The transport pathways of the mineral particles were studied by 3-D trajectory analyses of U. S. National Meteorological Center (NMC) data, which are reported twice daily. Most aerosol particles collected in the Antarctic upper troposphere originated from El Chichon volcano and had been transported downward from the stratosphere over Antarctica.

Aerosol particles for examination by electron microscopy have also been collected at a mountain site [54, 55], and from the upper troposphere and stratosphere by balloon-borne samplers [56-59].

The author expresses his great thanks to all of the researchers who have used the MRI electron microscope system.

1 Mouri, H., I. Nagao, K. Okada, S. Koga and H. Tanaka, 1996: Elemental composition of individual aerosol particles collected from the coastal marine boundary layer. *J. Meteor. Soc. Japan*., **74**, 585-591.

2 Roth, B. and K. Okada, 1998: On the modification of sea-salt particles in the coastal atmosphere. *Atmos. Environ*, **32**, 1,555-1,569.

3 Li, F., and K. Okada, 1999: Diffusion and modification of marine aerosol particles over the coastal areas in China - a case study using a single particle analysis. *J. Atmos. Sci*., **56**, 241-248.

4 Naoe, H.. and K. Okada, 2006. Modification of sea-salt particles in the remote marine atmosphere in the North Pacific. *Pap. Meteor. Geophys*, **57**, 47-54.

5 Mouri, H.., K. Okada and K. Shigehara, 1993: Variation of Mg, S, K and Ca contents in individual sea-salt particles. *Tellus*, **45B**, 80-85.

6 Mouri, H. and K. Okada, 1993: Shattering and modification of sea-salt particles in the marine atmosphere. *Geophys. Res. Lett*., **20**, 49-52.

7 Mouri, H., K. Okada and S. Takahashi, 1995: Giant sulfur-dominant particles in remote marine boundary layer. *Geophys. Res. Lett*., **22**, 595-598.

8 Mouri, H., I. Nagao, K. Okada, S. Koga and H. Tanaka, 1997: Elemental composition of individual aerosol particles collected over the Southern Ocean: A case study. *Atmos. Res*., **43**, 183-195.

9 Mouri, H., I. Nagao, K. Okada, S. Koga and H. Tanaka, 1999: Individual-particle analyses of coastal Antarctic aerosols. *Tellus*, **51B**, 603-611.

10 Zaizen, Y., K. Okada, M. Ikegami, T. Aoki, Y. Sawa, F. Nishio and Y. Tachibana, 1998: Size distribution of aerosols at Barrow in Alaska - A case study in spring. *Polar Meteor. Glaciol*., **12**, 40-48.

11 Ikegami, M., K. Okada, Y. Zaizen and Y. Makino, 1994: Sea-salt particles in the upper tropical troposphere. *Tellus*, **46B**, 142-151.

12 Ikegami, M., K. Okada, Y. Zaizen and Y. Makino, 1993: Aerosol particles in the middle troposphere over the northwestern Pacific. *J. Meteor. Soc. Japan*, **71**, 517-528.

13 Ikegami, M., K. Okada and Y. Zaizen, 1991: Sea-salt particles in the middle troposphere over the tropical Pacific Ocean. *Pap. Meteor. Geophys*, **42**, 31-41.

14 Ikegami, M., K. Okada, Y. Zaizen, Y. Tsutsumi, Y. Makino, J. B. Jensen and J. L. Gras, 2004: The composition of aerosol particles in the middle troposphere over the western Pacific Ocean: Aircraft observations from Australia to Japan, January 1994. *Atmos. Environ*, **38**, 5,945-5,956. (Erratum: *Atmos. Environ*., **40**, 793, 2006)

15 Okada, K., Y. Qin and K. Kai, 2005: Elemental composition and mixing properties of atmospheric mineral particles collected in Hohhot, China. *Atmos. Res*., **73**, 45-67.

16 Okada, K. and K. Kai, 1995: Features and elemental composition of mineral particles collected in Zhangye, China. *J. Meteor. Soc. Japan*, **73**, 947-957.

17 Okada, K. and K. Kai, 2004: Atmospheric mineral particles collected at Qira in the Taklamakan Desert, China. *Atmos. Environ*, **38**, 6,927-6,935.

18 Okada, K., A. Kobayashi, Y. Iwasaka, H. Naruse, T. Tanaka and O. Nemoto, 1987: Features of individual Asian dust-storm particles collected at Nagoya, Japan. *J. Meteor. Soc. Japan*, **65**, 515-521.

19 Okada, K., J. Heintzenberg, K. Kai and Yu Qin, 2001: Shape of atmospheric mineral particles collected in three Chinese arid-regions. *Geophys. Res. Lett.,* **28**, 3,123- 3,126.

20 Sakai, T., Y. Zaizen, C. Nishita, A. Matsuki, Y. Mano and K. Okada, 2008: Influence of particle nonsphericity on the size distribution measurement of submicrometer mineral dust by use of optical particle counter. Earozoru Kenkyu (formerly: *J. Aerosol Research Japan*), **23**, 269-277.

21 Sakai, T., T. Nagai, Y. Zaizen and Y. Mano, 2010: Backscattering linear depolarization ratio measurements of mineral, sea-salt, and ammonium sulfate particles simulated in a laboratory chamber. *Applied Optics*, **49**, 4,441-4,449.

22 Ishimoto, H., Y. Zaizen, A. Uchiyama, K. Masuda and Y. Mano, 2010: Shape modeling of mineral dust particles for light-scattering calculations using the spatial Poisson-Voronoi tessellation. *J. Quan. Spec. Rad. Trans*, **111**, 2434-2443.

23 Okada, K. and M. Ikegami, 2002: A case study of local wind-blown dust observed in Tsukuba, Japan. *Pap. Meteor. Geophys*, **52**, 9-18.

24 Niimura, N., K. Okada, X.-B. Fan, K. Kai, K. Arao and G.-Y. Shi, 1994: A method for the identification of Asian dust-storm particles mixed internally with sea salt. *J. Meteor. Soc. Japan*, **72**, 777-784.

25 Fan, X.-B., K. Okada, N. Niimura, K. Kai, K. Arao, G.-Y. Shi, Y. Qin and Y. Mitsuta, 1996: Mineral particles collected in China and Japan during the same Asian dust-storm event. *Atmos. Environ*, **30**, 347-351.

26 Niimura, N., K. Okada, X.-B. Fan, K. Kai, K. Arao, G.-Y. Shi and S. Takahashi, 1998: Formation of Asian dust-storm particles mixed internally with sea salt in the atmosphere. *J. Meteor. Soc. Japan*, **76**, 275-288.

27 Okada, K., H. Naruse, T. Tanaka, O. Nemoto, Y. Iwasaka, P.-M. Wu, A. Ono, R. A. Duce, M. Uematsu, J. T. Merrill and K. Arao, 1990: X-ray spectrometry of individual Asian dust-storm particles over the Japanese islands and the North Pacific Ocean. *Atmos. Environ*, **24A**, 1369-1378.

28 Zhou, M., K. Okada, F. Qian, P.-M. Wu, L. Su, B. E. Casareto and T. Shimohara, 1996: Charactersitics of dust storm particles and their long-range transport from China to Japan - Case studies in April 1993. *Atmos. Res*., **40**, 19-31.

29 Wu, P.-M. and K. Okada, 1994: Nature of coarse nitrate particles in the atmosphere- -A single particle approach. *Atmos. Environ*, **28**, 2053-2060.

30 Casareto, B. E., Y. Suzuki, K. Okada and M. Morita, 1996: Biological micro- particles in rain water. *Geophys. Res. Lett*., **23**, 173-176.

31 Pastuszka, J. S. and K. Okada, 1995: Features of atmospheric aerosol particles in Katowice, Poland. *Sci. Total Environ*, **175**, 179-188.

32 Okada, K. and R. M. Hitzenberger, 2001: Mixing properties of individual submicrometer aerosol particles in Vienna. *Atmos. Environ*, **35**, 5617-5628.

33 Naoe, H. and K. Okada, 2001: Mixing properties of submicrometer aerosol particles in the urban atmosphere - with regard to soot particles. *Atmos. Environ*, **35**, 5765-5772.

34 Heintzenberg, J., K. Okada and B. P. Luo, 2002: Distribution of optical properties among atmospheric submicrometer particles of given electrical mobilities. *J. Geophys. Res*., **107**, doi: 10.1029/2001JD000372

35 Okada, K. and J. Heintzenberg, 2003: Size distribution, state of mixture and morphology of urban aerosol particles at given electrical mobilities. *J. Aerosol Sci*., **34**, 1,539-1,553.

36 Heintzenberg, J., K. Okada, T. Trautmann and P. Hoffmann, 2004: Modeling of the signals of an optical particle counter for real nonspherical particles. *Applied Optics*, **43**, 5,893-5,900.

37 Okada, K., T. Tanaka, H. Naruse and T. Yoshikawa, 1990: Nucleation scavenging of submicrometer aerosol particles. *Tellus*, **42B**, 463-480.

38 Naruse, H. and K. Okada, 1989: Change in concentrations of cloud condensation nuclei and aerosol particles during the dissipation of fog. *Pap. Meteor. Geophys*, **40**, 125-137.

39 Akagawa, H. and K. Okada, 1993: Sizes of cloud droplets and cloud droplet residues near stratus cloud base. *Atmos. Res*., **30**, 37-49.

40 Hallberg, A., J. A. Ogren, K. J. Noone, K. Okada, J. Heintzenberg and I. B. Svenningsson, 1994: The influence of aerosol particle composition on cloud droplet formation. *J. Atmos. Chem*., **19**, 153-171.

41 Heintzenberg, J., K. Okada and J. Ström, 1996: On the composition of non-volatile material in upper tropospheric aerosols and cirrus crystals. *Atmos. Res*., **41**, 81- 88.

42 Ueda, S., K. Osada and K. Okada, 2011: Mixing states of cloud interstitial particles between water-soluble and insoluble materials at Mt. Tateyama, Japan: Effects of meteorological conditions. *Atmos. Res*., **99**, 325-336.

43 Naoe, H., S. Hasegawa, J. Heintzenberg, K. Okada, A. Uchiyama, Y. Zaizen, E. Kobayashi and A. Yamazaki, 2009: State of mixture of atmospheric submicrometer black carbon particles and its effect on particulate light absorption. *Atmos. Environ*, **43**, 1,296-1,301.

44 Wu, P.-M., A. Ono and K. Okada, 1987: On the mixture of submicrometer nitrate- containing particles in the urban atmosphere. *J. Meteor. Soc. Japan*, **65**, 1005- 1010.

45 Zaizen, Y., M. Ikegami, Y. Tsutsumi, Y. Makino, K. Okada, J. Jensen and J. L. Gras, 1996: Number concentration and size distribution of aerosol particles in the middle troposphere over the western Pacific Ocean. *Atmos. Environ*, **30**, 1755- 1762.

46 Okada, K., M. Ikegami, Y. Zaizen, Y. Tsutsumi, Y. Makino, J. B. Jensen and J. L. Gras, 2008: Submicrometer sulfur-rich particles in the middle troposphere: Aircraft observations from Australia to Japan. *Atmos. Res*., **88**, 185-198.

47 Ikegami, M., K. Okada, Y. Zaizen, Y. Makino, J. B. Jensen, J. L. Gras and H. Harjanto, 2001: Very high weight ratios of S/K in individual haze particles over Kalimantan during the 1997 Indonesian forest fires. *Atmos. Environ*, **35**, 4237- 4243.

48 Okada, K., M. Ikegami, Y. Zaizen, Y. Makino, J. B. Jensen and J. L. Gras, 2001: The mixture state of individual aerosol particles in the 1997 Indonesian haze episode. *J. Aerosol Sci*., **32**, 1269-1279. (Erratum: *J. Aerosol Sci*., **33**, 553, 2002)

49 Zaizen, Y., K. Okada, M. Ikegami, Y. Sawa and Y. Makino, 2004: Number-size distributions of aerosol particles in the free troposphere over the northwestern Pacific Ocean - Influence of Asian outflow and tropical air transport. *J. Meteor. Soc. Japan*, **82**, 1147-1160.

50 Okada, K., M. Ikegami, Y. Zaizen, Y. Tsutsumi, Y. Makino, J. B. Jensen and J. L. Gras, 2005: Soot particles in the free troposphere over Australia. *Atmos. Environ*, **39**, 5079-5089.

51 Okada, K., M. Ikegami, O. Uchino, Y. Nikaidou, Y. Zaizen, Y. Tsutsumi and Y. Makino, 1992: Kuwaiti soot over Japan. *Nature*, **355**, 120.

52 Okada, K., M. Ikegami, O. Uchino, Y. Nikaidou, Y. Zaizen, Y. Tsutsumi and Y. Makino, 1992: Extremely high proportions of soot particles in the upper troposphere over Japan. *Geophys Res. Lett*, **19**, 921-924.

53 Yamazaki, K., K. Okada and Y. Iwasaka, 1989: Where do aerosol particles in the Antarctic upper troposphere come from? - A case study in January 1983. *J. Meteor. Soc. Japan*, **67**, 889-906.

54 Naoe, H., J. Heintzenberg, K. Okada, Y. Zaizen, K. Hayashi, T. Tateishi, Y. Igarashi, Y. Dokiya and K. Kinoshita, 2003: Composition and size distribution of submicrometer aerosol particles observed on Mt Fuji in the volcanic plumes from Miyakejima. *Atmos. Environ*, **37**, 3047-3055.

55 Naoe, H., Y. Zaizen. K. Yanagida, K. Okada, H. Takahashi and Y. Igarashi, 2012: Mixing state of aerosol particles at Mt. Hotaka, Japan: A case study in winter. *Atmos. Res.*, **118**, 170-179.

56 Mouri, H., K. Okada and Y. Tazawa, 1992: Stratospheric solid particles collected at 24 km altitude over Japan using a balloon-borne impactor. *J. Meteor. Soc. Japan*, **70**, 67-75.

57 Wu, P.-M., K. Okada, T. Tanaka, T. Sasaki, T. Nagai, T. Fujimoto and O. Uchino, 1994: Balloon observation of stratospheric aerosols over Tsukuba, Japan: Two years after the Pinatubo volcanic eruption. *J. Meteor. Soc. Japan*, **72**, 475-480.

58 Okada, K., P.-M. Wu, T. Tanaka and M. Hotta, 1997: A light balloon-borne sampler collecting stratospheric aerosol particles for electron microscopy. *J. Meteor. Soc. Japan*, **75**, 753-760.

59 Xu, L., K. Okada, Y. Iwasaka, K. Hara, K. Okuhara, Y. Tsutsumi and G.-Y. Shi, 2001: On the composition of individual aerosol particle in the troposphere and stratosphere over Xianghe (39.45°N, 117.0°E), China. *Atmos. Environ*, **35**, 3,145-3,153.

Modification of dust particles by sea salt adherence and surface chemical reactions in the marine atmosphere

Daizhou Zhang[1,*], Guangyu Shi[2] and Yasunobu Iwasaka[3]

[1]Prefectural University of Kumamoto, Kumamoto 862-8502, Japan
[2]Institute of Atmospheric Physics, Chinese Academy of Science, Beijing 100029, China
[3]FSO, Kanazawa University, Kanazawa 920-1192, Japan

**Corresponding author. Tel.: +81 96 387 6712; Fax: +81 96 384 6765, Email address: dzzhang@pu-kumamoto.ac.jp (D. Zhang)*

Modifications to dust particles in the marine atmosphere detected by electron microscopy are briefly reviewed. Two processes are emphasized: the interaction of particles with gaseous species leading to the formation of chloride, sulfate, and nitrate, and the adherence of sea salt to particles.

Keywords: Mineral dust; Marine atmosphere; Long-range transport; Environmental subsequent effects

1. Introduction

Individual aerosol particle analysis can provide accurate information on the shape, size, composition, and other properties of particles. Unlike bulk, or integrated, sample analysis, which shows quantitative characteristics of all particles collected on a filter, individual particle analysis reveals the physical and chemical nature of a single atmospheric particle. Because it is tremendously time consuming and expensive, however, and because suitable standards are lacking, it is very hard to obtain good-quality quantitative data, although this situation is gradually improving owing to the commercial use of aerosol time-of-flight mass spectrometry (ATOFMS) in a limited series of field studies.

Here, dust particle changes that occur during transport in the atmosphere, caused by the formation of sulfate, nitrate, and chloride and by adherence of sea salt, are summarized, and their effects on the properties and fate of the dust particles are examined. In addition, important gaps in our knowledge and current topics of study relevant to individual particle analysis, as well as the potential subsequent environmental effects, are briefly described.

2. Sulfate, nitrate, and chloride formation

The formation of particulate sulfate and nitrate is substantially enhanced by the presence of dust particles in the atmosphere. Observations of Asian dust made at different sites, from dust source areas to remote marine areas, have shown that as the distance traveled by a dust plume increases, the number of sulfate- and nitrate-containing particles also increases. Furthermore, the formation of such compounds is much more efficient in the marine atmosphere than in the continental atmosphere, an effect that can be attributed to the greater humidity in the marine atmosphere. Although mineral dust containing substantial sulfate and/or nitrate has been reported in the urban atmosphere of Chinese cities, the weather conditions and records obtained at the time of sample collection indicate that these mineral particles were probably not from desert areas; more likely they derived from areas with active anthropogenic emissions such as road dust and coal burning emissions.

Moreover, the uptake of sulfate and nitrate by dust particles depends on the particle mineralogy; nitrate accumulation is more likely on calcium-rich particles, and sulfates tend to accumulate on aluminosilicate-rich dust. Further, the formation of nitrate on mineral particles relates mainly to their calcium carbonate content rather than to their silicon dioxide content.

The formation of sulfate on dust particles does not increase their hygroscopicity, whereas nitrate formation can remarkably increase particle hygroscopicity. The presence of nitrate on dust particles can also change the particles from hydrophobic to hydrophilic when the relative humidity is less than 30%, as shown by both laboratory studies and field measurements. Thus, the formation of nitrate on dust particles might increase their potential to act as cloud condensation nuclei (CCN) to produce cloud droplets.

A series of observations, for example, by ATOFMS, has provided evidence of hydrogen chloride (HCl) formation and deposition on dust particles in the marine atmosphere. HCl is a secondary acid released from sea salt by substitution reactions.

Ongoing analyses have shown that, in the absence of substantial sulfate and nitrate (i.e., in air masses less polluted by anthropogenic emissions), the effects of chloride formation on dust particles are likely important. Chloride on dust particles can also remarkably increase their hygrosco-

picity, suggesting that the chlorine-related chemistry of dust particles might substantially increase the ability of dust particles to act as CCN at high altitudes in the marine atmosphere. In addition, a recent report indicated that dust particles coated with organic acidic materials could more efficiently act as CCN.

3. Dust particles with adhering sea salt

Mineral dust particles frequently become mixed with sea salt during their transport in the marine boundary layer, and the mixed particles differ from mineral dust in size, hygroscopicity, and other physical-chemical characteristics.

Observational data and theoretical calculations have shown that the adherence of sea salt to dust particles can substantially enhance the settling of the particles. As a result, mixed particles composed of dust and sea salt are removed from the atmosphere faster than dust particles without sea salt. Since sea salt derives from sea spray, mixed particles are mainly found in the marine atmosphere. Thus, the gravitational settling of dust particles to the sea surface is fundamentally different from the settling of particles to the ground surface from the continental atmosphere. This sea salt effect on dust settling must therefore be taken into account to correctly map dust fluxes to the ocean. Studies comparing the effects of sulfate and sea salt on dust particles have shown that sulfate and nitrate formation on dust particles influences particle settling less than sea salt.

Unfortunately, the mechanism responsible for the mixing of dust and sea salt has yet to be elucidated. Coagulation of dust particles and sea salt particles that collide as a result of Brownian motion cannot explain the observed frequency of mixed particles, suggesting that some unknown process causes dust and sea salt mixing. Mixing in clouds has been suggested, but it cannot explain observations obtained during high-pressure conditions. Small-scale turbulences in the convective unstable mixed layer probably play a very important role in determining the fate of dust particles in the marine boundary layer. Horizontal roll vortices and streaks may alter the settling process to one very different from gravitational settling and delay the removal of particles, consequently increasing the likelihood that they will mix with gaseous species and other particulate matter.

Mixed particles of mineral dust and sea salt show stronger hydrophobicity than mineral dust particles. However, this characteristic is attributed to the sea salt component of the particles, which shows very strong hygroscopicity

In addition, when sea salt becomes mixed with mineral dust it may be less likely to lose chloride ions, as a result of the deposition of acidic materials such as sulfate and nitrate on the dust. This effect is plausible because most mineral dust particles are alkaline.

4. Remaining questions and challenges

Settling dust particles have an important influence on marine ecosystems by supplying nutrients such as iron. Early integrated sample analyses have shown that the iron in dust particles is water soluble. How much and by what processes the iron in dust particles becomes bioavailable is as yet unknown. Laboratory experiments have shown that the formation of acidic sulfate and nitrate materials can transform iron from a water-insoluble to a water-soluble form, although the experimental conditions differed greatly from those in the atmosphere. Model simulations have also evaluated these integrated sample results, but evidence from single particle analysis is not yet available.

Recent studies of integrated samples have reported that during long-distance transport in the atmosphere dust particles may become mixed with compounds such as halocarbons and polycyclic aromatic hydrocarbons and these mixed particles may importantly affect Earth geochemical cycles. However, methods have not yet been developed to detect these compounds on individual particles.

Atmospheric dust dispersion may play a role in the evolution and conservation of microorganism diversity in the natural environment. Some recent studies using culturing and staining techniques coupled with bioassays have confirmed that the abundance of microorganisms increases when there are dust plumes in the ambient air. However, methods to identify the microorganisms on a single particle are not available; consequently, whether microorganisms occur on dust particles is not clear, although it seems plausible, or even, probable, that they should.

The observations and analyses were conducted mainly within the scope of a series of Sino-Japan collaborative programs under the direction of Dr. Y. Iwasaka and Dr. G. Shi. A number of previous students of Dr. Iwasaka, Dr. Shi and Dr. Zhang contributed to the studies.

Aerosol particle shape revealed by transmission electron microscopy and the implications for its optical properties

Kouji Adachi[1]

[1]Meteorological Research Institute, 1-1 Nagamine, Tsukuba, Ibaraki 305-0052, Japan

**Corresponding author. Tel.: +81 29 853 8570, Email address: adachik@mri-jma.go.jp (K. Adachi)*

Aerosol particles in the atmosphere have various shapes, and their shape greatly influences light scattering and absorption by the particles. Direct observation by electron microscopy, including transmission electron microscopy (TEM), can reveal particle shapes. Current TEM techniques can determine the two-dimensional and three-dimensional shapes and hygroscopicity of aerosol particles. Optical properties of non-spherical three-dimensional aerosol particles with multiple components can be determined by using discrete dipole approximation (DDA). Here, I show how the combination of TEM techniques and DDA calculations can be used to determine the shape and configuration, and thus the optical properties, of realistic aerosol particles.

Keywords: Aerosol particles; Transmission electron microscopy; Discrete dipole approximation; Optical properties

1. Introduction

Atmospheric aerosol particles viewed by transmission electron microscopy (TEM) show various shapes, including fractal, aggregate, cubic, plate-like, and spherical. However, Mie theory, which is commonly used to estimate the optical properties of particles (e.g., absorption, scattering, and the asymmetry parameter), assumes that the particles are spherical. Here, I show the use of a discrete dipole approximation (DDA) calculation to determine the optical properties of non-spherical particles and electron tomography to determine the three-dimensional (3D) shapes and configurations of aerosol particles. I show several examples of the optical properties of non-spherical aerosol particles.

2. Material and methods

The electron tomography and DDA methods are described in detail by Adachi et al. (2010: Ref. 1) .

3. Results and discussion

3.1. Soot particle shape and configuration

Soot particles commonly have a fractal shape and are mixed with other particles. The amount of light absorption by a soot particle depends on its 3D shape and configuration. Adachi et al. (2010: Ref. 1) showed the effects of coatings on soot particles and particle configuration by simulating different particle shapes and coatings. Here, I describe how soot particle shape and configuration affect light absorption.

Coating enhances light absorption by soot particles [2] via a lens effect (Figure 1). Because of refraction of light within the coating, more light is focused on a coated soot particle than on one without coating.

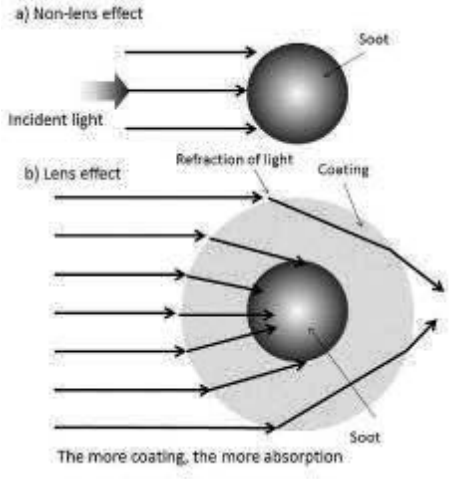

Figure 1 Schematic model of the lens effect. Light absorption by a) non-coated and b) coated soot particle.

The position of the soot within the coating determines the amount of light absorption [3]. Light tends to be focused on the center of the entire particles in the size range of ambient aerosol particles. Thus, when soot particles are centered within the coating, they absorb more light than when they are closer to one edge (Figure 2).

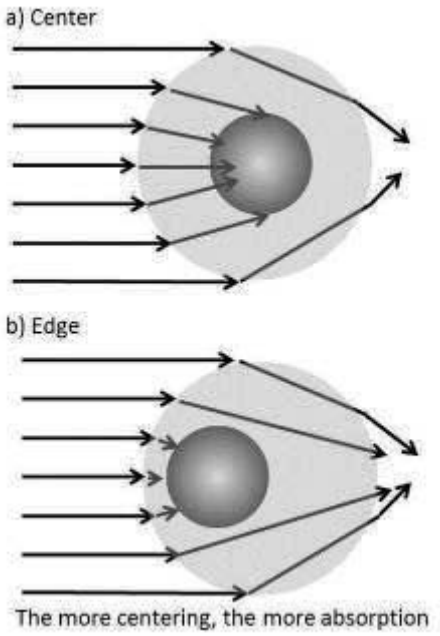

Figure 2 Schematic diagram of the position effect. Soot a) centered within and b) near the edge of the coating.

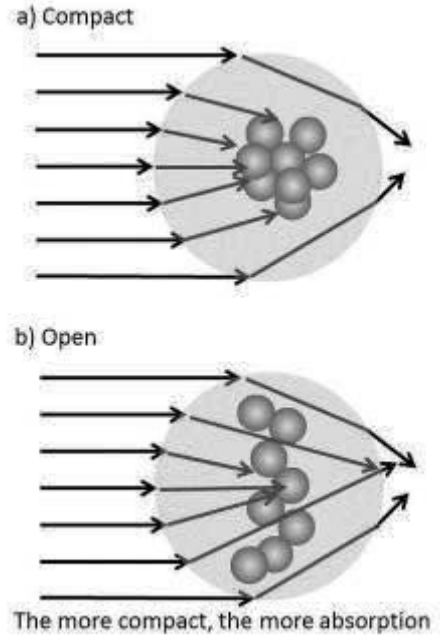

Figure 3 Schematic diagram of the soot shape effect. a) Compacted soot (high fractal dimension) and b) uncompacted soot (low fractal dimension).

Particle shape, that is, the degree of compaction, also affects absorption. Light absorption by a spherical soot particle depends on the particle size and the light wavelength. Light with a wavelength of 550 nm is efficiently absorbed by soot particles ~100 to 200 nm in diameter. Compacted soot has an apparent size within this range. When it is uncompacted, its apparent size is almost the same as that of the primary particles composing the soot, ~50 nm, and it does not absorb light efficiently.

3.2. Hygroscopic aerosol particles

Hygroscopic aerosol particles change their shape depending on the ambient relative humidity (RH); thus, changes in RH can increase or decrease the light scattering by the particles. An environmental TEM (ETEM) system, by controlling RH, can measure these shape changes, and then their shapes can be used determine the light scattering by the particles. Because particles change their shape and size after deliquescence, the scattering is different from that estimated by Mie theory [4, 5].

4. Summary

Particle shapes vary depending on the sampling location and time and RH. As a result, light scattering and absorption by particles will be increased or decreased compared with that determined by assuming a simple spherical model. Thus, particle shape needs to be considered by climate models.

I thank Peter R. Buseck (Arizona State University) and Yasuhito Igarashi (MRI) for supporting this research. I acknowledge the use of TEM facilities within the LeRoy Eyring Center for Solid State Science at Arizona State University.

1 Adachi, K., S. H. Chung and P. R. Buseck, 2010: Shapes of soot aerosol particles and implications for their effects on climate, *J. Geophys. Res.*, **115**, D15206.
2 Bond, T. C., G. Habib and R. W. Bergstrom, 2006: Limitations in the enhancement of visible light absorption due to mixing state, *J. Geophys. Res.*, **111**, D20211, doi: 10.1029/2006JD007315.
3 Fuller, K. A., W. C. Malm and S. M. Kreidenweis, 1999: Effects of mixing on extinction by carbonaceous particles, *J. Geophys. Res.*, **104**, 15,941–15,954.
4 Adachi, K., E. Freney and P. R. Buseck, 2011: shapes of internally mixed hygroscopic aerosol particles after deliquescence, and their effect on light scattering, *Geophys. Res. Let.*, **38**, L13804.
5 Freney, E., K. Adachi, and P. R. Buseck, 2010: Internally mixed atmospheric aerosol particles: Hygroscopic growth and light scattering, *J. Geophys. Res.*, **115**.

Internal mixtures of diesel nanoparticles investigated by FIB-SIMS microscopy

Yuji Fujitani[1,*], Tetsuo Sakamoto[2] and Kentaro Misawa[3]

[1]National Institute for Environmental Studies, 16-2 Onogawa, Tsukuba, Ibaraki 305-8506, Japan
[2]Kogakuin University, 2665-1 Nakanocho, Hachioji, Tokyo 192-0015, Japan
[3]Tokyo Institute of Technology, 4259 Nagatsuta-cho, Midori-ku, Yokohama, Kanagawa 226-8503, Japan

Corresponding author. Tel.: +81 29 850 2014; Fax: +81 29 850 2014, Email address: fujitani.yuji@nies.go.jp (Y. Fujitani)

Information about the physicochemical properties of particles composed of internal mixtures of inorganic and organic materials is necessary to predict particle fate after deposition in the lung and to assess particle toxicity. To measure internal mixtures of inorganic and organic materials in diesel exhaust nanoparticles, we applied a scanning electron microscopy technique, in which Ga-focused ion beam-secondary ion mass spectrometry (FIB-SIMS) is coupled with laser ionization, for observation of diesel particles. We collected particles, generated by an engine operating under no-torque conditions, with aerodynamic diameters of 100–630 nm (subdivided into four size fractions) and with mobility diameters of 30, 50, and 100 nm. By using FIB-SIMS observations, we classified the particles into seven types according to their physical size and chemical composition.

Keywords: Nanoparticle; Ultrafine particle; FIB-SIMS; Imaging; Laser ionization

1. Introduction

Particles, especially insoluble and ultrafine particles (diameter < 100 nm), deposited in the human alveoli are thought to penetrate the cell membrane and enter the bloodstream to be transported to other organs [1, 2]. The adverse health effects due to such insoluble nanoparticles may depend on their chemical composition and shape, as well as on the dose received (number and surface area of the particles). In contrast, the adverse health effects of soluble nanoparticles may depend primarily on their chemical composition and the dose. Thus, the physicochemical properties of nanoparticles, including internal mixtures of inorganic and organic materials, need to be known to predict the toxicity and likely fates of particles after deposition in the lung. Particle fate depends on its solubility in the lung fluid, which in turns depends the particle's composition and how the components are mixed.

In this study, we applied a scanning electron microscopy technique, in which ion beam-secondary ion mass spectrometry (FIB-SIMS) to measure the internal mixture of inorganic and organic materials in diesel exhaust particles and nanoparticles.

2. Methods

An apparatus consisting of a scanning electron microscope and a focused ion beam secondary ion mass spectrometer [3] was used to measure the internal mixture of inorganic and organic material in diesel exhaust nanoparticles. A gallium liquid metal ion source (^{69}Ga and ^{71}Ga mixture) was used for the FIB. Resonance enhanced multi-photon ionization was used for the detection of organic species. Image resolution of up to 50 nm was achieved. Particle morphology was also observed by transmission electron microscopy (TEM; JEM-2010, JEOL).

An 8-L diesel engine (1997 emission regulations) that was not fitted with any after-treatment devices in the Nanoparticle Health Effect Laboratory, National Institute for Environmental Studies [4], was used to generate diesel exhaust particles. The engine was operated at a steady state of 2000 rpm and 0 Nm. Low-sulfur diesel fuel (JIS No. 2 light oil, available and generally used in Japan) and lubricant oil (E Pro Extra 10W-30, Hino) were used. The exhaust was introduced into a primary dilution tunnel and diluted with particle-free clean air with a dilution ratio of about 10 times.

Particles were collected in a size-resolved manner because the depositional area after inhalation is a function of the particle aerodynamic diameter or diffusive equivalent diameter [5], not the physical particle size. Size-resolved particles (aerodynamic diameter, D_{ae} = 100–630 nm, divided into four size fractions) were collected on a silicon wafer by a low-pressure impactor (DLPI, Dekati) in the primary

dilution tunnel. The sample flow rate was 10 L min^{-1} and the sampling duration depended on the targeted size fraction, because particle number concentrations differ according to the size fraction and the particles collected on the silicon wafer in the microscope were required not to overlap. Particles smaller than 100 nm are likely to overlap on the impaction plate because of their high number concentration; therefore, we used a differential mobility analyzer (DMA) and electrical precipitator to distribute the sample evenly on the silicon wafer. Particles with a mobility diameter (D_m) of 30, 50, and 100 nm were collected on the silicon wafer or on collodion membrane-coated copper grids with an electrical precipitator operated at 9 kV after passing through the DMA (SIBATA) with a sheath flow rate of 24 L min^{-1} and a sample flow rate of 2.4 L min^{-1}. The aerodynamic diameter and electrical mobility diameter were equivalent, as shown by the mass size distribution determined by DLPI measurement and the volume size distribution determined by a scanning mobility particle sizer (3034, TSI), in the primary dilution tunnel during sampling. Therefore, we considered there to be no systematic difference between particles >100 nm and <100 nm obtained by the different sampling methods.

3. Results and discussion

Three kinds of physical particles were detected as having D_{ae} = 100–630 nm for each size fraction: agglomerated particles a few micrometers in diameter, oily spot, and smaller particles with a diameter similar to their D_{ae}. Agglomerated particles were apparently soot particles; clusters of ions (C_3, C_4, C_5, C_6), detecting mainly of elemental carbon, were detected. Further, their surface seemed to be coated with an oily substance, because they suddenly shrank when exposed to FIB irradiation. Ca and carbon were detected in the oily spots, indicating that oil mist particle is derived from lubricant oil (Figure 1). The smaller particles consisted mainly of Ca and Cl (Figure 1), or they corresponded to oxidized particles containing Na and K. Carbonaceous particles were also detected without Na or K. We classified the particles with D_{ae} = 100–630 nm into five types according to their physical size and chemical composition. TEM observation indicated that the number of primary particles (about 10 nm) increased as the particle size increased (Figure 2). FIB-SIMS observation showed that particles with D_m = 30–100 nm were of two types, oil mist particles and carbon particles covered with fluorine.

To simulate particle fate after deposition in the lung, the soot particles were exposed to micro mist of acetone generated by electrical spray. FIB-SIMS observation showed that after exposure, the aliphatic hydrocarbons on the soot particle dissolved and dispersed around particle, creating many small particles from the soot particle fragments. From this we infer that after deposition in the alveoli agglomerated particles become disagglomerated in the alveolar lining. Smaller particles can more easily penetrate the cell membrane and enter the bloodstream, to be transported to other organs. Thus, the fate of these particles after deposition in the lung can be predicted from our data.

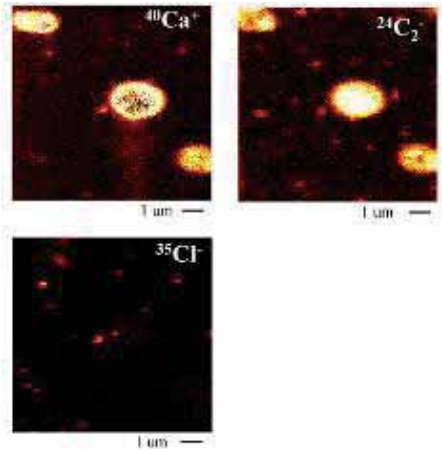

Figure 1 Elemental mapping of Ca^+, C_2^-, and Cl^{-1} for particles of D_{ae} = 390–630 nm

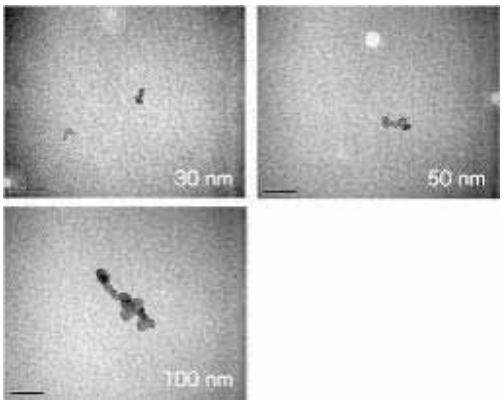

Figure 2 TEM images of particles with D_m = 30, 50, and 100 nm. Scale bar is 100 nm.

This research was supported by the Environment Research and Technology Development Fund (C-1002) of the Ministry of the Environment, Japan.

1 Takenaka, S., E. Karg, C. Roth, H. Schulz, A. Ziesenis, U. Heinzmann, P. Schramel and J. Heyder, 2001: Pulmonary and systemic distribution of inhaled ultrafine silver particles in rats. *Environ. Health Per.,* **109**,547–551

2 Oberdorster, G., Z. Sharp, V. Atudorei, A. Elder, R. Gelein, A. Lunts, W. Kreyling and C. Cox, 2002: Extrapulmonary translocation of ultrafine carbon particles following whole-body inhalation exposure of rats. *J. Toxicol. Env. Heal. A,* **65**,1,531–1,543

3 Sakamoto, T., M. Koizumi, J. Kawasaki and J. Yamaguchi, 2008: Development of a High Lateral Resolution TOF-SIMS Apparatus for Single Particle Analysis. *Applied Surface Science,* **255**, 1,617-1,620

4 Fujitani, Y., S. Hirano, S. Kobayashi, K. Tanabe, A. Suzuki, A. Furuyama and T. Kobayashi, 2009: Characterization of Dilution Conditions for Diesel Nanoparticle Inhalation Studies. *Inhal Toxicol*, **21**: 200-209

5 ICRP, Human Respiratory Tract Model for Radiological Protection. *ICRP Publication,* 66, Pergamon Press, Oxford.

Modeling atmospheric transport of fine particulate matter with WRF/CMAQ in the Kanto region in summer 2007

Hikari Shimadera[1,*], Hiroshi Hayami[1], Yu Morino[2], Toshimasa Ohara[2], Satoru Chatani[3] and Naoki Kaneyasu[4]

[1]Central Research Institute of Electric Power Industry, 1646 Abiko, Abiko, Chiba 270-1194, Japan
[2]National Institute for Environmental Studies, 16-2 Onogawa, Tsukuba, Ibaraki 305-8506, Japan
[3]Toyota Central R&D Labs., Inc., Nagakute-cho, Aichi-gun, Aichi 480-1192, Japan
[4]National Institute of Advanced Industrial Science and Technology, 16-1 Onogawa, Tsukuba, Ibaraki 305-8569, Japan

Corresponding author. Tel.: + 81 4 7182 1181; Fax: +81 4 7183 2966, Email address: simadera@criepi.denken.or.jp (H. Shimadera)

The Community Multiscale Air Quality model was used to analyze atmospheric transport of elemental carbon (EC) and sulfate (SO_4^{2-}) in the Kanto region of Japan in summer 2007. Although the model captured well the long-range transport of EC from the Asian continent, the simulation results indicated that local emissions dominantly contributed to EC concentrations in urban parts of the Kanto region. The model also approximately captured the concentration of SO_4^{2-} and its temporal variation in the region. The simulation results indicated that both domestic emissions in Japan and long-range transport from the Asian continent contribute to SO_4^{2-} concentrations in the Kanto region. When a Pacific high-pressure system covered the Kanto region, local circulation was well developed and consequently domestic emissions, including volcanic emissions, were the dominant contributors, whereas when a high-pressure system prevailed over the East China Sea and low-pressure systems passed north of Japan, synoptic-scale winds associated with this pressure pattern transported large amounts of SO_4^{2-} from the Asian continent to the Kanto region. In addition, although heavy precipitation decreased SO_4^{2-} concentrations near the center of a typhoon, peripheral typhoon winds occasionally played an important role in the long-range transport of SO_4^{2-} from the Asian continent to the Kanto region.

Keywords: $PM_{2.5}$; Air quality model; Sulfate; Elemental carbon; Long-range transport

1. Introduction

Fine particulate matter ($PM_{2.5}$) has several major components, including elemental carbon (EC) and sulfate (SO_4^{2-}). $PM_{2.5}$ has been of increasing concern because it can seriously affect human health. The Ministry of the Environment of Japan established an air quality standard for $PM_{2.5}$ in 2009. Although $PM_{2.5}$ concentrations have decreased in recent years in Japan, the standard for $PM_{2.5}$ is seldom attained in most urban areas. Therefore, better understanding of $PM_{2.5}$ behavior in the atmosphere is required so that measures to attain the standard can be developed.

In this study, the Community Multiscale Air Quality model (CMAQ) [1] driven with meteorological fields produced by the Weather Research and Forecasting model (WRF) [2] was applied to the Kanto region of Japan in summer 2007. In summer, a Pacific high-pressure system often covers Honshu, the main island of Japan. Under this condition, local circulation is well developed and long-range transport is likely to be of small importance. However, Aikawa et al. (2010: Ref. 3) showed that long-range transport of SO_4^{2-} from the Asian continent contributes importantly to air quality in Japan even in summer. In Japan, summer is also the typhoon season and the heavy precipitation and strong winds associated with typhoons can also affect air quality. The present study analyzed summertime atmospheric transport of EC and SO_4^{2-} in $PM_{2.5}$.

2. Methods

The Advanced Research WRF version 3.2.1 and CMAQ version 4.7.1 were used. The WRF/CMAQ modeling system was run for July and August 2007 with three nested modeling domains, from domain 1, covering a wide area of East Asia, to domain 3, covering most of the Kanto region. Mesoscale and regional-scale objective analysis data of the Japan Meteorological Agency and the final analysis data of the U.S. National Centers for Environmental Prediction

were used for initial and boundary conditions and grid nudging in the WRF simulation. Initial and boundary conditions for the CMAQ simulation were obtained from the Model for Ozone and Related Chemical Tracers version 4 [4]. Emission data were derived from Ohara et al. (2007: Ref. 5) and Zhang et al. (2009: Ref. 6), and estimated by the method described by Chatani et al. (2011: Ref. 7). The CMAQ simulations were conducted for two cases: a baseline simulation case (CB), and a case in which EC and sulfur compound emissions outside Japan and their domain 1 boundary concentrations were set to 0 (CJ).

3. Results and discussion

The simulated EC concentration of CB agreed with the observed black carbon (BC) concentration at the Chichi-Jima Island (about 1000 km south of the center of Tokyo; Figure 1). This result indicates that the model reproduced well the long-range atmospheric transport of EC. It also captured well the temporal variations of EC and SO_4^{2-} concentrations at Komae (about 10 km southwest of the center of Tokyo; Figures 2 and 3). The EC concentration of CB was slightly higher than but similar to that of CJ, indicating that local emissions dominantly contributed to the EC concentration in urban areas of the Kanto region. The differences in the SO_4^{2-} concentrations between CB and CJ indicate that long-range transport from the other countries contributed substantially to SO_4^{2-} concentrations in the Kanto region even in summer. On 15 July, heavy precipitation associated with typhoon 0704 Man-Yi decreased the SO_4^{2-} concentration. On 20 July, the typhoon and the low-pressure system that succeeded it transported EC from the Yellow Sea coastal area to the Chichi-Jima Island, and a volcanic plume from the Miyake-Jima Island increased the SO_4^{2-} concentration at Komae. During 26–29 July and 25–28 August, a high-pressure system prevailed over the East China Sea and low-pressure systems passed north of Japan. Under this typical summertime pressure pattern, the associated synoptic-scale winds transported large amounts of SO_4^{2-} from the Yellow Sea coastal area to Japan. From 31 July to 5 August, peripheral winds of typhoon 0705 USAGI controlled the SO_4^{2-} concentration in the Kanto region by transporting a polluted air mass from the Asian continent and a clean air mass from the Pacific Ocean. After the passage of the typhoon, a Pacific high-pressure system often covered the Kanto region. Under this very typical summer pressure pattern, local sea and land breezes were well developed and the region tended to be less affected by Asian continental outflow. On 21 August, the local circulation accumulated local air pollutants and volcanic gases from Miyake-Jima, and caused high SO_4^{2-} concentrations at Komae.

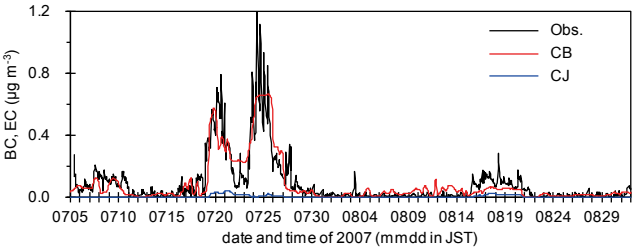

Figure 1 Hourly time series of observed BC and simulated EC concentrations at Chichi-jima.

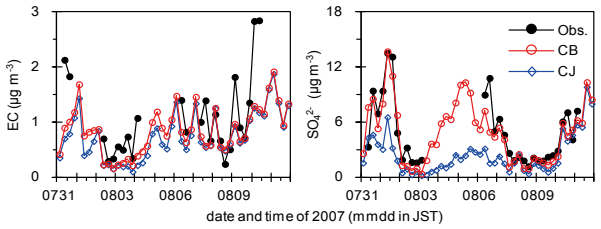

Figure 2 Time series of observed and simulated 6-hour EC and SO_4^{2-} concentrations at Komae.

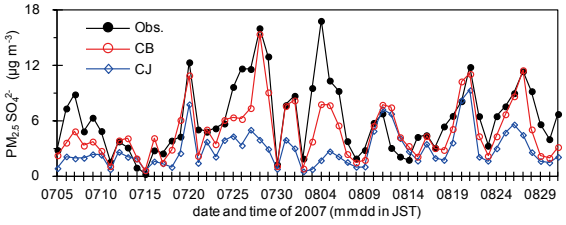

Figure 3 Time series of the observed and simulated daily SO_4^{2-} concentrations at Komae.

This research was supported by the Environment Research and Technology Development Fund (C-1001) of the Ministry of the Environment, Japan.

1 Byun, D. W. and J. K. S. Ching,1999: Science Algorithms of the EPA Models-3 Community Multi-scale Air Quality (CMAQ) Modeling System. NERL, Research Triangle Park, NC.

2 Skamarock, W. C., J.B. Klemp, J. Dudhia, et al. 2008: A description of the advanced research WRF version 3. NCAR Technical Note, NCAR/TN-475+STR.

3 Aikawa, M., T. Ohara, T. Hiraki, et al. 2010: Significant geographic gradients in particulate sulfate over Japan determined from multiple-site measurements and a chemical transport model: Impacts of transboundary pollution from the *Asian continent. Atmos Environ,* **44**, 381–391

4 Emmons, L K., S. Walters, P. G. Hess, et al. 2010: Description and evaluation of the Model for Ozone and Related chemical Tracers, version 4 (MOZART-4). *Geosci Mod Dev*, **3**, 43–67.

5 Ohara, T., H. Akimoto, J. Kurokawa, et al. 2007: An Asian emission inventory of anthropogenic emission sources for the period 1980-2020. *Atmos Chem Phys*, **7**, 4,419–4,444.

6 Zhang, Q., D. G. Streets, G. R. Carmichael, et al. 2009: Asian emissions in 2006 for the NASA INTEX-B mission. *Atmos Chem Phys,* **9**, 5,131–5,153

7 Chatani, S., T. Morikawa, S. Nakatsuka, et al.2011: Development of a framework for a high-resolution, three-dimensional regional air quality simulation and its application to predicting future air quality over Japan. *Atmos Environ,* **45**, 1,383–1,393

Treatment of black carbon by a global climate model and the potential contribution of electron microscopy

Daisuke Goto[1*], Naga Oshima[2], Teruyuki Nakajima[3] and Toshihiko Takemura[4]

[1]National Institute for Environmental Studies, 16-2 Onogawa, Tsukuba, Ibaraki 305-8506, Japan
[2]Meteorological Research Institute, 1-1 Nagamine, Tsukuba, Ibaraki 305-0052, Japan
[3]Atmosphere and Ocean Research Institute, University of Tokyo, 5-1-5 Kashiwanoha, Kashiwa, Chiba 277-8568, Japan
[4]Research Institute for Applied Mechanics, Kyusyu University, 6-1 Kasuga-koen, Kasuga, Fukuoka 816-8580, Japan

Corresponding author. Tel.: +81 29 850 2899; fax: +81 29 850 2580, Email address: goto.daisuke@nies.go.jp (D. Goto)

Black carbon (BC) is the most strongly light-absorbing component of aerosols, and the accurate simulation of BC-containing aerosols is required to properly predict aerosol radiative forcing (ARF) and climate change. Different global climate models differently treat categories of BC-containing aerosols and their behaviors in the atmosphere. In this study, we implemented newly parameterized BC aging processes depending on sulfuric acid, BC, and total aerosols into a global three-dimensional aerosol transport–radiation model, SPRINTARS. ARF as predicted by the traditional aging process and a new process differed from that calculated by the original SPRINTARS by about 0.30 Wm^{-2}, a value comparable to the uncertainty suggested by international model intercomparison (AeroCom) results.

Keywords: Black carbon (BC); BC Aging process; Global aerosol model; BC radiative forcing

1. Introduction

Black carbon (BC) aerosol particles strongly absorb shortwave radiation and thus influence radiative perturbation more strongly than other aerosol components [1-3]. Estimates of the direct radiative impacts of an aerosol due to BC derived from fossil fuel and biomass burning still include large uncertainty, with positive forcings of +0.20 ± 0.15 and +0.03 ± 0.12 W m^{-2}, respectively [3]. The uncertainty of the BC radiative effects may reflect uncertainties in both the spatial distribution of BC, which depends on various atmospheric processes such as emission, transport, chemical transposition (BC aging), and deposition processes [4-7], and BC optical properties [8]. Among general circulation models (GCMs) and models included in the AeroCom model intercomparison project, differences in the BC aging process are large (Table 1). Most aerosol climate models still use parameterization to simplify the BC aging process.

Therefore, in this study, we investigated how differences in the treatment of the BC aging process affected the BC spatial distribution and thus BC radiative forcing. For this purpose, we performed numerical experiments with SPRINTARS, a global aerosol transport–radiation model [9-13], which also is a participant in the AeroCom project, using three different types of treatment for BC aging processes: (1) the original SPRINTARS method (ORIG); (2) the traditional method, which uses a constant aging timescale with e-fold lifetime (τBC) through coagulation and condensation and is widely used in global models (AGF); (3) a method similar to AGF but using a variable τBC value that is calculated online by a new parameterization of BC aerosols based on a spectral-binning method (AGV) [14].

Table 1 Summary of BC aging processes used in global models

Name[a]	Method[b]	Time scale of BC aging[c]	Computer cost[d]
UMI	None	Zero (No aging)	---
UIO_CTM	Param.	Const.	Light
LOA	Param.	Const.	Light
LSCE	Param.	Const.	Light
MPI_HAM	Explicit	Var.	Heavy
GISS	Param.	Const.	Light
UIO_GCM	Explicit	Var.	Heavy
SPRINTARS	Param.	Zero[e]	Light
ULAQ	Param.	Const.	Light
GOCART	Param.	Const.	Light

[a] Model name as shown in the AeroCom project [4]
[b] Param., parameterization; Explicit, explicit expression
[c] Zero, no decay; Const., constant timescale of decay; Var., variable timescale of decay
[d] CPU time required to calculate the process
[e] See section 2

2. Methods

2.1. Global aerosol radiation model (SPRINTARS)

We implemented three different BC aging processes in a global three-dimensional aerosol transport-radiation model, the Spectral Radiation-Transport Model for Aerosol Species (SPRINTARS) [9-13, 15, 16]. SPRINTARS has been implemented within an atmospheric GCM developed by the former Center for Climate System Research (now Atmosphere and Ocean Research Institute) of the University of Tokyo, National Institute for Environmental Studies, and the Frontier Research Center for Global Change, and used for climate modeling [17]. The model has also been implemented within a radiation scheme called MSTRN-8 [18, 19]. SPRINTARS calculates the mass mixing ratios of the main tropospheric aerosols, namely, carbonaceous aerosols, including water-soluble BC (WSBC), water-insoluble BC (WIBC), and organic particles (OC); sulfate, soil dust, sea salt, and the precursor gases of sulfate (SO_2 and dimethyl sulfide). SPRINTARS considers atmospheric processes, including emission, advection, diffusion, sulfur chemistry, deposition, and gravitational settling. We used emission inventories and nudging conditions described previously [10, 15]. The spatial and vertical resolutions were set to T42 (i.e., 2.8° × 2.8° horizontally and 20 vertical layers).

2.2. Treatment of BC

The three ways of treating BC aging processes implemented in SPRINTARS are shown schematically in Figure 1.

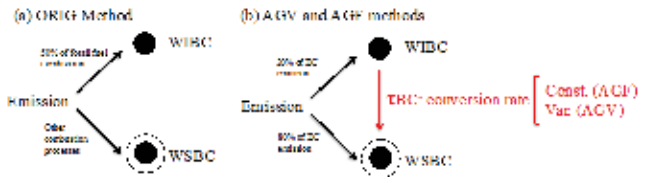

Figure 1 Schematic diagram of the three BC aging processes implemented.

2.2.1. Original method (ORIG)

In ORIG, WIBC is not converted to WSBC; that is, it is assumed that no BC aging occurs in the atmosphere. BC aerosols are categorized into three types: pure BC (i.e., WIBC) and two types of WSBC (BC/OC = 6.67 or 3.33). In the original SPRINTARS, the partitioning ratio of WSBC into each mode is diagnosed by the fractions of WSBC and OC in one grid cell of the GCM. Therefore, ORIG treats three carbonaceous tracers: OC, WSBC, and WIBC. In ORIG, half of the BC emitted by fossil fuel combustion is assumed to be externally mixed with other species (i.e., WIBC), whereas the BC from biomass burning, agricultural activities, and biofuel combustion is considered to become internally mixed with OC (i.e., WSBC) within one time step (about 20 min) of the GCM in one grid cell (about 300 km by 300 km).

2.2.2. AGV and AGF

In AGV and AGF, BC aging in the atmosphere is expressed by the conversion timescale with e-fold lifetime, τBC, from WIBC to WSBC. The change in WIBC in time t can be expressed in terms of τBC as follows:

$$[WIBC](t) = [WIBC](t-1) + [WIBC](t-1) \times \exp(-t/\tau BC), \quad (1)$$

$$[WSBC](t) = [WSBC](t-1) - [WIBC](t-1) \times \exp(-t/\tau BC), \quad (2)$$

where [WIBC] and [WSBC] are the concentrations of WIBC and WSBC, respectively. In AGF the τBC value is generally fixed at 1 to 1.2 days (see section 1) [20, 21]. In AGV, however, τBC is allowed to vary, depending on the number concentration of the particles to be aged and the concentrations of condensed gases. In this method, we used a new parameterization of τBC that takes into account the dependence of the aging process on various conditions. This parameterization was developed by Liu et al. [5], who used a detailed physics-based aerosol mixing state-resolved box model for the purpose [22, 23]. However, this parameterization only addresses the growth of BC by condensation, and ignores other BC aging processes (e.g., by coagulation). Therefore, we set the maximum τBC to 20 days following [7].

3. Results

We compared three methods using the horizontal distribution of the annually averaged BC mass concentration at the surface (Figure 2). We found that the difference in the calculated BC mass concentration among the three methods was at most 10% near aerosol sources and at most 50% over remote areas (Figures 2b and 2c). The differences among the methods near aerosol source regions such as North America exceeded the differences between the simulations and the observations (not shown). Therefore, these differences may reflect mainly the uncertainty of the BC emission inventory.

We also compared the annually averaged ratio of WIBC to total BC (WIBC + WSBC) (hereafter, the WIBC ratio) at the surface with that at the sigma 0.5 level (Figure 3). In ORIG, the WIBC ratio at the surface ranged from 10% to 30% over the BC source regions (United States, Europe, China, and India) and were smaller over oceans (from 30% to 40%), because the WIBC particles, which are inefficiently removed by rainout during precipitation events, do not age in ORIG but remain in the atmosphere, whereas WSBC particles are efficiently removed. In contrast, in both AGF and AGV, the WIBC ratios at the surface over most land areas become much larger than those over oceans. In AGV, the WIBC ratios are larger than those in AGF over most of the world, because the magnitude of the conversion timescale is smaller in AGV than in AGF. As a result,

WIBC ages more rapidly in AGF than in AGV and more is scavenged by wet deposition. Therefore, the contrast in the WIBC ratio between land and ocean in ORIG is very different from that in both AGV and AGF. Theoretically, the WIBC ratio tends to be higher over BC source regions (land) than over outflow regions (ocean), because the amount of BC that is aged by condensation of gases or other aerosols is in proportion to the amount of time the BC particles remain suspended in the atmosphere [24-27].

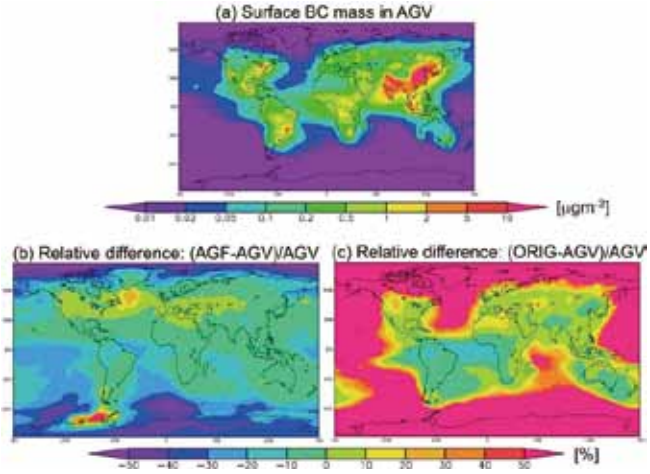

Figure 2 Global distributions of annually averaged (a) surface BC mass concentrations obtained by the AGV method, and the relative differences in BC mass concentrations (b) between AGF and AGV and (c) between ORIG and AGV.

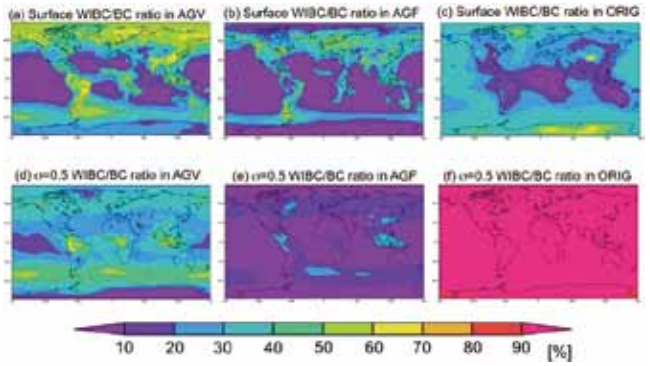

Figure 3 Annual mean ratio of WIBC to total BC at the surface and at the sigma 0.5 level.

These differences in the WSBC ratio among the methods result in differences in the absorption aerosol optical thickness (AAOT) (Figure 4). The AAOT values in AGV tend to be larger than those in the other two methods, especially over biomass burning regions. This difference can be explained in part by the gap in AAOT between simulation and observation [4].

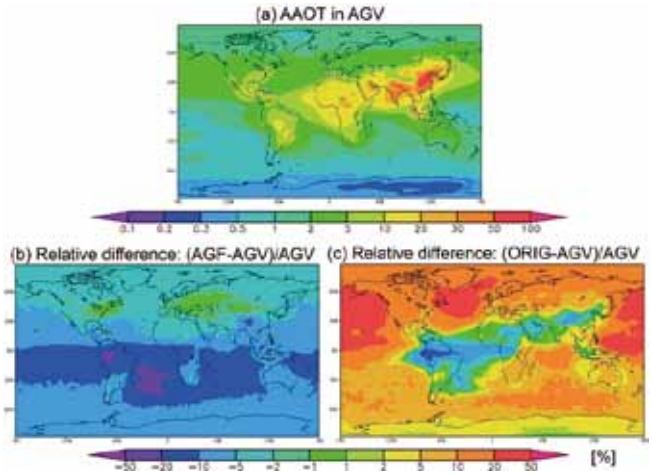

Figure 4 Global distribution of annually averaged (a) AAOT obtained by the AGV method and the relative differences in AAOT (b) between AGF and AGV and (c) between ORIG and AGV.

Finally, we estimated aerosol radiative forcing caused by the aerosol direct effect due to anthropogenic BC to be +0.300 Wm^{-2} (AGV), +0.047 Wm^{-2} (AGF), and +0.356 Wm^{-2} (ORIG). Thus, AGF tended to underestimate the amount of aerosol light absorption compared with the other methods (AGV and ORIG).

4. Conclusions

Differences in the treatment of BC aging in aerosol modeling studies can cause differences of up to about 0.3 Wm^{-2} in the aerosol radiative forcing due to BC. This value is comparable to the uncertainty suggested by AeroCom results. Therefore, this problem needs to be addressed further by obtaining new information from field measurements and in situ experiments. In this regard, electron microscopy could contribute to global modeling by providing microphysical information, for example, the fraction of BC-containing particles relative to total atmospheric particles and the proportion of BC in BC-containing particles.

Some of the authors received support from MEXT/RECCA/SALSA, JAXA/EarthCARE, MEXT/VL for Climate System Diagnostics, MOE/Global Environment Research Fund B-0803 and A-1101, NIES/GOSAT, or NIES/CGER (NEC SX-8R). We acknowledge the PIs and their staff for IMPROVE, EMEP, and AERONET, many researchers for the NCAR/NCEP reanalysis and HadISST data, and the developers of the MIROC and SPRINTARS models.

1 Hansen, J., M. Sato and R. Ruedy, 1997: Radiative forcing and climate response, *J. Geophys. Res.*, **102**, D6, 6,831-6,864.
2 Jacobson, M. Z., 2002: Control of fossil-fuel particulate black carbon and organic matter possibly the most effective method of slowing global warming, *J. Geophys. Res.*, **107**(D19), 4,410, doi: 10.1029/2001JD001376.
3 Forster, P., V. Ramaswamy, P. Artaxo, T. Berntsen, R. Betts, D. W. Fahey, J. Haywood, J. Lean, D. C. Lowe, G. Myhre, J. Nganga, R. Prinn, G. Raga, M. Schulz and R. Van Dorland, 2007: Changes in Atmospheric

Constituents and in Radiative Forcing. In: Climate Change 2007: The Physical Science Basis. Contribution of Working Group I to the Fourth Assessment Report of the Intergovernmental Panel on Climate Change (Solomon, S. et al. (eds.). Cambridge University Press, Cambridge, United Kingdom and New York, NY, USA.

4 Koch, D., M. Schulz, S. Kinne, C. McNaughton, J. R. Spackman, Y. Balkanski, S. Bauer, T. Berntsen, T. C. Bond, O. Boucher, M. Chin, A. Clarke, N. De Luca, F. Dentener, T. Diehl, O. Dubovik, R. Easter, D. W. Farey, J. Feichter, D. Fillmore, S. Freitag, S. Ghan, P. Ginoux, S. Gong, L. Horowitz, T. Iversen, A. Kirkevåg, Z. Klimont, Y. Kondo, M. Krol, X. Liu, R. Miller, V. Montanaro, N. Moteki, G. Myhre, J. E. Penner, J. Perlwitz, G. Pitari, S. Reddy, L. Sahu, H. Sakamoto, G. Schuster, J. P. Schwarz, Ø. Seland, P. Stier, N. Takegawa, T. Takemura, C. Textor, J. A. van Aardenne and Y. Zhao, 2009: Evaluation of black carbon estimations in global aerosol models. *Atmos. Chem. Phys.*, **9**, 9,001-9,026.

5 Liu, J. F., S. M. Fan, L. W. Horoqitz and H. Levy II, 2011: Evaluation of factors controlling long-range transport of black carbon to the Arctic, *J. Geophys. Res.*, **116**, D04307, doi: 10.1029/2010JD015145.

6 Schulz, M., C. Textor, S. Kinne, Y. Balkanski, S. Bauer, T. Bertsen, T. Berglen, O. Boucher, F. Dentener, S. Guibert, I. S. A. Isaksen, T. Iversen, D. Koch, A. Kirkevag, X. Liu, V. Montanaro, G. Myhre, J. E. Penner, G. Pitari, S. Reddy, O. Seland, P. Stier and T. Takemura, 2006: Radiative forcing by aerosols as derived from the AeroCom present-day and pre-industrial simulations, *Atmos. Chem, Phys.*, **6**, 5,225-5,246.

7 Shindell, D. T., M. Chin, F. Dentener, R. M. Doherty, G. Faluvegi, A. M. Fiore, P. Hess, D. M. Koch, I. A. MacKenzie, M. G. Sanderson, M. G. Schultz, M. Schulz, D. S. Stevenson, H. Teich, C. Textor, O. Wild, D. J. Bergmann, I. Bey, H. Bian, C. Cuvelier, B. N. Duncan, G. Folberth, L. W. Horowitz, J. Jonson, J. W. Kaminski, E. Marmer, R. Park, K. J. Pringle, S. Schroeder, S. Szopa, T. Takemura, G. Zeng, T. J. Keating and A. Zuber, 2008: A multi-model assessment of pollution transport to the Arctic, *Atmos. Chem. Phys.*, **8**, 5,353-5,372.

8 Bond, T. C. and R. W. Bergstrom, 2006: Light absorption by carbonaceous particles: an investigative review, *Aerosol Science and Tech.*, **40**, 27-67.

9 Goto, D., T. Takemura and T. Nakajima, 2008: Importance of global aerosol modeling including secondary organic aerosol formed from monoterpene, *J. Geophys. Res.*, **113**, D07205, doi: 10.1029/2007JD009019.

10 Goto, D., T. Nakajima, T. Takemura and K. Sudo, 2011: A study of uncertainties in the sulfate distribution and its radiative forcing associated with sulfur chemistry in a global aerosol model. *Atmos. Chem. Phys.*, **11**, 10,889-10,910.

11 Takemura, T., H. Okamoto, Y. Maruyama, A. Numaguti, A. Higurashi and T. Nakajima, 2000: Global three-dimensional simulation of aerosol optical thickness distribution of various origins, *J. Geophys. Res.*, **105**, 17,853–17,873.

12 Takemura, T., T. Nakajima, O. Dubovik, B. N. Holben and S. Kinne, 2002: Single scattering albedo and radiative forcing of various aerosol species with a global three-dimensional model, *J. Climate*, **15**, 333–352.

13 Takemura, T., T. Nozawa, S. Emori, T. Y. Nakajima and T. Nakajima, 2005: Simulation of climate response to aerosol direct and indirect effects with aerosol transport-radiation model, *J. Geophys. Res.*, **110**, D02202, doi: 10.1029/2004JD005029.

14 Oshima, N. and M. Koike, 2012: Development of a parameterization of black carbon aging for use in general circulation models, *Geo. Model Dev. Discuss*, **5**, 1,263-1,293.

15 Goto, D., N. A. J. Schutgens, T. Nakajima and T. Takemura, 2011: Sensitivity of aerosol to assumed optical properties over Asia using a global aerosol model and AERONET, *Geophys. Res., Lett.*, **38**, L17810, doi: 10.1029/20011GL048675.

16 Goto, D., T. Takemura, T. Nakajima and K. V. S. Badarinath, 2011: Global aerosol model-derived black carbon concentration and single scattering albedo over Indian region and its comparison with ground observations, *Atmos. Environ.*, **45**, 3,277-3,285.

17 Hasumi, H. and S. Emori, 2004: K-1 Model Developers: K-1 coupled GCM (MIROC) description, *K-1 Tech. Rep.* **1**, Univ. of Tokyo, Tokyo.

18 Nakajima, T., M. Tsukamoto, Y. Tsushima, A. Numaguti and T. Kimura, 2000: Modeling of the radiative process in an atmospheric general circulation model, *Appl. Opt.*, **39**, 4,869–4,878

19 Sekiguchi, M. and T. Nakajima 2008: A k-distribution-based radiation code and its computational optimization for an atmospheric general circulation model. *J. Quant. Spectrosc. Radiat. Transfer*, **109**, 2,779-2,793.

20 Chin, M., P. Ginoux, S. Kinne, O. Torres, B. N. Holben, B. N. Duncan, R. V. Martin, J. A. Logan, A. Higurashi and T. Nakajima, 2002: Tropospheric aerosol optical thickness from the GOCART model and comparisons with satellite and sun photometer measurements, *J. Atmos. Sci.,* **59**, 461-483

21 Chung, S. H. and J. H. Seinfeld, 2002: Global distribution and climate forcing of carbonaceous aerosols, *J. Geophys. Res.*, **107**(D19), 4407, doi: 10.1029/2001JD001397.

22 Oshima, N., M. Koike, Y. Zhang, Y. Kondo, N. Moteki, N. Takegawa and Y. Miyazaki, 2009: Aging of black carbon in outflow from anthropogenic sources using a mixing state resolved model: Model development and evaluation, *J. Geophys. Res.*, **114**, D06210, doi: 10.1029/2008JD010680.

23 Oshima, N., M. Koike, Y. Zhang and Y. Kondo, 2009: Aging of black carbon in outflow from anthropogenic sources using a mixing state resolved model: 2. Aerosol optical properties and cloud condensation nuclei activities, *J. Geophys. Res.*, **114**, D18202, doi: 10.1029/2008JD011681.

24 Moteki, N., Y. Kondo, Y. Miyazaki, N. Takegawa, Y. Komazaki, G. Kurata, T. Shirai, D. R. Blake, T. Miyakawa and M. Koike, 2007: Evolution of mixing state of black carbon particles: Aircraft measurements over the western Pacific in March 2004, *Geophys. Res., Lett.*, **34**, L11803, doi: 10.1029/2006GL028943.

25 Clarke, A. D., Y. Shinozuka, V. N. Kapustin, S. Howell, B. Huebert, S. Doherty, T. Anderson, D. Covert, J. Anderson, X. Hua, K. G. Moore II, C. McNaughton, G. Carmichael and R. Weber, 2004: Size distributions and mixtures of dust and black carbon aerosol in Asian outflow: Physiochemistry and optical properties, *J. Geophys. Res.*, **109**, D15S09, doi: 10.1029/2003JD004378

26 Schwarz, J. P., R. S. Gao, D. W. Fahey, D. S. Thomson, L. A. Watts, J. C. Wilson, J. M. Reeves, M. Darbeheshti, D. G. Baumgardner, G. L. Kok, S. H. Chung, M. Schulz, J. Hendricks, A. Lauer, B. Kärcher, J. G. Slowik, K. H. Rosenlof, T. L. Thompson, A. O. Langford, M. Loewenstein and K. C. Aikin, 2006: Single-particle measurements of midlatitude black carbon and light-scattering aerosols from the boundary layer to the lower stratosphere, *J Geophys. Res.*, **111**, D16207, doi: 10.1029/2006JD007076.

27 Shiraiwa, M., Y. Kondo, N. Moteki, N. Takegawa, Y. Miyazaki and D. R. Blake, 2007: Evolution of mixing state of black carbon in polluted air from Tokyo, *Geophys. Res. Lett.*, **34**, L16803, doi: 10.1029/2007GL029819.

Aerosol particle analysis with INCAFeature TEM

Chizu Mitsui[1*], Chieko Hamamoto[2] and Hideo Nishioka[2]

[1]Oxford Instruments KK, 2-11-6, Tomioka, Koto-ku, Tokyo 135-0047, Japan
[2]JEOL Ltd., 3-1-2 Musashino, Akishima, Tokyo 196-8558, Japan

**Corresponding author. Tel.: +81 3 5245 3591; Fax: +81 3 5245 4477, Email address: chizu.mitsui@oxinst.com (C. Mitsui)*

Energy dispersive X-ray spectroscopy (EDS) is an established technique used to characterize the elemental composition of a sample under the beam of an electron microscope. INCAFeature is an automated feature detection and analysis system in which an electron microscope is used for feature detection and EDS is used to determine the chemistry of each feature. Although a particle analysis with an scanning electron microscopy-EDS system is often used for non-metallic inclusions in steel or gunshot residue, few studies have used a transmission electron microscopy (TEM)-EDS system because of sample size and focusing difficulties. In this study, we conducted a first trial of automated particle analysis with a TEM-EDS system and succeeded in automatically detecting and analyzing 158 particles in just 31 min. By automating labor-intensive statistical calculations, INCAFeature can accelerate the progress of aerosol studies.

Keywords: Aerosol particles; Energy dispersive X-ray spectroscopy; Elemental composition; Automated analysis; Particle analysis; Electron microscopy

1. Introduction

Energy dispersive X-ray spectroscopy (EDS) is an established technique used to characterize the elemental composition of a sample under the beam of an electron microscope. INCAFeature is an automated particle detection and analysis system that uses electron microscopy for feature detection and EDS for determining the chemistry of each particle. Although a scanning electron microscopy-EDS system is often used for particle analysis of non-metallic inclusions in steel or gunshot residue, few studies have used a transmission electron microscopy (TEM)-EDS system because of sample size and focusing difficulties. In this study, we conducted a first trial of automated particle analysis with a TEM-EDS system.

2. Instrument configuration

EDS system: INCAFeature, a particle detection and identification system
EDS detector: X-MAXTEM, 80 mm^2 (Oxford Instruments Ltd.)
TEM: JEM-1400 (JEOL Ltd.)

3. Aerosol particles

An aerosol is a colloid suspension of fine particles in a gas. Aerosols scatter and absorb solar and terrestrial radiation. Moreover, by forming clouds, they influence climate and meteorology. Aerosol particles have complex chemical compositions and vary over a wide size range, depending on their origin and on atmospheric processes. The number, size and chemical composition of aerosol particles have important consequences for meteorological phenomena. In this study, aerosol particles were applied to a carbon filter for TEM imaging and EDS analysis.

4. Results

On a TEM image (Figure 1), aerosol particles appear as small dark particles and brighter amorphous features. The dark particles are composed mainly of carbon, silicon, and some metals (data not shown), whereas the brighter particles are sulfate.

Gray-level thresholding of the image is used to identify the gray particles on the filter. Figure 2 shows aerosol particles imaged by TEM and scanning TEM (STEM; dark-field), and detected by INCAFeature. Sulfate particles are brighter than the filter used to obtain the STEM image. Detected particles were colored individually.

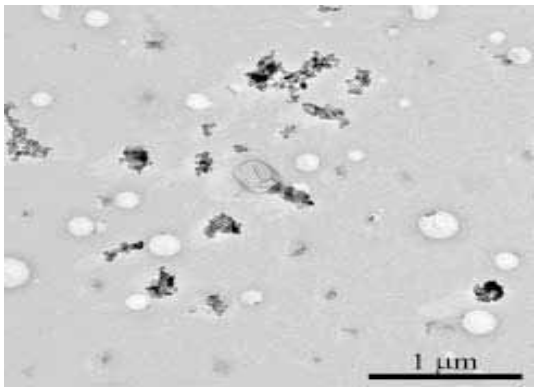

Figure 1 TEM image of aerosol particles applied to a carbon film.

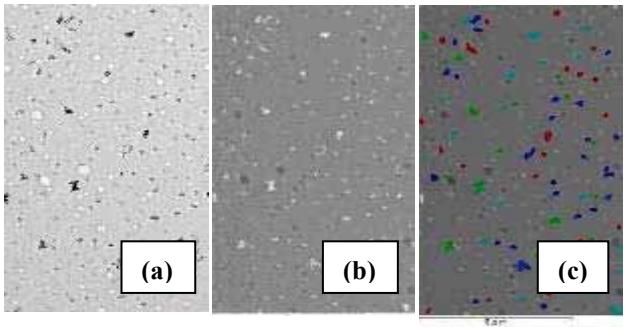

Figure 2 Aerosol particles imaged by (a) TEM and (b) STEM (dark-field) and (c) detected by using INCAFeature

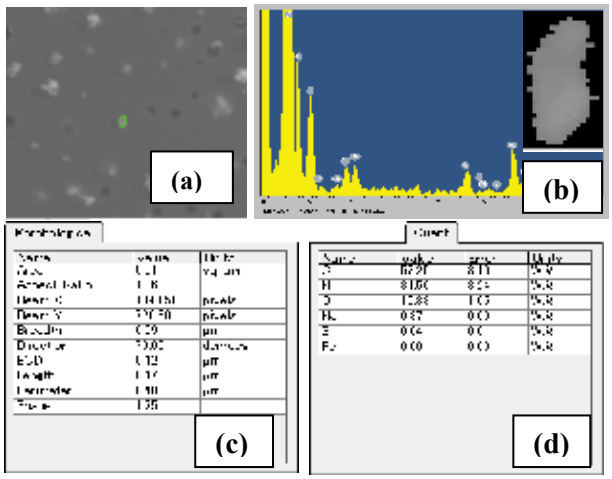

Figure 3 INCAFeature TEM results for a single particle: (a) STEM image, (b) binary image and X-ray spectrum, and information on the particle's (c) morphology and (d) chemistry.

To acquire a STEM image for morphological measurement, all detected particles were scanned again; the electron beam scanned each particle continuously and its X-ray spectrum was determined with the EDS detection system. The automated analysis of a particle by INCA Feature produces a STEM image of the particle and its X-ray spectrum, and information on its morphology and chemical composition (Figure 3). Then, the particle is classified on the basis of its morphology and chemistry (Figure 4).

In this trial, 158 particles were detected automatically in a 12 µm × 12 µm area, and particle detection and measurement took just 31 min. The automated statistical data processing can be performed using the particle chemistry or its morphology, or a combination of the two (Figures 5 and 6).

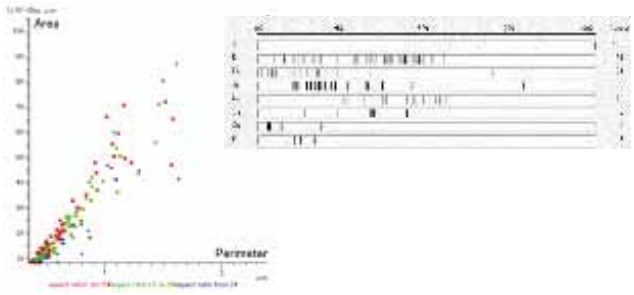

Figure 4 Example of particle data. Scatter plot of area vs perimeter (left), and a quant bar summarizing all of the elements and their concentrations (right)

Classe	Number of particles	% of total particles	Particle area (sq.µm)	% of total area
Includes S, Aspect ratio 1~1.5	70	44.3	1.63E+00	1.146
Includes S, Aspect ratio 1.5~2	60	38.0	1.67E+00	1.170
Includes S, Aspect ratio 2~	20	12.7	5.63E+01	0.396

Figure 5 Example statistical analyses

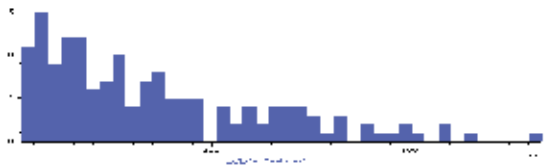

Figure 6 Histogram showing the frequency distribution of one morphological measurement. Most particles were smaller than 200 µm equivalent circle diameter (ECD).

5. Conclusion

INCAFeature, an automated particle analyzing system used in conjunction with TEM, is a powerful tool for aerosol studies. Typically, particle analysis by TEM-EDS is done manually point by point, which requires an immense amount of time and effort. With INCAFeature, we succeeded in automatically detecting and analyzing 158 particles in just 31 min, and data processing was done in parallel. Thus, by automating labor-intensive statistical processing, INCA Feature can further the progress of aerosol studies.

The authors thank Dr. Yasuhito Igarashi, Meteorological Research Institute, for the aerosol sample.

Aerosol isotope analysis by secondary ion mass spectrometry

Masashi Nojima

[1]Research Institute of Science and Technology, Tokyo University of Science, 2461 Yamazaki, Noda-shi, Chiba 278-8510, Japan

**Corresponding author. Tel.: +81 4 7124 1501 (Ext. 5025), Email address: mnojima@rs.noda.tus.ac.jp (M. Nojima)*

This study focuses on radioisotopes on aerosols exposed to radionuclides produced by the Fukushima Daiichi nuclear disaster. Radioisotopes are transported by wind in the gas phase or adsorbed onto aerosol particles. The distribution of radioisotopes in the environment depends on the aerosol particle size and the radionuclides present, factors that must be considered when investigating the areas polluted by radioisotopes and internal contamination in our bodies. In this study, size-classified aerosol particle samples were collected with a cascade impactor and analyzed by secondary ion mass spectrometry.

Keywords: Size-classified analysis; Radioisotope aerosol; Fukushima Daiichi nuclear disaster; SIMS

1. Introduction

This study focused on radioisotopes on aerosols that were exposed to radionuclides produced by the Fukushima Daiichi nuclear disaster. Radioisotopes are carried by winds in gas phase or adsorbed onto aerosol particles. The distribution of radioisotopes in the environment depends on the aerosol particle size and the radionuclides present, and these factors must be considered in investigations of the areas polluted by radioisotopes and internal contamination in our bodies.

Radioactive contamination is frequently discussed only in terms of dose. The objective of this study was to clarify the relationship between radionuclide distribution in the environment and the size of aerosol particles, which is not taken into account by the Japanese System for Prediction of Environmental Emergency Dose Information. In this study, size-classified aerosol particle samples were collected by cascade impactor and analyzed by secondary ion mass spectrometry (SIMS).

2. Methods

Aerosols were sampled with an MCAS-03 aerosol sampler (Murata Inc.) that filtered the particles into three size fractions according to their aerodynamic diameter: >10 μm, 2.5–10 μm, and <2.5 μm.

The sampling locations were Katsuomura, in Fukushima Prefecture, almost 20 km from the Fukushima Daiichi nuclear power plant; Noda, in Chiba Prefecture, which is near a nuclear fallout hot spot; and Aihara, in Tokyo, where the dose measured after the disaster was nearly the same as that before the disaster. In some locations, the aerosol sampler was powered by electricity provided by an AC backup system; MBS-300S-TR1 (Miyauchi works).

The aerosol samples on the sampling plates were introduced into a dynamic SIMS system (IMS-4f; AMETEK, Inc.) and supplied with 4.5 kV of energy. The primary ion beam was O_2^+ (acceleration energy, 10 kV; beam current, 30 nA). In this system, secondary ions generated by a sputtering process are separated by their energy and mass by a mass spectrometer.

3. Estimation of size-classified aerosols

In addition to the SIMS analysis, the size-classified aerosol particles were examined by scanning electron microscopy (SEM) and energy dispersive X-ray spectroscopy (EDX) (Figure 1). In this figure, the SEM images show each size fraction of the aerosol sampled at Noda. Fine aerosol particles (<2.5 μm) are observed on the resin fibers, and an aggregate of aerosol particles of intermediate size . A single aerosol particle of the >10 μm size fraction is also shown.

The mass spectrum of the <2.5 μm aerosol particles shows a strong peak at m/z = 131. The peak may represent radioiodine already transformed by beta decay to ^{131}Xe in the nuclear reactor [1]. The mass spectrum of the aerosol particle > 10 μm in diameter shows two strong peaks at m/z = 139 and 141. These may represent the main fission products of the following nuclear reactions:

$$^{235}\mathrm{U} + \mathrm{n} \rightarrow {}^{92}\mathrm{Kr} + {}^{141}\mathrm{Ba} + 3\mathrm{n} \quad (1)$$

$$^{235}\mathrm{U} + \mathrm{n} \rightarrow {}^{95}\mathrm{Y} + {}^{139}\mathrm{I} + 2\mathrm{n} \quad (2)$$

These elements are not stable, and by the time they were released into the atmosphere their decay products were no

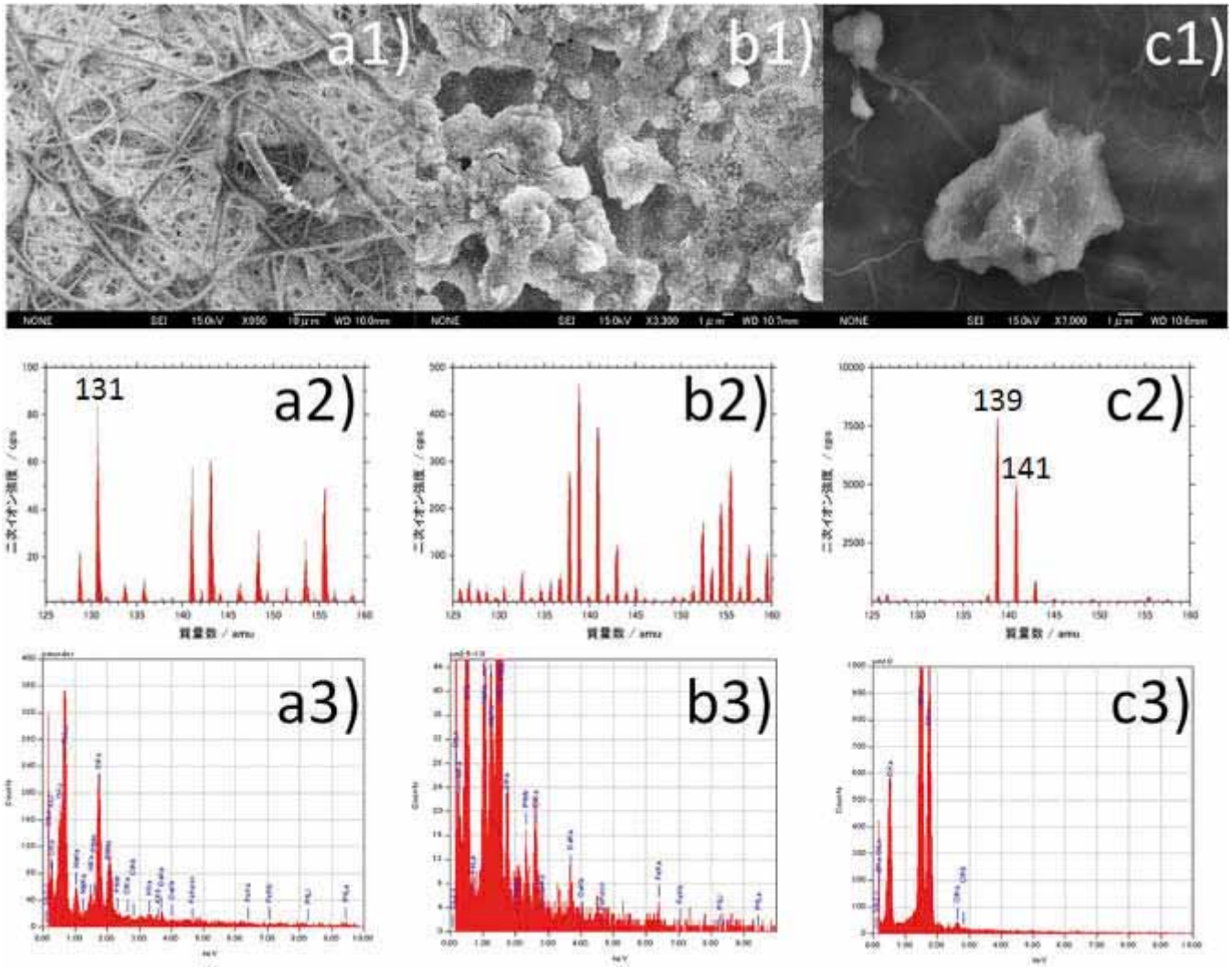

Figure 1 SEM images (top row), mass spectra (middle), and EDX spectra (bottom) of size-classified aerosol particles: a) <2.5 μm; b) 2.5–10 μm; c) >10 μm.

longer radioactive.

The EDX spectra show that the main elements in the sampled aerosol were carbon, oxygen, and silicon. No elements generated by the nuclear disaster were detected. Small particles also included sodium and chlorine, probably from sea salt.

4. Concluding remarks

To clarify the size relationship between aerosol particles and radionuclides, a size-classified aerosol sample was obtained by cascade impactor and analyzed by SIMS.

The mass spectrum of particles < 2.5 μm showed a strong peak at m/z = 131, suggesting radioiodine already transformed by beta decay to ^{131}Xe in the nuclear reactor. The mass spectrum of particles > 10 μm showed two peaks (m/z = 139 and 141) that may have originated as the main fission products of the nuclear reactions.

This study was supported in part by the Research Fund of the Tokyo University of Science. I am grateful to Dr. Yasuhito Igarashi, Prof. Kazuhiko Miura, and Prof. Ken Takada for technical support and helpful suggestions.

1 Aregbe, Y., K. Mayer, S. Valkiers and P. De Bièvre, 1996: *International Journal of Mass Spectrometry and Ion Processes*, Volume **154**, Issues 1–2, Pages 89–97.

Aging of black carbon and its impact on aerosol optical properties and cloud condensation nuclei activities using a mixing state resolved model

Naga Oshima*

[1]Atmospheric Environment and Applied Meteorology Research Department, Meteorological Research Institute, 1-1 Nagamine, Tsukuba, Ibaraki 305-0052, Japan

Corresponding author. Tel.: +81 29 853 8712; Fax: +81 29 855 7240, Email address: oshima@mri-jma.go.jp (N. Oshima)

The mixing state of black carbon (BC) aerosols, namely, the degree to which BC particles are coated with other aerosol components, has been recognized as important for evaluating aerosol radiative forcing. In order to resolve the BC mixing state explicitly in model simulations, the Model of Aerosol Dynamics, Reaction, Ionization, and Dissolution with resolution of the mixing state of BC (MADRID-BC) was developed. MADRID-BC uses a two-dimensional (2-D) aerosol representation, in which aerosols are given for individual particle diameters and BC mass fractions, and it can accurately simulate changes in the entire BC mixing state resulting from condensation/evaporation processes. Aircraft observations conducted in March 2004 show that the mass fraction of thickly-coated BC particles increased in air horizontally transported out from an urban area in Japan within the planetary boundary layer (PBL) over the ocean. MADRID-BC generally reproduces this feature well when observed bulk aerosol concentrations are used as constraints. MADRID-BC was applied to evaluate the influence of changes in the BC mixing state on aerosol optical properties and cloud condensation nuclei (CCN) activities in these air parcels. The evaluation shows that coatings on BC particles enhance light absorption at a wavelength of 550 nm by 38% in air leaving the source region, and by 59% after transport over the ocean for half a day. When the model treats aerosols using the conventional size-resolved sectional representation that does not resolve BC mixing states, the simulated absorption coefficients and single scattering albedos are greater by 35–44% and smaller by 7–13%, respectively, than those from a simulation that resolves the BC mixing state. These results indicate that it is essential for atmospheric models to take into account BC-free particles for accurate prediction of aerosol optical properties, because the conventional representation cannot separately treat BC-containing and BC-free particles in each size bin. Moreover, 55% and 83% of BC-containing particles (by BC mass concentration) can act as CCN at a supersaturation of 0.05% when they leave the source region and after transport for half a day, respectively. These results suggest the importance of the uplift of BC particles from the PBL near source regions for their efficient long-range transport in the free troposphere.

Keywords: Aerosol modeling; Black carbon; Mixing state; Aging; Aerosol optical properties; Cloud condensation nuclei

1. Introduction

Black carbon (BC) aerosols (soot) in the atmosphere efficiently absorb solar radiation and are recognized as one of the most important aerosols for climate forcing. In evaluating aerosol radiative effects, the mixing state of BC particles, namely, the degree to which BC particles are coated with other aerosol components, is a key parameter. Freshly emitted BC particles are generally bare (hydrophobic BC) and become internally mixed with other aerosols through condensation, coagulation, and photochemical oxidation processes in the atmosphere (referred to as "aging processes" hereafter). Coatings on BC particles with sufficient water-soluble compounds, such as ammonium sulfate ($(NH_4)_2SO_4$) and organic acids, change hydrophobic BC to hydrophilic BC, which can serve as cloud condensation nuclei (CCN) at a given supersaturation. Therefore, the coatings on BC particles increase their wet scavenging efficiency and influence the atmospheric lifetime of BC Stier et al., (2006: Ref. 1) through their removal from the atmosphere by precipitation Oshima et al., (2012: Ref. 2). At the same time, coatings on BC particles with non-absorbing compounds enhance the BC absorption efficiency of solar radiation Bond et al., (2006: Ref. 3) This enhancement and the CCN activity of a BC-containing particle primarily depend on the diameters of the BC core and the particle shell, which consists of both the BC core and the coating materials. Consequently, to accurately estimate the aerosol optical properties and CCN activities of BC-containing particles,

one needs to know the entire BC mixing state, namely, the size distribution of BC-containing particles as a function of both the BC core diameter and the BC mass fraction. Although previous modeling studies have evaluated the radiative effects of aerosols including BC, some uncertainties remain in their results because the entire BC mixing state was not accurately treated in most of these studies.

In this study, a new mixing state resolved box model is developed to explicitly simulate the entire BC mixing state resulting from condensation/evaporation processes. This paper presents comparisons of the model simulation results with the aircraft observations and the influences of changes in the BC mixing state on aerosol optical properties and CCN activities for air parcels sampled by the aircraft.

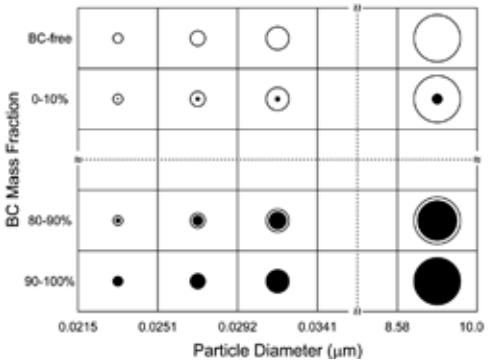

Figure 1 Schematic diagram of the two-dimensional (2-D) aerosol representation adopted in the MADRID-BC box model.

2. Methods

A new box model, called Model of Aerosol Dynamics, Reaction, Ionization, and Dissolution (MADRID) [4] with resolution of the mixing state of BC (MADRID-BC), was developed as a stand-alone model that includes gas-phase chemistry. Oshima et al. (2009a, b: Ref. 5, 6) describe MADRID-BC in detail. MADRID-BC uses a 2-D aerosol representation, in which aerosol mass and number are given for individual particle diameters and BC mass fractions, so that the coexistence of BC particles with different shell diameters but with the same BC core diameter can be tracked for all ranges of BC core diameter (Figure 1). In this study, 40 size sections, ranging from 0.0215 μm to 10 μm, are employed, and BC mass fractions are divided into ten even sections between 0 and 100%. In addition to BC-containing particles, externally mixed "BC-free" particles are treated separately. Aerosol species treated in MADRID-BC include sulfate (SO_4^{2-}), ammonium (NH_4^+), nitrate (NO_3^-), sodium (Na^+), chloride (Cl^-), aerosol water, BC, and organic aerosol (OA). Note that the 2-D aerosol representation allows the coexistence of particles having different BC mass fractions with any given particle diameter. However, when aerosols are represented only by particle diameters, as used in most aerosol models (i.e., a one-dimensional (1-D) aerosol representation or a conventional sectional aerosol representation), the variability in aerosol mixing states cannot be represented.

MADRID-BC treats condensation/evaporation due to mass transfer between gas and particulate phases by a dynamic (kinetic) non-equilibrium approach developed by Meng et al. (1998: Ref. 7). BC aging processes due to coagulation and photochemical oxidation are not included in this study, although the contribution of coagulation may be important under certain circumstances. MADRID-BC treats heterogeneous reactions on the surface of particles and homogeneous nucleation processes [4], however, the nucleation process is not used in this study. The dilution of air, dry and wet deposition, and aqueous-phase chemistry in cloud particles are not included.

Aerosol optical properties (e.g., absorption and scattering coefficients of aerosol particles) are calculated based on the core-shell treatment according to the Mie code of Bohren and Huffman (1983: Ref. 8) for concentrically coated spheres. A complex refractive index of (1.85, –0.71i) at a wavelength of 550 nm [3] is used for the concentric core of pure BC. The CCN activities of BC-containing particles are estimated by calculating the critical supersaturation of particles with the Köhler equation. In this study, BC is treated as the insoluble concentric core of BC-containing particles, and other aerosol components are assumed to be soluble materials. When the critical supersaturation of BC-containing particles is lower than a given air supersaturation, these particles are defined as hydrophilic BC (i.e., CCN).

3. Results and discussion

3.1. Observed evolution of the BC mixing state

The Pacific Exploration of Asian Continental Emission phase C (PEACE-C) aircraft campaign was conducted over the western Pacific around Japan between 22 and 27 March 2004 [9]. Kinematic back trajectories of air parcels sampled from the aircraft were calculated using the method described by Tomikawa and Sato (2005: Ref. 10). Figure 2 shows two-day back trajectories for two air parcel groups, which were transported horizontally from over the Nagoya urban area, Japan, within the planetary boundary layer (PBL), during flight 5. Within air parcels sampled by the aircraft in the PBL, these two groups had the shortest (2 hours) and longest (13 hours) transport times over the ocean after leaving the coastline of Japan, and hereafter they are referred to as "fresh" and "aged" air, respectively. Both air parcels had likely been influenced by anthropogenic emission sources. During flight 5, the air parcels had very little chance to encounter clouds or precipitation.

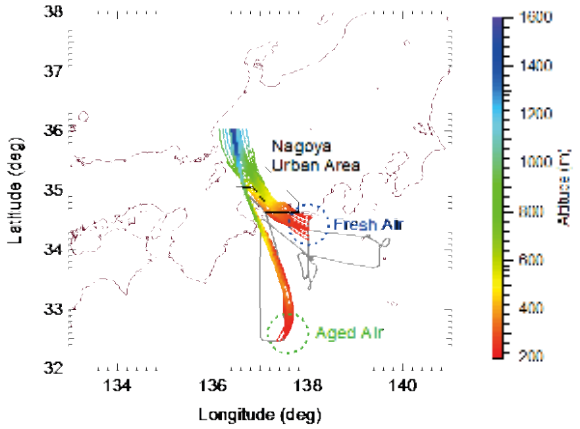

Figure 2 Flight tracks of the aircraft observations during PEACE-C flight 5 (gray lines) and two-day back trajectories of "fresh" and "aged" air parcels (colored lines).

During the PEACE-C aircraft measurements, thinly- and thickly-coated BC particles were discriminated by using a single-particle soot photometer (SP2) [9]. These two types of aerosols generally correspond to BC particles with a shell/BC-core ratio smaller or greater than a particular threshold value. The mass fraction of thickly-coated BC particles, $f_{thick}(D_{BC})$, is defined for individual BC core diameters, D_{BC}, as follows,

$$f_{thick}(D_{BC}) = \frac{[BC_{thick}(D_{BC})]}{[BC_{thick}(D_{BC})]+[BC_{thin}(D_{BC})]} \qquad (1)$$

where $[BC_{thick}(D_{BC})]$ and $[BC_{thin}(D_{BC})]$ are the total BC mass concentrations of thickly- and thinly-coated BC particles, respectively, for a given BC core diameter (D_{BC}).

Consistent with the shortest and longest transport times of the "fresh" and "aged" air parcels, the smallest and greatest $\Delta SO_4^{2-}/\Delta BC$ ratios were observed in "fresh" and "aged" air, respectively (Figure 3), where ΔSO_4^{2-} and ΔBC are the differences between observed and background concentrations of SO_4^{2-} and BC, respectively. In Figure 3, observed $f_{thick}(D_{BC})$ values are shown as a function of the $\Delta SO_4^{2-}/\Delta BC$ ratios for D_{BC} of 155–185 nm. Observed $f_{thick}(D_{BC})$ values increased continuously from 0.34 ("fresh" air) to 0.62 ("aged" air) as the $\Delta SO_4^{2-}/\Delta BC$ ratio increased from 1.3 to 3.5. This result shows that $f_{thick}(D_{BC})$ values increased as the photochemical production of SO_4^{2-} proceeded during transport. This increasing tendency can be viewed as a Lagrangian time evolution of the BC mixing state from "fresh" to "aged" air parcels during transport over the ocean.

3.2. Model-predicted evolution of BC mixing states

MADRID-BC was applied to the flight 5 case to validate the model simulations and examine changes in the entire BC mixing state. To simulate the entire BC mixing state in air sampled during flight 5, simulations for two consecutive regimes were performed. The simulation for the first regime

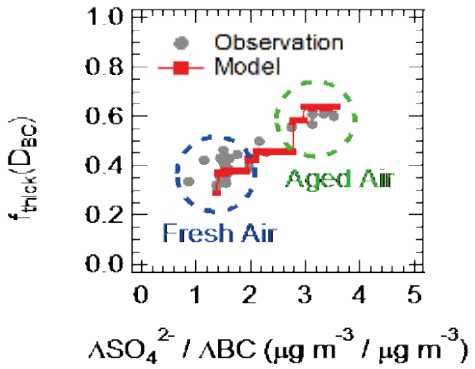

Figure 3 Observed and model-predicted mass fractions of thickly-coated BC particles, $f_{thick}(D_{BC})$, defined by equation (1), as a function of the bulk $\Delta SO_4^{2-}/\Delta BC$ ratio. Results are shown for BC core diameters (D_{BC}) of 100–200 nm (model) and 155–185 nm (observation).

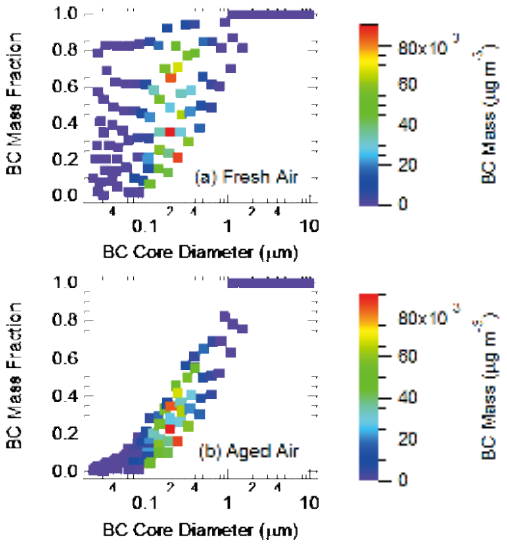

Figure 4 Entire BC mixing states predicted by the model for (a) "fresh" and (b) "aged" air parcels. The BC mass concentrations in individual grid cells are denoted by colored squares.

was for the source region, where emissions of BC particles were continuously introduced, and concurrent coatings due to condensation were calculated. The second regime simulation, which followed the first regime simulation, was for the outflow region over the ocean, where the coating process took place without emissions. These simulations were performed using observed bulk amounts of aerosols and gaseous concentrations as constraints so that the predicted bulk $\Delta SO_4^{2-}/\Delta BC$ ratio became equal to that observed in "fresh" and "aged" air, respectively.

As shown in Figure 3, MADRID-BC reproduced well the observed increase in $f_{thick}(D_{BC})$ values with the increase in the $\Delta SO_4^{2-}/\Delta BC$ ratio from "fresh" to "aged" air for the observed BC core diameter ranges. The agreement in $f_{thick}(D_{BC})$ values of this particular case suggests the validity of the time evolution of the model-predicted entire BC mixing state. The validity found in this study also suggests that

general features of the evolution of BC mixing states can be interpreted at least by the condensational growth process in this particular case.

In the predicted entire BC mixing states for "fresh" and "aged" air (Figures 4a and 4b, respectively), BC-containing particles with different BC mass fractions (coating thicknesses) coexist for individual BC core diameters. The mass of BC particles is concentrated at a BC core diameter of around 200 nm, reflecting the input BC core size distribution. Comparison of the entire BC mixing state between "fresh" and "aged" air shows two distinguishing features. First, compared with "fresh" air, BC mass fractions in "aged" air are systematically smaller for particles with BC core diameters smaller than 1 μm, and BC mass fractions of smaller BC particles show larger decreases. Second, the spread of the BC mass fraction at a given individual BC core diameter is systematically smaller in "aged" air than in "fresh" air. These two features are consistent with both condensation theory, which predicts that the rate of change in particle diameter is greater for a smaller particle, and also with the absence of BC emissions in the outflow region over the ocean, in contrast to continuous emissions of uncoated BC over the source region.

3.3. Aerosol optical properties and CCN activities

Aerosol optical properties were estimated at a wavelength of 550 nm using MADRID-BC based on the validated BC mixing states for "fresh" and "aged" air parcels (Table 1). In this particular case, the BC coatings enhance the overall absorption of particles by 38% and 59% in "fresh" and "aged" air, respectively. The overall single scattering albedo (SSA) of particles increases from 0.81 in "fresh" air to 0.85 in "aged" air. CCN activities were also estimated for a supersaturation of 0.05% for "fresh" and "aged" air parcels (Table 1). The overall hydrophilic BC mass fraction increases from 0.55 in "fresh" air to 0.83 in "aged" air, although these values are quite sensitive to the given supersaturation. This result suggests the importance of the uplift of BC particles near source regions for their efficient long-range transport through the free troposphere, because precipitation generally takes place in association with vertical transport of air.

Another simulation using a conventional sectional (1-D) aerosol representation was conducted to evaluate possible errors in aerosol optical properties and CCN activities calculated using the 1-D aerosol representation instead of the BC-mixing-state-resolved (2-D) aerosol representation (Table 1). In comparison with the 2-D aerosol representation results, the 1-D case simulation gives considerably larger overall absorption coefficients (by 35–44%), a much smaller overall SSA (by 7.2–13%), and a larger overall fraction of hydrophilic BC mass (by 7.9–34%) for particles in air. The absence of efficiently scattering BC-free particles in the conventional sectional (1-D) aerosol representation, which causes not only smaller scattering effects but also greater coating amounts on BC-containing particles, can explain these differences. These results demonstrate the importance of a BC-mixing-state-resolved aerosol representation in aerosol modeling to accurately predict the optical properties and CCN activities of BC particles.

Table 1 Aerosol optical properties and CCN activities calculated by MADRID-BC using a 2-D aerosol representation and a conventional sectional (1-D) aerosol representation (in parentheses)

Parameter	Fresh air	Aged air
Extinction coefficient	75.1 (69.7)	107 (103)
Scattering coefficient	60.9 (49.3)	90.9 (80.8)
Absorption coefficient	14.2 (20.4)	16.4 (22.1)
Absorption amplification	1.38 (1.77)	1.59 (1.92)
Single scattering albedo	0.811 (0.708)	0.847 (0.786)
Fraction of hydrophilic BC mass	0.552 (0.738)	0.831 (0.897)

This work was supported by the Ministry of Education, Culture, Sports, Science and Technology (MEXT) of Japan and in part by the Global Environment Research Fund of the Japanese Ministry of the Environment (A-0803 and A-1101). This study was conducted as a part of the Mega-Cities: Asia Task under the framework of the International Global Atmospheric Chemistry (IGAC) project. The trajectory calculation program used in this paper was developed by Y. Tomikawa of the National Institute of Polar Research and K. Sato of the University of Tokyo, Japan.

1 Stier, P., J. H. Seinfeld, S. Kinne, J. Feichter and O. Boucher 2006: Impact of nonabsorbing anthropogenic aerosols on clear-sky atmospheric absorption, *J. Geophys. Res.,* **111**, D18201, doi: 10.1029/2006JD007147.

2 Oshima, N., Y. Kondo, N. Moteki, N. Takegawa, M. Koike, K. Kita, H. Matsui, M. Kajino, H. Nakamura, J. S. Jung and Y. J. Kim, 2012: Wet removal of black carbon in Asian outflow: Aerosol Radiative Forcing in East Asia (A-FORCE) aircraft campaign, *J. Geophys. Res.,* **117**, D03204, doi: 10.1029/2011JD016552.

3 Bond, T. C., G. Habib and R. W. Bergstrom, 2006: Limitations in the enhancement of visible light absorption due to mixing state, *J. Geophys. Res.,* **111**, D20211, doi: 10.1029/2006JD007315.

4 Zhang, Y., B. Pun, K. Vijayaraghavan, S. Wu, C. Seigneur, S. N. Pandis, M. Z. Jacobson, A. Nenes, and J. H. Seinfeld 2004: Development and application of the Model of Aerosol Dynamics, Reaction, Ionization, and Dissolution (MADRID), *J. Geophys. Res.,* **109**, D01202, doi: 10.1029/2003JD003501.

5 Oshima, N., M. Koike, Y. Zhang, Y. Kondo, N Moteki, N. Takegawa and Y. Miyazaki, 2009a: Aging of black carbon in outflow from anthropogenic sources using a mixing state resolved model: Model development and evaluation, *J. Geophys. Res.,* **114**, D06210, doi:10.1029/2008JD010680.

6 Oshima, N., M. Koike, Y. Zhang and Y. Kondo, 2009b: Aging of black carbon in outflow from anthropogenic sources using a mixing state resolved model: 2. Aerosol optical properties and cloud condensation nuclei activities, *J. Geophys. Res.,* **114**, D18202, doi:10.1029/2008JD011681.

7 Meng, Z., D. Dabdub and J. H. Seinfeld, 1998: Size-resolved and chemically resolved model of atmospheric aerosol dynamics, *J. Geophys. Res.,* **103**, 3,419–3,435.

8 Bohren, C. F. and D. R. Huffman, 1983: *Absorption and Scattering of Light by Small Particles*, John Wiley, Hoboken, N. J.

9 Moteki, N., Y. Kondo, Y. Miyazaki, N. Takegawa, Y. Komazaki, G. Kurata, T. Shirai, D. R. Blake, T. Miyakawa and M. Koike, 2007: Evolution of mixing state of black carbon particles: Aircraft measurements over the western Pacific in March 2004, *Geophys. Res. Lett.,* **34**, L11803, doi: 10.1029/2006GL028943.

10 Tomikawa, Y. and K. Sato, 2005: Design of the NIPR trajectory model, *Polar Meteorol. Glaciol.,* **19**, 120-137.

Formation and variations of aerosols around Beijing using the WRF-chem model

Hitoshi Matsui[1,*], Makoto Koike[1], Yutaka Kondo[1] and Nobuyuki Takegawa[1]

[1]University of Tokyo, Hongo 7-3-1, Bunkyo-ku, Tokyo 113-0033, Japan

**Corresponding author. Tel.: +81 3 5841 4550; Fax: +81 3 5841 8318, Email address: matsui@eps.s.u-tokyo.ac.jp (H. Matsui)*

Model calculations were conducted with the Weather Research and Forecasting model coupled with a chemistry scheme (WRF-chem) for the region around Beijing, China, in summer 2006, when the CAREBeijing-2006 intensive campaign was conducted. In this paper, we interpret aerosol optical properties in terms of aerosol mass concentrations and their chemical compositions by linking model calculations with measurements.

Keywords: Aerosol; Regional three-dimensional model; Optical property; Mass concentrations; Spatial and temporal variations; Urban; East Asia

1. Introduction

The mega-cities of East Asia are large emission sources that have considerable impacts on regional climate and air quality. We performed three-dimensional aerosol model simulations for the region around Beijing with the Weather Research and Forecasting model coupled with a chemistry scheme (WRF-chem). The purposes of this study were (1) to validate the model-simulated spatial and temporal variations of aerosol mass concentrations and optical properties and (2) to systematically understand the spatial and temporal variations of aerosol mass concentrations and their optical parameters around Beijing. This study is one of the first applications of the WRF-chem model to the simulation of aerosol optical properties associated with mega-city emissions in East Asia.

2. Methods

2.1. Three-dimensional model (WRF-chem)

WRF-chem version 2.2 was used as a regional three-dimensional model [1, 2]. The details of the calculation settings and parameterization schemes used are described elsewhere [3, 4]. Model calculations were conducted for two domains with horizontal resolutions of 27 and 9 km. The simulation period was from 10 August to 11 September 2006. For the aerosol calculations, the Model for Simulating Aerosol Interactions and Chemistry (MOSAIC) was used, and a sectional representation of the aerosol size distribution was adopted to simulate both particle number and mass in each aerosol size bin [2, 5]. An eight-bin representation was adopted. Aerosol species included were sulfate, nitrate, ammonium, elemental carbon (EC), primary organic aerosols, nonreactive dust, and aerosol water. Anthropogenic emission inventories for 2004 were used [3, 6]. The Global Emissions Inventories Activity [7] was used for biogenic emission inventories.

Aerosol optical parameters were calculated offline using the WRF-chem-simulated aerosol mass concentration and size distributions, rather than using those calculated online, within WRF-chem. The offline optical calculation approach adopted an algorithm based on Mie theory [8] to estimate differences in aerosol optical properties calculated using three different aerosol mixing state treatments, namely, well-mixed internally (WMI), core-shell internally mixed (CSI), and externally mixed (EM) [4]. Here, we mainly use the aerosol optical properties calculated using the WMI treatment (at 550 nm) in the comparison with the measurement data, because this treatment was also used in the online WRF-chem calculations.

2.2. Measurements

Model calculations of aerosol optical properties were compared with various in situ measurements made during the CAREBeijing-2006 campaign, which was conducted between 10 August and 11 September 2006. Intensive aerosol measurements were carried out at Yufa, a site about 50 km south of Beijing. Details of the observation sites and CAREBeijing-2006 measurements are reported in other papers [9, 10]. In this study, we used mass concentrations of inorganics (obtained with an Aerodyne Aerosol Mass Spectrometer), EC/organic carbon (OC) (Sunset Laboratory semi-continuous EC/OC analyzer), and $PM_{2.5}$ (tapered element oscillating microbalance), aerosol size distributions

(twin differential mobility particle sizer and aerodynamic particle sizer), the absorption coefficient (b_{abs}) at 532 nm (photoacoustic spectrometer), and the scattering coefficient (b_{scat}) at 550 nm (nephelometer).

3. Results: mass and optical properties

3.1. Variations in aerosol mass concentrations

Model calculations generally captured the temporal variations of primary (such as EC) and secondary (such as sulfate) aerosols observed at Yufa (Figure 1). Model calculations showed distinct differences in spatial distribution between primary and secondary aerosols in association with synoptic-scale meteorology. Under an anticyclonic pressure system, secondary aerosols increased in the air around Beijing within an area of about 1000 × 1000 km^2. This polluted air mass had been transported northward from the area of high anthropogenic emissions and continuous photochemical production in the region south of Beijing. Then, the subsequent passage of a cold front brought clean air from the north, and the polluted air around Beijing was swept southward. This cycle was repeated about once a week and was found to be responsible for observed enhancements and reductions of aerosols at the intensive measurement sites. In contrast to the secondary aerosols, the spatial distributions of primary aerosols (EC) reflected those of emissions, resulting in only slight variability despite changes in the synoptic-scale meteorology. In accordance with these results, source apportionment simulations revealed that primary aerosols in Beijing were controlled by emissions emitted within 100 km of Beijing and within the preceding 24 hours, whereas emissions emitted as far as 500 km of Beijing and within the preceding 3 days were found to affect secondary aerosols.

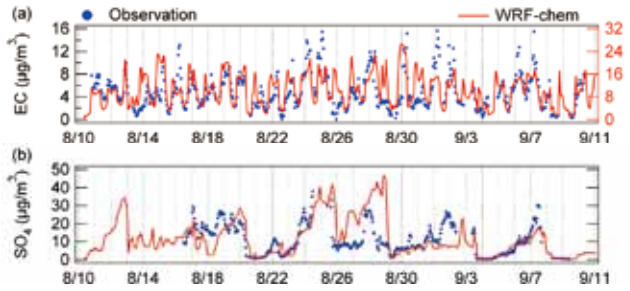

Figure 1 Time series of (a) EC and (b) sulfate at the Yufa site.

3.2. Variations in aerosol optical properties

Model calculations generally reproduced well the temporal variability of the local aerosol optical properties at Yufa (Figure 2). Because of the reasonable agreement with measurements, spatial and temporal variations of aerosol optical properties around Beijing were interpreted from the model results from the viewpoint of regional-scale aerosol mass distributions of individual chemical components. The spatial and temporal variations of b_{abs}, b_{scat}, and the extinction coefficient (b_{ext}) and the single scattering albedo (SSA) corresponded well to those of the mass concentrations of EC, sulfate, and $PM_{2.5}$, and the mass fractions of secondary aerosols, respectively. Therefore, aerosol optical parameters can be interpreted by considering in combination the spatial variations of EC, which are controlled by local-scale emissions (within 100 km of Beijing during the preceding 24 h), and those of sulfate, which are controlled by regional-scale emissions (within 500 km of Beijing during the preceding 3 days), as well as by synoptic meteorological conditions. These results explain why b_{scat} and b_{ext} exhibited multi-day variations, whereas b_{abs} primarily exhibited diurnal variations at Yufa.

On the other hand, the model calculations underestimated the absolute values of b_{ext}, b_{scat}, and SSA by 40%, 50%, and 20%, respectively, and overestimated the absolute value of b_{abs} by 60%. The underestimation and overestimation exceed the uncertainties in the measurements. Possible causes of the discrepancies between measurements and model calculations are discussed in section 3.3

.

3.3. Offline sensitivity calculations

Here we discuss possible factors accounting for the overestimation and underestimation by the aerosol optical parameter calculations, including uncertainties in the aerosol physical parameters (aerosol density and refractive index), size distribution, and mixing state (adopted for aerosol optical calculations). We first examine b_{ext} (sections 3.3.1 and 3.3.2) because it is rather insensitive to the aerosol mixing state, and we examine the other optical parameters (b_{abs}, b_{scat}, and SSA) in section 3.3.3.

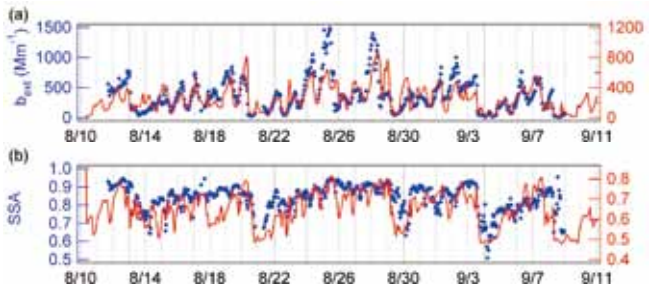

Figure 2 Time series of (a) b_{ext} and (b) SSA at the Yufa site.

3.3.1. Total mass and b_{ext}

We examine closure among the measurements themselves in terms of aerosol mass, size distribution, and optical properties to separate the uncertainties in the model calculations from those in the measurements. First, we examine the closure between aerosol mass concentrations and size distributions. When we estimated $PM_{2.5}$ mass concentrations from the size distribution measurements using an aerosol density of 1.6 g cm^{-3}, as assumed in the aerodynamic particle sizer measurements [11], their absolute values and temporal variation agreed with those of measured

$PM_{2.5}$ within the uncertainty of the measurements.
Second, we examine the closure between b_{ext} and size distributions. We estimated b_{ext} values of PM_{10} from the measured size distribution and chemical composition by the WMI treatment. When we compared these with the measurements obtained by the photoacoustic spectrometer and nephelometer, they agreed within 3%. We also found a quite good agreement of their temporal variations (correlation coefficient = 0.99 for hourly data).

We found reasonably good measurement closure, within the uncertainties in observed aerosol mass, size distribution, and b_{ext} values. These results suggest that the disagreement in b_{ext} values between measurements and model calculations is not due to the Mie theory algorithm itself but instead is due mainly to the uncertainties/errors in the parameters used for the Mie calculations, such as the refractive index and the size distributions of aerosols in the model calculations.

3.3.2. Aerosol density, refractive index, and size distribution: b_{ext}

The average aerosol density in the WRF-chem calculations of approximately 2.0 g cm^{-3} was greater than the density of 1.6 g cm^{-3} assumed in the measurements [11]. This discrepancy is partly because the density of unidentified species is unknown and a high aerosol density (2.6 g cm^{-3}) is assumed for dust species in the model calculations. Some organic aerosols in the real atmosphere with densities as low as 1 g cm^{-3} may also contribute to this discrepancy, because they are not included in our WRF-chem calculations. In addition, non-spherical aerosol particles in the real atmosphere (under dry conditions) may in part account for this discrepancy because spherical particles are assumed in the model calculations. In this study, the discrepancy in "aerosol density" between measurements and model calculations includes all of the above potential effects related to mass-to-volume conversion.

The period average of the volume-averaged aerosol refractive index in the WRF-chem calculations is 1.545 + 0.091i, whereas an estimate obtained by using the observed PM_1 chemical composition is 1.545 + 0.103i. Consequently, errors due to the refractive index are expected to be small in this study.

To obtain a quantitative understanding of the discrepancies in b_{ext} between model calculations and measurements, we conducted simple sensitivity studies in which model-calculated aerosol density, refractive index, and the shape of the size distribution were individually replaced with values estimated from the measurements. In these sensitivity calculations, total aerosol mass concentrations at each time point were constrained by the results of the WRF-chem calculations. In addition, we assumed that aerosol density and refractive index did not influence each other (e.g., we used measurement-derived density with the model-calculated refractive index). Note that the replacement of the refractive index, aerosol density, and the shape of size distribution is equivalent to making changes in chemical composition, volume, and the size distribution with constant volume, respectively.
The use of measurement-derived values for both density and the refractive index causes a 37% increase in b_{ext} (orange square in Figure 3a), leading to much better agreement with the measurements (blue circle in Figure 3a). Most of the increase was due to the aerosol density change (28% increase in b_{ext}) because a lower density (1.6 g cm^{-3} instead of 2.0 g cm^{-3}) results in a larger total aerosol volume and mass extinction efficiency and therefore a larger b_{ext} value.

Similarly, we conducted sensitivity calculations to estimate errors in b_{ext} caused by errors in the shape of the aerosol size distributions calculated by WRF-chem. In this sensitivity calculation we used the shape of the observed aerosol size distributions without changing the model-calculated aerosol total mass, density, or volume-averaged refractive index. As a result, the period-averaged b_{ext} value increased by 9.1% (green square in Figure 3a).
Finally, we conducted sensitivity calculations in which all three aerosol parameters (aerosol density, refractive index, and the shape of the size distribution) were replaced with measurement-derived values, while using model-calculated mass concentrations. As a result, the calculated b_{ext} value (black square in Figure 3a) agrees with observed b_{ext} within 0.5%.

These sensitivity calculations demonstrate that the discrepancies in b_{ext} between the calculations and measurements are due mostly to the treatment of aerosol density (disagreement between the calculated mass-to-volume conversion and the measurements) in the model calculations.

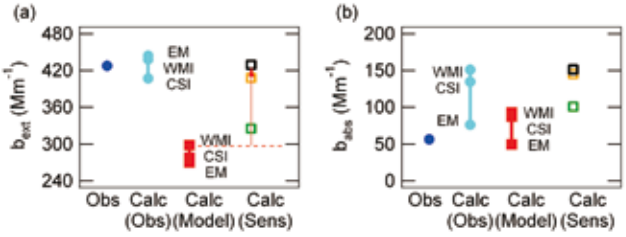

Figure 3 Period-averaged (a) b_{ext} and (b) b_{abs} at Yufa. The results of the optical sensitivity calculations are also shown.

The contributions of the refractive index and the shape of the size distribution to b_{ext} discrepancies were estimated to be small. Good agreement with measurements is achieved when these aerosol properties are accurately predicted or assumed; however, a notable bias can result when these properties are inadequately treated, even if total aerosol mass concentrations are reproduced well in the model calculations.

3.3.3. Aerosol mixing states: b_{abs}, b_{scat}, and SSA

Optical parameters were also estimated from the ob-

served size distribution and chemical composition for the CSI and EM aerosol mixing state treatments. Although b_{ext} was insensitive to the aerosol mixing state treatment, b_{abs} and SSA were sensitive to the treatment and agreed better with direct measurements when the EM treatment was adopted (Figure 3b). These results are consistent with the observed features of the aerosol mixing states during the CAREBeijing-2006 campaign [11].

When b_{abs} and SSA were calculated using the results of the WRF-chem calculations, similar tendencies were found: namely, b_{abs} values were largest (lowest) and SSA values were lowest (largest) when the WMI (EM) treatment was adopted. Because the aerosol mixing state is essential information for reproducing SSA in model calculations, it is quite important to improve regional aerosol models to represent multiple mixing states and their aging processes.

4. Summary

Regional aerosol model calculations were made using WRF-chem to study spatial and temporal variations of aerosol mass concentrations of individual chemical components and their optical properties around Beijing, China. Model calculations reproduced the temporal variations of aerosol mass concentrations and optical properties observed during the CAREBeijing-2006 campaign.

The spatial and temporal variations of the absorption, scattering, and extinction coefficients and SSA corresponded well with those of the mass concentrations of EC, sulfate, and $PM_{2.5}$ and the mass fractions of secondary aerosols, respectively. Therefore, aerosol optical parameters can be interpreted by considering the combination of spatial variations of primary aerosols (EC), which are controlled by local-scale emissions, and those of secondary aerosols (sulfate), which are controlled by regional-scale emissions, along with synoptic meteorological conditions. These results explain why the scattering and extinction coefficients exhibited multi-day variations, while the absorption coefficient primarily exhibited diurnal variations, at Yufa.

Model calculations, however, underestimated or overestimated the absolute levels of aerosol optical properties around Beijing by up to 60%. Offline sensitivity calculations showed that the treatment of aerosol mixing states and aerosol "density" (parameters related to mass-to-volume conversion) in the model calculations mainly contributed to these over- and underestimations. Good agreement with measurements is achieved when these aerosol parameters are accurately predicted or assumed; however, a notable bias can result when these properties are inadequately treated, even if total aerosol mass concentrations are reproduced well in the model calculations.

We are indebted to all of the CAREBeijing-2006 campaign participants for their cooperation and support. This study was conducted as a part of the Mega-Cities: Asia Task under the framework of the International Global Atmospheric Chemistry (IGAC) project.

1 Grell, G. A., S. E. Peckham, P. Schmitz, et al. 2005: Fully coupled "online" chemistry within the WRF model, *Atmos. Environ*, **39**, 6,957 – 6,975.
2 Fast, J. D., W. I. Gustafson, R. C. Easter, et al. 2006: Evolution of ozone, particulates, and aerosol direct radiative forcing in the vicinity of Houston using a fully coupled meteorology-chemistry-aerosol model, *J. Geophys. Res*., **111**: D21305, doi: 10.1029/2005JD006721.
3 Matsui, H., M. Koike, Y. Kondo, et al. 2009: Spatial and temporal variations of aerosols around Beijing in summer 2006: Model evaluation and source apportionment, *J. Geophys. Res.,* **114**: D00G13, doi: 10.1029/2008JD010906.
4 Matsui, H., M. Koike, Y. Kondo, et al. 2010: Spatial and temporal variations of aerosols around Beijing in summer 2006: 2. Local and column aerosol optical properties, *J. Geophys. Res.,* **115**: D22207, doi: 10.1029/2010JD013895.
5 Zaveri, R. A., R. C. Easter, J. D. Fast, et al. 2008: Model for Simulating Aerosol Interactions and Chemistry (MOSAIC), *J. Geophys. Res*., **113**: D13204, doi: 10.1029/2007JD008782.
6 Zhang, Q., D. G. Streets, G. R. Carmichael, et al. 2009: Asian emissions in 2006 for the NASA INTEX-B mission, *Atmos. Chem. Phys*., **9**, 5,131 – 5,153.
7 Guenther, A., C. N. Hewitt, D. Erickson, et al. 1995: A global model of natural volatile organic compound emissions, *J. Geophys. Res*., **100**, 8,873 – 8,892.
8 Bohren, C. F., and D. R. Huffman, 1998:Absorption and Scattering of Light by Small Particles, John Wiley, Hoboken, N. J.
9 Takegawa, N., T. Miyakawa, M. Kuwata, et al. 2009: Variability of submicron aerosol observed at a rural site in Beijing in the summer of 2006, *J. Geophys. Res*., **114**: D00G05, doi: 10.1029/2008JD010857.
10 Garland, R. M., O. Schmid, A. Nowak, et al. 2009: Aerosol optical properties observed during Campaign of Air Quality Research in Beijing 2006 (CAREBeijing-2006): Characteristic differences between the inflow and outflow of Beijing city air, *J. Geophys. Res*., **114**: D00G04, doi: 10.1029/2008JD010780.
11 Cheng, Y. F., M. Berghof, R. M. Garland, et al. 2009: Influence of soot mixing state on aerosol light absorption and single scattering albedo during air mass aging at a polluted regional site in northeastern China, *J. Geophys. Res*., **114**: D00G10, doi: 10.1029/2008JD010883.

Shape modeling of dust and soot particles for remote sensing applications by considering the geometrical features of sampled aerosols

Hiroshi Ishimoto[1*], Yuji Zaizen[2], Kazuhiko Masuda[1], Yuzo Mano[1] and Akihiro Uchiyama[3]

[1]Meteorological Satellite and Observation System Research Department, Meteorological Research Institute, 1-1 Nagamine, Tsukuba, Ibaraki 305-0052, Japan
[2]Atmospheric Environment and Applied Meteorology Research Department, Meteorological Research Institute, 1-1 Nagamine, Tsukuba, Ibaraki 305-0052, Japan
[3]Climate Research Department, Meteorological Research Institute, 1-1 Nagamine, Tsukuba, Ibaraki 305-0052, Japan

**Corresponding author. Tel.: +81 29 853 8676; Fax: +81 29 856 0644, Email address: hishimot@mri-jma.go.jp (H. Ishimoto)*

We present shape models for dust and soot particles that were developed by taking into account the geometrical features of sampled aerosols and using an assumed cell-type structure. We examined the spatial Poisson-Voronoi tessellation by considering the assumed basic structure of the material, and determined the particle shapes by extracting cells from the tessellation. Using these procedures, hundreds of "Voronoi aggregates" were prepared for use in a dust particle model. To determine the final model, we used two-dimensional images of dust particles collected at Fukuoka, Japan, on 16 March 2009, during a time when dust particles transported from China were widely observed in this part of western Japan. For the shape analysis, we used silicate-dominated particles, which were identified by transmission electron microscopy spectral analysis. For the modeling of soot particles, selected fractal structures with arbitrary fractal dimensions were examined and compared to the sampled images of complex-shaped aerosols, under the assumption that the aerosol particles with highly complex shapes were soot particles. A database of the optical properties of these aerosol models was compiled from calculations by the finite-difference time-domain method, the geometric optics integral equation method, and a conventional geometric optics method. The database will be made available for use in analyses of aerosol remote sensing data.

Keywords: Mineral dust; Soot; Irregular shape; Optical modeling

1. Introduction

Together with particle size and chemical composition, the shape characteristics of aerosol particles must be considered in their optical modeling. Because dust and soot particles generally have irregular and complex shapes, some models assuming simple shapes (e.g., spheres and spheroids) may produce large errors when estimating the radiative properties of particles in the visible and near-infrared wavelengths. There is also an increasing demand for models using realistic aerosol shapes for various applications of multi-channel and polarization observations by satellite and ground-based active or passive sensors.

With advances in computer performance, it is possible to create a database of the optical properties of modeled particles over a wide size range that takes into account their realistic shapes and structures. For nonspherical and inhomogeneous particles with small size parameters $x = \pi d / \lambda$, where d is the size of the particle and λ is the wavelength, discrete-dipole approximation and finite-difference time-domain (FDTD) methods are widely used for the accurate determination of their light-scattering properties. These numerical methods can be used for most of the typical size range of soot particles at visible and near-infrared wavelengths.

For relatively large aerosol particles, such as mineral dust, improved geometrical optics approximations (GOM2 or geometric optics integral equation: GOIE), which use the integral equation of electromagnetic wave theory, produce reasonably accurate results (e.g., [1, 2]). Therefore, formulating realistic and sophisticated aerosol shape models for use with these numerical methods is vital for improving remote sensing analysis and radiative models of the atmosphere. To create realistic shape models, geometrical information collected from microscopic images of sampled aerosols is important.

In this paper, we propose an approach for modeling the three-dimensional shape of mineral dust and soot particles

from geometrical information provided by aerosol images.

2. Methods

Shape models of mineral dust and soot particles were created by the following procedure.

(i) The basic structure of the shape model was obtained by applying certain microphysical assumptions.
(ii) By a Monte Carlo approach, a number of particle models were created by changing various parameters to modify the shape characteristics of the structure assumed in (i).
(iii) A final shape model was determined by statistical comparison of two-dimensional geometrical features between randomly oriented model particles and sampled aerosols.

In this method, the basic structure assumed in (i) is crucial for producing a reasonable shape model. The final shape model determined was not a copy of a specific aerosol particle seen in the microscopic images, but a virtual particle with geometrical features similar to those of an ensemble average of the sampled aerosols. The intention was to simulate the average optical properties of the sampled aerosols by using a small number of shape models in order to reduce the computational cost of light-scattering calculations.

2.1. Mineral dust model

We used a spatial Poisson-Voronoi tessellation to simulate the basic structure of mineral dust particles [3]. A Poisson-Voronoi structure has been used as a simple crystal growth model in structural analysis studies [4], where the structure is defined by nucleation points within a numerical field. The structure consists of Voronoi cells with each cell sharing a facet with a neighboring cell, and aggregates of Voronoi cells (hereafter, Voronoi aggregate: VA) are determined by extracting the cells enclosed within an assumed spheroid. Therefore, the shape of the VA depends on the number of initial nucleation points and their locations in the numerical field, and on the shape of the assumed outer spheroid. In this study, we randomly selected 100 nucleation points in the numerical field and then examined different spheroid shapes, creating hundreds of aggregates for each combination of tessellation and outer spheroid. Examples of numerically created VAs are shown in Figure 1.

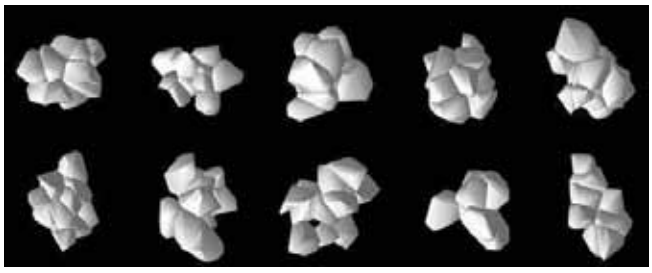

Figure 1 Examples of numerically created Voronoi aggregates

To determine the mineral dust shape model from the large number of created VA particles, geometrical information obtained from microscopic images of sampled aerosols was considered. For the shape analysis, images of particles larger than 0.1 μm were used. Furthermore, silicate-dominated particles (Si weight ratio more than 65%) were chosen following chemical analysis with an energy-dispersive X-ray (EDX) analyzer. We also removed particles that included materials soluble in water or other liquids detected by electron beam irradiation. These elemental analyses were performed on 91 particles on the sample plate, leaving 18 particles for image analysis (see Figure 2).

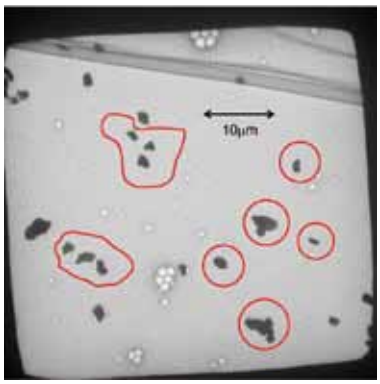

Figure 2 Microscopic image of aerosols sampled at Fukuoka, Japan, on 16 March 2009. Mineral dust particles identified by EDX analysis are encircled by red lines.

We calculated two non-dimensional shape parameters (α, β) for the 18 dust particle images and numerically created VAs:

$$\alpha \equiv \frac{4A}{\pi D^2}, \ \beta \equiv \frac{4\pi A}{L^2} \tag{1}$$

where A is the area, D is the maximum dimension, and L is the perimeter of the projected particle image. Figure 3 shows scatter plots of (α, β) for the 18 mineral dust particle samples (Figure 3a) and for 100 VAs created by using a prolate spheroid with an axis ratio of 1:2 for the outer shape (Figure 3b).

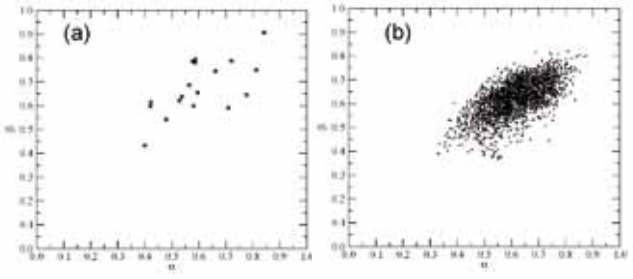

Figure 3 Scatter plots of the geometrical parameters (α, β) of 18 aerosol particles (a) and 100 selected Voronoi aggregates (VAs) (b) The calculated values for 46 orientations of each VA are plotted.

By using a least-squares analysis for correlation of the (α, β) distribution, we determined the final shape model for mineral dust particles. The resultant shape model consisted of four Voronoi cells and was relatively simple compared with other possible shape models (Figure 1). Because of the small number of mineral dust samples, we neglected the particle size dependence of (α, β) and proposed only one shape model.

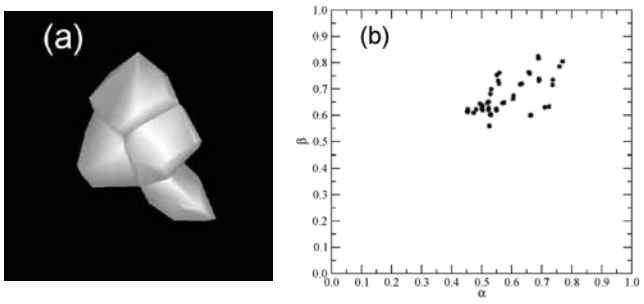

Figure 4 Shape model for mineral dust particles (a) and the (α, β) distribution of its 46 orientations (b).

2.2. Soot model

There is a large body of previous work on determining soot particle shape. A typical assumption is that soot particles consist of primary particles (monomers) and have a fractal structure with a specific fractal dimension (e.g., Ref. [5]). We also assumed a fractal structure for soot particles. Moreover, we considered aerosol particles with a highly complex structure on the microscopic images to be soot and used them as the reference soot particles, because it was difficult to identify soot particles directly by elemental analysis. From microscopic images of aerosol samples obtained at Tsukuba, Japan, we selected 52 complex-shaped aerosols with the geometrical parameter $\beta \leq 0.3$ and assumed that they were soot particles (Figure 5).

We created many fractal structures with a specific fractal dimension d_f between 1.5 and 2.4 at intervals of 0.1, by using the numerical procedure described in [6]. Then we created spatial Poisson-Voronoi tessellations with an average cell size of ~30 nm. To restrict the size variation for each Voronoi cell, a Matérn hard-core point field (e.g., Ref. [4]) was applied to determine the distribution of the initial nucleation points for generating tessellations. After applying the prepared fractal structure to the Voronoi tessellation, Voronoi cells that overlapped the fractal shape were extracted [7]. Examples of aggregates of Voronoi cells are shown in Figure 6.

Figure 5 Reference particles for soot modeling selected from microscopic images. The largest particle has $D = \sim 3$ μm.

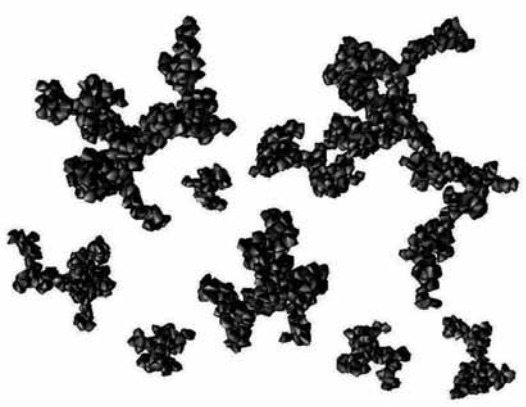

Figure 6 Voronoi aggregates created by using fractal structures (fractal dimension $d_f = 1.7$ in box-count method).

Figure 7 shows the geometrical parameters α and β with respect to the maximum dimension D for the soot particles and for the orientation-averaged fractal aggregates, where 10 size categories and 10 modeled particles of each size were used for the fractal aggregate. For particles with $D \geq 1$ μm, the aggregates with fractal dimensions between 1.5 and 1.8 agreed well with the selected soot samples, for both parameters α and β. However, a bias was confirmed in values of β for particles with $D \leq 0.5$ μm. Because we considered the average cell size of the aggregate to be 30 nm, the small modeled aggregates became more compact than the sampled soot particles. This result indicates that it is difficult to simulate the size dependence of the shape properties of whole soot particles, such as those shown in Figure 5, by using only one fractal dimension and one average monomer size. To improve the $\beta - D$ relationship for the modeled particles, we further considered the particle size dependence of the monomer (size of the Voronoi cell). The final soot model was selected from 10 sets of modified fractal aggregates with a fractal dimension $d_f = 1.7$ (Figure 8).

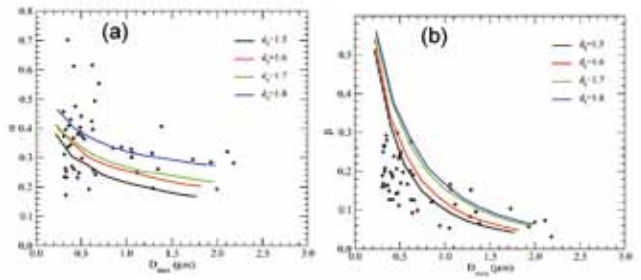

Figure 7 Size dependence of the geometrical parameters α (a) and β (b) for the assumed soot particles (*) and the simulated fractal-Voronoi aggregates with fractal dimensions $d_f = 1.5 - 1.8$ (lines).

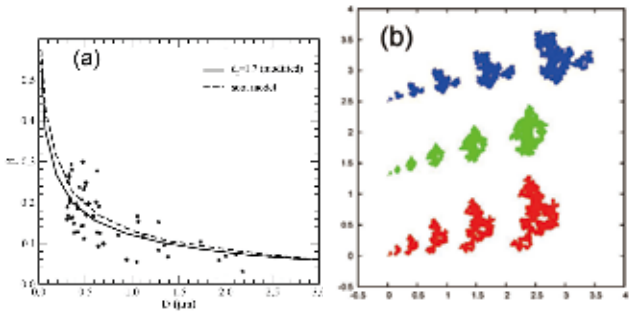

Figure 8 (a): The same as Figure 7b but for particles with modified $d_f = 1.7$ (solid line) and for the soot shape model determined by light scattering calculations (dashed line). (b): The shapes of six soot models of different sizes. Different colors indicate views from different angles.

3. Database of optical properties

Optical properties of the mineral dust and soot models were calculated by using FDTD, GOIE, and conventional geometrical optics methods for various size parameters and refractive indices. A database of these optical properties is scheduled to be used for data analysis by the Second-generation Global Imager onboard the Global Change Observation Mission Climate (GCOM-C1) satellite. Furthermore, we inserted our mineral dust model, called MRIDUST, into the RSTAR atmospheric radiative transfer model developed by the Atmosphere and Ocean Research Institute, Tokyo University [8], as an optional calculation scheme for "Yellow sand" (i.e., mineral dust) (currently only available to model developers).

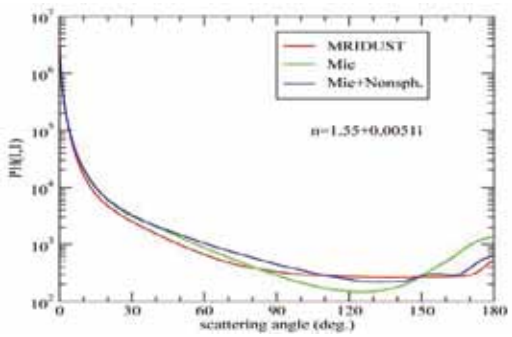

Figure 9 Size averaged phase function of the mineral dust model MRIDUST (red), based on the size distribution of the "yellow sand" model in the RSTAR code and refractive index $n = 1.55 + 5.102 \times 10^{-3} i$ at wavelength $\lambda = 0.5\mu m$. Results of the Mie calculation (green) and the Mie calculation modified by an empirical formula for nonsphericity (blue) are shown for comparison.

4. Discussion

Mineral dust and soot particle shapes were modeled by assuming microphysical constraints on the particle structure and the geometrical features of sampled aerosols. For the mineral dust model, we neglected the size dependence of particle shape irregularities because of the small number of dry dust samples. Because the surface roughness of dust particles is likely important in determining their optical properties, in future work, the size dependence of the shape properties of dust particles should be considered. In addition, the relationship between water-soluble components of particles and their optical effects for dust and soot particles should be investigated. The transmission electron microscopy tomography imaging technique is expected to be useful for three-dimensional shape modeling of internal mixtures of such aerosols.

This work was supported by the Global Change Observation Mission-Climate (GCOM-C1) research project of the Japan Aerospace Exploration Agency (JAXA).

1 Yang, P. and K. N. Liou, 1996: Geometric-optics-integral-equation method for light scattering by nonspherical ice crystals, *Appl. Opt.* **35**, 6,568-6,584.
2 Masuda, K., H. Ishimoto, Y. Mano, 2012: Efficient method of computing a geometric optics integral for light scattering by nonspherical particles, Papers in *Meteorology and Geophysics*. **63**: 15-19.
3 Ishimoto, H., Y. Zaizen, A. Uchiyama, K. Masuda and Y. Mano, 2010: Shape modeling of mineral dust particles for light-scattering calculations using the spatial Poisson-Voronoi tessellation, *Journal of Quantitative Spectroscopy & Radiative Transfer*. **111**, 2,434-2,443.
4 Ohser, J. and F. Mücklich, 2000: Statistical analysis of microstructures in materials science, Chichester: John Wiley & Sons.
5 Mikhailov, E. and S. S. Vlasenko, 2006: Podgorny I A, Ramanathan V, Corrigan C E. Optical properties of soot-water drop agglomerates: *An experimental study, JGR*. **111**: D07209, doi: 10.1029/2005JD006389.
6 Ishimoto, H., 2008: Radar backscattering computations for fractal-shaped snowflakes, *Journal of the Meteorological Society of Japan*. **86**, 459-469.
7 Ishimoto, H., K. Masuda, Y. Mano, N. Orikasa and A. Uchiyama 2012: Irregularly shaped ice aggregates in optical modeling of convectively generated ice clouds, *Journal of Quantitative Spectroscopy & Radiative Transfer*. **113**, 632-643.
8 Nakajima, T. and M. Tanaka, 1986: Matrix formulations for the transfer of solar radiation in a plane-parallel scattering atmosphere, *Journal of Quantitative Spectroscopy & Radiative Transfer*. **35**, 13-21.

Single particle analysis of aerosols and cloud residues in the Arctic troposphere

Atsushi Matsuki[1,*], Alfons Schwarzenboeck[2], Boris Quennehen[2], Karine Deboudt[3], Guy Febvre[2], Olivier Jourdan[2], Christophe Gourbeyre[2] and Jean-François Gayet[2]

[1]Institute of Nature and Environmental Technology, Kanazawa University, Kakuma, Kanazawa, Ishikawa 920-1192, Japan
[2]LaMP, Université Blaise Pascal, Clermont-Ferrand II, 24 avenue des Landais 63171 Aubière, France
[3]LPCA, Université du Littoral Côte d'Opale, 189A avenue Maurice Schumann, 59140 Dunkerque, France

**Corresponding author. Tel.: +81 76 264 6510, Email address: matsuki@staff.kanazawa-u.ac.jp (A. Matsuki)*

The compositions of individual cloud residues and interstitial aerosol particles collected in northern Scandinavia during the POLARCAT 2008 spring campaign were investigated. Individual aerosol particles and residues from various clouds (ice, liquid, or mixed phase) extracted by an aircraft-borne counterflow virtual impactor were analyzed by both scanning and transmission electron microscopy systems equipped with energy dispersive X-ray detectors. Supermicrometer-sized residues of clouds containing ice crystals tended to be dominantly clay-like mineral dust, whereas marine particles were relatively more important within lower altitude, liquid-phase clouds, indicating distinctly different interactions of different particle types with Arctic clouds. Submicrometer-sized biomass burning (BB) particles (enriched in potassium and often internally mixed with soot) were characteristically found in polluted air masses in the Arctic troposphere. BB particles were also extracted from liquid-phase clouds, and less frequently from ice-phase clouds. In contrast, mineral dust, bare soot, fly ash, and K-rich marine particles dominated submicrometer-sized ice-phase cloud residues. These results suggest that BB particles may be efficient cloud condensation nuclei but their internal mixing can delay or inhibit the ice nucleating properties of bare soot particles. These results show that continental particles are actively transported to the Arctic, where they interact with Arctic clouds.

Keywords: Aerosol particles; Cloud residues; Single particle analysis; Aircraft; Cloud condensation nuclei; Ice nuclei

1. Introduction

In the past 100 years, average Arctic temperatures have been rising at almost twice the rate of temperatures in the rest of the world [1], and global circulation models agree that Arctic warming will continue to exceed the global mean warming [2]. High surface albedo in the Arctic region can amplify both the direct and indirect radiative effects of aerosols. Over the ice, even weakly absorbing aerosol layers can heat the Earth/atmosphere system [3], making the Arctic climate especially vulnerable to any changes in aerosol and cloud microphysical properties.

POLARCAT (POLar study using Aircraft, Remote sensing, surface measurements and modeling of Climate, chemistry, Aerosols and Transport) is an international program endorsed as part of the 4th International Polar Year (2007–2008), which aims to quantify the impact of trace gases, particulate aerosols, and heavy metals transported to the Arctic and their contribution to pollutant deposition and climate change in the region. The POLARCAT-France team used in situ aircraft measurements to better quantify the impact of aerosol particle properties on cloud characteristics in the Arctic during the spring 2008 campaign. The focus of this particular study is the detailed characterization of individual cloud residual and interstitial aerosol particles collected with an airborne counterflow virtual impactor (CVI) to provide insights into the cloud nucleating properties of Arctic aerosols.

2. Methods

The ATR-42 research aircraft was stationed at Kiruna airport (67°50′N, 20°20′E, 460 m a.m.s.l.) in northern Sweden from 30 March to 11 April 2008 during the POLARCAT-France spring measurement campaign. The aircraft made multiple level flights when cloud layers and pollution plumes were present in the low to mid troposphere (0.3–6 km). Tropospheric aerosol particles as well as residues from

various clouds (ice-, liquid-, or mixed-phase) extracted by the CVI were analyzed later in the laboratory on an individual particle basis by both scanning and transmission electron microscopy systems equipped with energy dispersive X-ray detectors (SEM- and TEM-EDX systems).

3. Results and discussion

Supermicrometer-sized residues of clouds containing ice crystals tended to be dominantly clay-like mineral dust, whereas marine particles were relatively more important within lower-altitude liquid-phase clouds, indicating distinctly different interactions of the different particle types with Arctic clouds.

Submicrometer-sized biomass burning (BB) particles (enriched in K and S and often internally mixed with soot) were characteristically found in polluted air masses in the Arctic troposphere (Figures 1 and 2). BB particles were primarily extracted from liquid-phase clouds and less frequently from ice-phase clouds. In contrast, mineral dust, bare soot, fly ash, and marine (sea salt, often enriched in K) particles dominated submicrometer-sized ice cloud residues. These results suggest that BB particles may be efficient cloud condensation nuclei (CCN) but that their internal mixing can delay or inhibit the ice nucleating properties of bare soot particles. These results show that continental particles are actively transported to the Arctic, where they interact with the Arctic clouds.

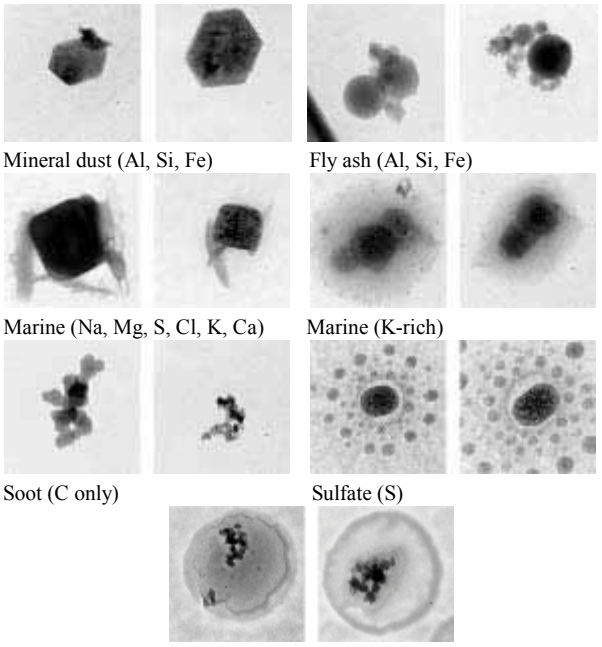

Figure 1 Representative TEM images of submicrometer-sized cloud residual and aerosol particles collected during the POLARCAT-France spring measurement campaign. Particle types were distinguished by their characteristic morphology and the elements detected by EDX. Each image is 500 nm wide.

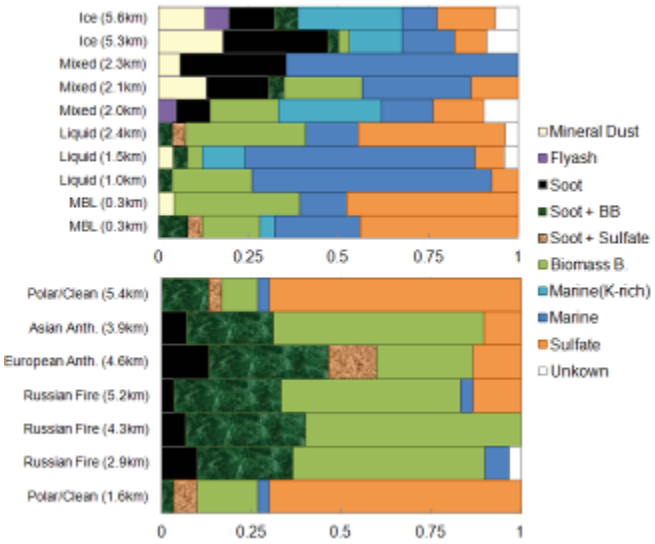

Figure 2 Relative abundance of particle types among submicrometer-sized cloud residues (ice, mixed, and liquid phases) and aerosols in the marine boundary layer (upper panel), following manual identification by TEM-EDX analysis. The particle types of free tropospheric aerosol particles collected under polluted and clean Arctic conditions [4] are also shown for comparison (lower panel).

The enrichment of marine particles in ice- and mixed-phase residues and the abundance of BB particles in interstitial aerosols found in this study are surprisingly consistent with the results of CRYSTAL-FACE experiments [5], which found a high abundance of sea salt in ice residues but a low quantity in interstitial aerosols. Conversely, the vast majority of interstitial aerosol particles, but not ice residues, were BB-related particles (those with mass spectral features of sulfates, K^+, organics, and NO^+). This similarity is striking considering the different analytical methods used and the different geographical settings (i.e., cirrus clouds at 13 km over Florida).

POLARCAT-France campaigns were funded by the French research agencies ANR, CNES, CNRS-INSU (LEFE-CHAT), IPEV, EUFAR, and CLIMSLIP-LEFE. Special thanks to SAFIRE for support during the planning and execution of the French ATR-42 campaigns, and to DT-INSU for help with the instrument integration.

1 Intergovernmental Panel on Climate Change, Climate Change 2007: The Physical Science Basis, in: Contribution of Working Group I to the Fourth Assessment Report of the Intergovernmental Panel on Climate Change, *Cambridge Univ. Press*. Cambridge, UK, 2007.

2 ACIA, 2004: Impacts of a Warming Arctic, Arctic Climate Impact Assessment, *Cambridge Univ. Press*.

3 Pueschel, R. F. and S. A. Kinne, 1995: Physical and radiative properties of Arctic atmospheric aerosols, *Sci. Total Environ.* **160/161**, 811-824.

4 Quennehen, B., A. Schwarzenboeck, A. Matsuki, J. F. Burkhart, A. Stohl, G. Ancellet and K. S. Law, 2012: Anthropogenic and forest fire pollution aerosol transported to the Arctic: observations from the POLARCAT-France spring campaign, *Atmos. Chem. Phys. Discuss.* **12**, 4,541-4,588.

5 Cziczo, D. J., D. M. Murphy, P. K. Hudson and D. S. Thomson, 2004: Single particle measurements of the chemical composition of cirrus ice residue during CRYSTAL-FACE., *J. Geophys. Res.*, **109**, D04201.

Determination of the aerosol direct effect over the East China Sea using ground-based remote sensing and aircraft observation data

Pradeep Khatri[1]*, Tamio Takamura[1], Akhiro Yamazaki[2], Yutaka Kondo[3], Atsushi Shimizu[4], and Nobuo Sugimoto[4]

[1]Center for Environmental Remote Sensing, Chiba University, 1-33 Yayoi, Inage, Chiba, Japan
[2] Meteorological Research Institute, 1-1 Nagamine, Tsukuba, Ibaraki 305-0052, Japan
[3]Department of Earth and Planetary Science, The University of Tokyo, 7-3-1 Hongo, Bunkyo, Tokyo 113-0033, Japan
[4]National Institute for Environmental Studies, 16-2 Onogawa, Tsukuba, Ibaraki 305-8506, Japan

Corresponding author. Tel.: +81 43 290 3869; Fax: +81 43 290 3857, Email address: pradeep.nep@gmail.com (P. Khatri)

Meteorological and aerosol data observed from aircraft over the East China Sea region as well as aerosol radiative parameters and surface irradiances observed by ground-based remote sensing instruments were input a radiative transfer model to study the vertical profiles of aerosol radiative forcing and the aerosol heating rate over the study region. The results showed that in spring, some aerosol layers above the boundary layer can have a strong heating effect comparable to that of aerosols within the boundary layer. This result suggests that aerosols above the boundary layer can have important effects on the atmospheric heat budget over the East China Sea region in spring.

Keywords: Aerosol particles; Aerosol optical thickness; Single scattering albedo; Aerosol radiative forcing

1. Introduction

Despite the important effects of East Asian aerosols on climate change, how those aerosols are linked with regional and global climate change, a major scientific question, is not well understood because of their spatial and temporal variations as well as the complexity of their physical, chemical, and optical characteristics. Efforts are being made by the scientific community to understand the characteristics of East Asian aerosols and their roles in the climate system. One important reason for the poor understanding of the direct and indirect effects of East Asian aerosols on climate is the inadequate understanding of the vertical profiles of aerosol optical parameters and aerosol radiative forcing. Widely used instruments for aerosol observation such as the Prede sky radiometer and the CIMEL sun photometer can provide information about only columnar aerosols, and lidar systems are capable of providing only limited information about the vertical profile of aerosols. The most important parameter for estimating aerosol radiative forcing, single scattering albedo (SSA), cannot be measured directly. Implementation of the vertical profiles of SSA and other radiative parameters in radiative transfer models is necessary for precise calculation of the aerosol direct effect. Aircraft observations are very useful for understanding the vertical distribution of aerosols and other atmospheric parameters. This study utilized simultaneous aircraft observation data and ground-based remote sensing data to investigate the vertical profiles of aerosol radiative parameters and the aerosol direct effect over the East China Sea in spring.

2. Data and study method

We used observation data collected at the Fukue-Jima Island (32.752°N, 128.682°E) on 30 March and 5 April 2009. Vertical profiles of black carbon concentration and relative humidity were observed by aircraft over Fukue-jima, and spectral aerosol optical thickness and SSA at wavelengths of 399.1, 499.0, 675.6, 870.6, and 1020.2 nm were retrieved by using spectral irradiances measured with an MS-700 spectroradiometer and the algorithm of Khatri et al. (2012: Ref. 1). Further, we used the spectral asymmetry parameter (ASY) retrieved by a sky radiometer (Manufacture: PREDE Co. Ltd., Japan, model: POM-02) as well as vertical profiles of the aerosol extinction coefficient and yellow sand index (YSI) at 532 nm measured by a lidar. YSI is defined as the contribution of non-spherical (dust) aerosol optical thickness to the total aerosol optical thickness [2].

By assuming that the three types of aerosols, namely water soluble, dust, and black carbon, were externally mixed, we derived the vertical profiles of the extinction coefficient, SSA, and ASY at the wavelengths of 399.1, 499.0, 675.6, 870.6, and 1020.2 nm in such a way that the integrated vertical profiles of those optical parameters would produce the best agreement with the columnar values measured at ground level by the MS-700 spectroradiometer and the sky radiometer. For this purpose, we used the optical data given in the Optical Properties of Aerosols and Clouds (OPAC) software [3]. Finally, vertical profiles of the extinction coefficient, SSA, and ASY as well as the columnar water vapor content measured by a microwave radiometer and surface reflectance measured by MODIS were input into the Santa Barbara DISORT atmospheric radiative transfer (SBDART) model [4] to estimate the vertical profiles of aerosol direct radiative forcing and of the heating rate.

3. Results and discussion

In Figure 1, the vertical profiles of heating rate caused by aerosol light absorption are shown for aircraft observation days of 30 March, 2009 (14.17JST) and 05 April, 2009(14.67 JST). Figure 1 shows that some aerosol layers within an altitude of 2-6 km have strong heating rates comparable to the aerosols near the surface. For the aerosols that have relatively high heating rate, we noted that YSI and SSA values were relatively higher and lower, respectively (not shown here).This indicates that such strong heating rates over the boundary layer were likely to be caused by the mixture of dust and light absorbing aerosols. This result indicates that strongly light absorbing aerosols can be transported by dust aerosols at altitudes above the boundary layer in the spring season. Backward trajectories were used to trace the paths for aerosols on those layers. Backward trajectory analyses also emphasized that such light absorbing aerosol layers above the boundary layer were likely due to the mixture of aerosols transported from the desert and urban areas.

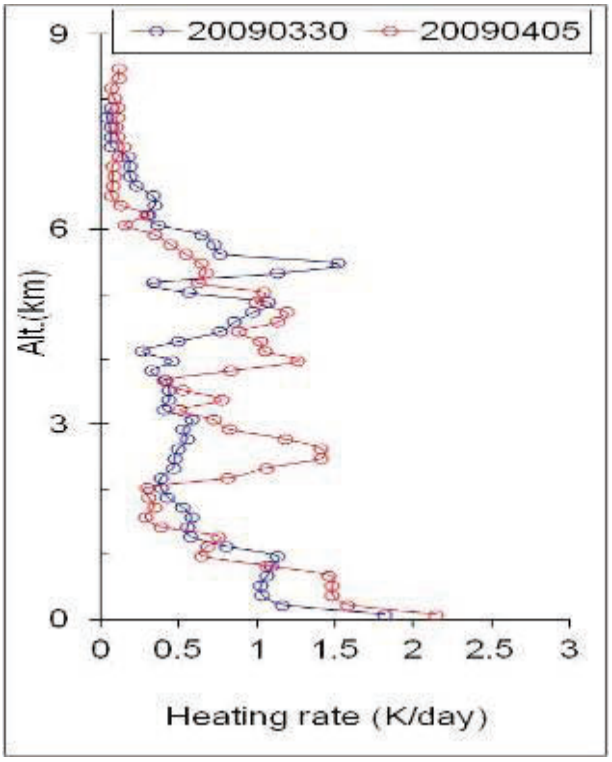

Figure 1 Vertical profiles of the heating rate due to aerosol absorption over Fukue-jima on 30 March 2009 (14.17 JST) and 05 April (14.67 JST) 2009. The vertical profiles were calculated from a combination of aircraft, lidar, and surface observation data.

1 Khatri, P., A. Yamazaki and Y. Kondo, 2012: Retrieval of key aerosol optical parameters from spectral direct and diffuse irradiances measured by a radiometer with nonideal cosine response characteristics, *J. Atmos. Oceanic Technol.*(in press)

2 Takamura, T., N. Sugimoto, A. Shimizu, A. Uchiyama, A. Yamazaki, K. Aoki, T. Nakajima, B. J. Sohn and H. Takenaka, 2007: Aerosol radiative characteristics at Gosan, Korea, during the Atmospheric Brown Cloud East Asian Regional Experiment 2005, *J. Geophys. Res.*,**112**, D22S36, doi: 10.1029/2007JD008506

3 Hess, M., P. Koepke and I. Schult, 1998: Optical Properties of Aerosols and Clouds: The software package OPAC, *Bull. Am. Met. Soc*., **79**, 831-844

4 Ricchiazzi, P., S. Yang, C. Gautier and D. Sowle, 1998: SBDART: A research and teaching software tool for plane-parallel radiative transfer in the Earth's atmosphere. *Bull. Amer. Meteor. Soc*., **79**, 2,101-2,114.

Particle effective density measurement using a DMA-APM-CPC system in Nagoya, Japan: Estimation of mixing state and shape

Tomoki Nakayama[1,*], Yuuki Sawada[1], Yuka Ikeda[1], Yutaka Matsumi[1], Yoshitaka Setoguchi[2], Kaori Kawana[2] and Michihiro Mochida[2]

[1]Solar-Terrestrial Environment Laboratory and Graduate School of Science, Nagoya University, Furo-cho, Chikusa-ku, Nagoya 464-8601, Japan
[2] Graduate School of Environmental Studies, Nagoya University, Furo-cho, Chikusa-ku, Nagoya 464-8601, Japan

Corresponding author. Tel.: +81 52 747 6413; Fax: +81 52 789 5787, Email address: nakayama@stelab.nagoya-u.ac.jp (T. Nakayama)

Simultaneous observations of particle density distributions and chemical properties of ambient aerosols were conducted at an urban site in Nagoya, Japan, during summer, by a system consisting of a differential mobility analyzer, an aerosol particle mass analyzer, and a condensation particle counter, and a time-of-flight aerosol mass spectrometer. Bimodal effective density distributions consisting of non-volatile black carbon particles and volatile compounds such as organics and sulfate were observed. Temporal variations of effective densities were found to be related to chemical composition. From the effective density distributions with and without heating, relative abundance of externally mixed soot particles was also estimated.

Keywords: Particle density distribution; Mixing state; Chemical property, Aerosol particle mass analyzer (APM); Time of flight aerosol mass spectrometer (ToF-AMS); Ambient measurement

1. Introduction

Tropospheric aerosols are a complex mixture, including mineral dust, inorganic salts, organic compounds, and soot particles. The climate impact of aerosols depends on their physical and chemical properties such as size, shape, density, mixing state, and chemical composition. Therefore, accurate knowledge of these properties is essential for modeling climate forcing by aerosols.

Particle density is an important parameter that links particle mass and particle volume (or diameter). However, detailed knowledge of the density distributions of ambient particles is still limited [e.g. 1-3], because filter-based techniques can provide only average densities of internally and externally mixed particles.

In this work, real-time measurements of effective density distributions and chemical properties of ambient particles were made at an urban site in Nagoya, Japan, and the relationship between them was examined. In addition, the mixing state of the aerosols, another important parameter for determining optical properties, was also estimated by using the measured particle density distributions.

2. Methods

Observations of aerosol density distributions and chemical properties were conducted on 16–25 August 2011 at the Higashiyama campus of Nagoya University. A schematic diagram of the experimental setup used for the ambient measurements is shown in Figure 1. The effective density of particles with mobility diameters of 100 and 200 nm was measured by a system consisting of a differential mobility analyzer (DMA, TSI model 3081), an aerosol particle mass analyzer (APM, Kanomax model 3601), and a condensation particle counter (CPC TSI, model 3776).

Nearly monodisperse aerosols were selected by the DMA, which was upstream of the APM. The APM then transmitted particles of known mass, determined by the balance of

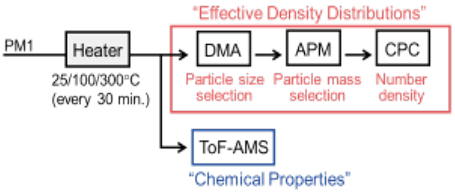

Figure 1 The experimental setup.

centrifugal and electrostatic forces, to the CPC, which was connected downstream of the APM and which counted the particles selected by the APM. By scanning the APM voltage with a fixed rotational velocity, the effective density distributions of the ambient particles were then determined [1].

Chemical compositions of the aerosol were measured by a time-of-flight aerosol mass spectrometer (ToF-AMS, Aerodyne). The density distributions and chemical compositions were measured after the aerosol had passed through a PM1 cyclone, diffusion dryers, and one of three heaters, controlled at 25, 100, and 300 °C, by switching ball valves every 30 min.

3. Results and discussion

The ambient aerosols typically had two distinct density peaks, at 0.7–0.9 g/cm^3 (peak 1) and 1.2–1.6 g/cm^3 (peak 2) (Figure 2). The changes in the peak areas after heating implied that peak 1 and peak 2 consisted mainly of soot and volatile compounds (such as inorganic salts and organics), respectively.

Observation data were divided into three periods on the basis of particle chemical properties and the observed meteorological conditions: A, 00:00 16 August to 06:00 20 August; B, 06:00 20 August to 12:00 22 August; and C 12:00 22 August to 06:00 25 August. These periods were characterized as follows: period A, increased mass concentration of organics and of the low-volatility oxygenated organic aerosol (LV-OOA) fraction during the afternoon (12:00–18:00) accompanied by clear weather conditions;

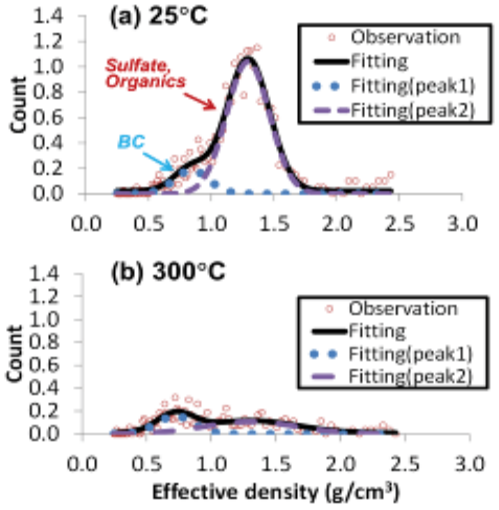

Figure 2 Average density distributions of ambient particles with a mobility diameter of 100 nm observed at an inlet temperature of (a) 25 °C and (b) 300 °C at 6:00–18:00 on 21 August 2011.

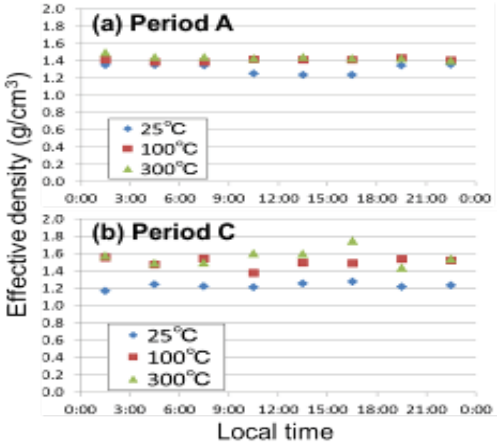

Figure 3 Diurnal variations of the average effective density of peak 2 during periods (a) A and (b) C (mobility diameter, 100 nm).

period B, lower abundance of volatile compounds (organics and inorganics) associated with rainfall; period C, higher sulfate/organics ratio (typically >2).

Analysis of the diurnal variation of the effective density of peak 2 during these periods (examples shown in Figure 3) showed that during period A, the effective density at 25 °C decreased during the afternoon (12:00–18:00), whereas no significant diurnal variations of effective density were observed at 100 °C or 300 °C. This result may be attributable to higher contributions of photochemically generated LV-OOA during the afternoon, because LV-OOA possibly has a relatively lower density. During period C, a larger difference in effective density was observed between 25 °C and 100 °C, which may be due to a higher contribution of sulfate during that period, because sulfate has a higher density and volatilization temperature than organics.

The peak area ratio of peak 1 to the sum of the areas of peak 1 and peak 2 gives information about the relative abundance of externally mixed black carbon (BC) particles. The ratio typically was between 0.05 and 0.15 at 25 °C for particles with a diameter of 100 as well as those with a diameter of 200 nm. The absolute peak area of peak 1 tended to increase after heating. This result implies that at 25 °C some of the BC particles were internally mixed with volatile compounds.

This work was partly supported by the Global Environment Research Fund of the Japanese Ministry of the Environment (RF-1008) and the Ministry of Education, Culture, Sports, Science and Technology (KAKENHI 20671001, 21710007, 22310015, 20120007).

1 McMarry, P. H., X. Wang, K. Park and K. Ehara, 2002: The relationship between mass and mobility for atmospheric particles: A new technique for measuring particle density, *Aerosol Sci Technol*. **36**: 227-238

2 Geller, M., S. Biswas and C. Sioutas, 2006: Determination of particle effective density in urban environments with a differential mobility analyzer and aerosol particle mass analyzer. *Aerosol Sci Technol*. **40**: 709-723

3 Spencer, M. T., L. G. Shields, K. Shields and A. Shields, 2007: Simultaneous measurement of the effective density and chemical composition of ambient aerosol particles. *Environ Sci Technol*. **41**, 1,303-1,309

Measurements of light absorption enhancement of black carbon using a photoacoustic spectrometer in Nagoya, Japan

Tomoki Nakayama[1,*], Yuka Ikeda[1], Yuuki Sawada[1], Yutaka Matsumi[1], Yoshitaka Setoguchi[2], Kaori Kawana[2] and Michihiro Mochida[2]

[1]Solar-Terrestrial Environment Laboratory and Graduate School of Science, Nagoya University, Furo-cho, Chikusa-ku, Nagoya 464-8601, Japan
[2]Graduate School of Environmental Studies, Nagoya University, Furo-cho, Chikusa-ku, Nagoya 464-8601, Japan

Corresponding author. Tel.: +81 52 747 6413; Fax: +81 52 789 5787, Email address: nakayama@stelab.nagoya-u.ac.jp (T. Nakayama)

Simultaneous observations of optical and chemical properties of ambient aerosols were conducted at an urban site in Nagoya, Japan, during summer by using a multi-wavelength photoacoustic spectrometer and a time-of-flight aerosol mass spectrometer. By comparing absorption coefficients at 781 nm with and without heating (300 °C), the increase in BC light absorption due to particle coating was estimated to be 10–40%. A slightly larger amplification factor was observed when the sulfate/organics ratio was high. The contribution to light absorption of organic carbon, which is vaporized at 300 °C, was small (<5%) at 405 nm, at least during the summer at Nagoya.

Keywords: Aerosol optical properties; Chemical properties; Absorption enhancement; Light absorbing organic carbon; Photoacoustic spectroscopy (PAS); Time-of-flight aerosol mass spectrometer (ToF-AMS); Ambient measurement

1. Introduction

Aerosol particles play an important role in the radiation balance in the atmosphere by absorbing and scattering incident light. Black carbon (BC) particles are an important global warming agent with radiation forcing similar in magnitude to that of CO_2. Light absorption by BC is generally considered to be increased by internal mixing with other compounds, but the amount of absorption enhancement depends on factors such as the refractive index of the BC and the coating materials and the size and location of the BC core. In addition, light-absorbing organic carbon ("brown carbon"), including humic-like substances (HULIS), organonitrates, and nitro-aromatics, has recently been proposed to be a cause of substantial absorption, particularly in the shorter visible and UV wavelengths. However, observational studies of the enhancement of BC light absorption and of brown carbon are still limited, mainly because it is difficult to directly measure light absorption by internally mixed BC particles without collecting them on a filter [1, 2].

In this work, photoacoustic spectroscopy was applied to examine light absorption enhancement of BC and the contribution of brown carbon to aerosol light absorption at an urban site in Nagoya, Japan.

2. Methods

Observations of aerosol optical and chemical properties were conducted during 16–25 August 2011 at the Higashiyama campus of Nagoya University. A schematic diagram of the experimental setup is shown in Figure 1. The optical properties and chemical compositions were measured after the aerosols were passed through a PM1 cyclone, diffusion dryers, and one of three heaters, controlled at 25, 100, and 300 °C, by switching ball valves every 30 min. Optical properties were measured using a photoacoustic soot spectrometer (PASS-3, Droplet Measurement Technologies). Chemical composition of the aerosol was measured by a time-of-flight aerosol mass spectrometer (ToF-AMS, Aerodyne). Mass concentrations of elemental carbon (EC) and organic carbon (OC) were also measured by a thermo-optical technique (Sunset Lab.) every 90 min.

3. Results and discussion

Observation data were divided into three periods on the basis of particle chemistry and meteorological conditions: A 23:00 15 August to 12:00 19 August; B, 12:00 19 August to12:00 22 August; and C, 12:00 22 August to 06:00 25 August. These periods were characterized as follows: period

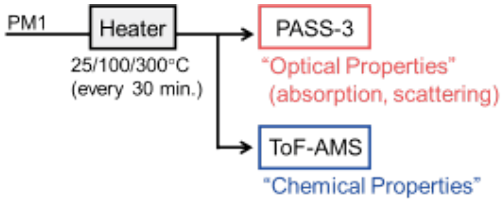

Figure 1 The experimental setup.

A, increased mass concentration of organics and of the low-volatility oxygenated organic aerosol fraction during the afternoon accompanied by clear weather conditions; period B, lower abundance of volatile compounds (organics and inorganics) associated with rainfall; and period C, higher sulfate/organics ratio (typically > 2), possibly due to long-range transport of sulfate.

Changes in the inlet temperature from 25 °C to 300 °C led to a slight decrease in the absorption coefficient ($b_{abs}(\lambda)$), but a significant decrease in the scattering coefficient ($b_{sca}(\lambda)$). As a result, small single scattering albedo (SSA; $b_{sca}(\lambda)/(b_{abs}(\lambda) + b_{sca}(\lambda))$) values of around 0.4 were observed at 300 °C (Figure 2). The ToF-AMS data showed that sulfate, nitrate, and a large part of the organics were volatized at the inlet temperature of 300 °C. These results suggest that the observed optical properties at 300 °C are mainly due to non-volatile BC particles.

Relatively smaller SSA values at 25 °C were observed during period B, when smaller mass concentrations of volatile compositions such as sulfate and organics were observed. These results may be explained by the hypothesis that lower photochemical activities due to a stationary front suppressed secondary formation of aerosols containing sulfate and organics, and resulted in larger contributions by light-absorbing BC particles during the period.

The amplification factor (F_A), which represents enhancement of light absorption by BC due to its coating, is calculated under the assumption that light absorption by OC is negligible at 781 nm as follows.

$$F_A = b_{abs}(781\ \text{nm}, 25\ °\text{C}) / b_{abs}(781\ \text{nm}, 300\ °\text{C}) \qquad (1)$$

Average F_A ($\pm 1\sigma$) (Figure 3a) during periods A, B, and C was 1.22 ± 0.16, 1.26 ± 0.14, and 1.29 ± 0.13, respectively. Although average F_A during period C, when the contributions of sulfate were large, was slightly higher than that during the other two periods, the small difference in F_A among the three periods suggests that the degree of enhancement of light absorption by BC due to its coating did not significantly depend on photochemical activities and aging processes in this observation.

The absorption coefficient of OC at 405 nm ($b_{abs,OC}$(405 nm, 25 °C)) was calculated under the assumption that F_A does not depend on wavelength as follows.

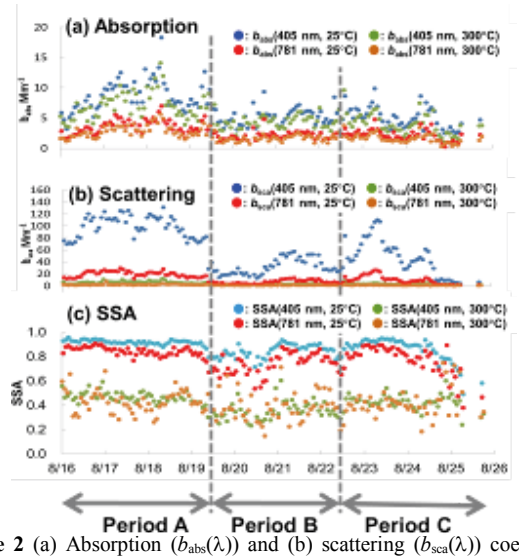

Figure 2 (a) Absorption ($b_{abs}(\lambda)$) and (b) scattering ($b_{sca}(\lambda)$) coefficients and (c) single scattering albedo (SSA; $b_{sca}(\lambda)/(b_{abs}(\lambda)+ b_{sca}(\lambda))$) at 405 and 781 nm measured at the inlet temperature of 25 °C and 300 °C. All data are 30-min averages.

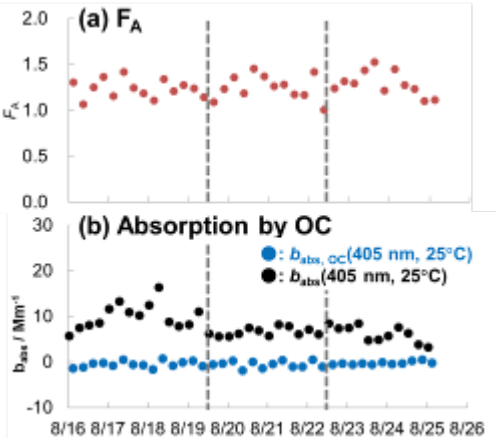

Figure 3 (a) Amplification factor (F_A) calculated with eq. (1) and (b) absorption coefficients for OC at 405 nm calculated with eq. (2) (see text). All data are 6-h averages.

$$b_{abs,OC}(405\ \text{nm}, 25\ °\text{C}) = b_{abs}(405\ \text{nm}, 25\ °\text{C}) - F_A \times b_{abs}(405\ \text{nm}, 300\ °\text{C}) \qquad (2)$$

The calculated $b_{abs,OC}$ values and the observed total aerosol light absorption at 405 nm show that the contribution of light absorption by OC, which is vaporized at 300 °C, was small (<5%) at 405 nm, at least during summer at Nagoya (Figure 3b).

This work was partly supported by the Global Environment Research Fund of the Japanese Ministry of the Environment (RF-1008) and the Ministry of Education, Culture, Sports, Science and Technology (KAKENHI 20671001, 21710007, 22310015, 20120007).

1 Flowers, B. A., M. K. Dubey, C. Mazzoleni, et al. 2010: Optical-chemical-microphysical relationships and closure studies for mixed carbonaceous aerosols observed at Jeju Island; 3-laser Photoacoustic spectrometer, particle sizing, and filter analysis, *Atmos Chem Phys*. **10**, 10,387-10,398.
2 Lack, D. A., M. S. Richardson, D. Law, et al. 2012: Aircraft instrument for comprehensive characterization of aerosol optical properties, Part 2: Black and brown carbon absorption and absorption enhancement measured with photoacoustic spectroscopy, *Aerosol Sci Technol*. **46**, 555-568.

Changes in chemical compositions of sea-salt particles collected at Mt. Rokko, Kobe, Japan

Shohei Mukai[1,*] and Ken'ichi Ohkushi[1]

[1]The Graduate School of Human Development and Environment, Kobe University, 3-11 Tsurukabuto, Nada-ku, Kobe 657-8501, Japan

Corresponding author. Email address: mukaishohei76@gmail.com (S. Mukai)

We collected aerosol particles at the summit of Mt. Rokko, Kobe, Japan, at 15:00 JST every day for one month from 31 July to 1 September 2011, and analyzed a total of 21 aerosol samples with a transmission electron microscopy system equipped with an energy-dispersive X-ray analyzer. Various aerosol particles having different chemical compositions were identified. In particular, the chemical compositions of sea-salt particles differed from that of typical seawater. We focused on four sea-salt particles from two samples. The amount of Cl varied with the sampling day, and the Na to Mg ratio in sea-salt particles differed from that of seawater.

Keywords: Aerosol particles; Sea-salt particles; Elemental composition; Single particle analysis; Electron microscopy; Chemical compositions; Electron micrograph

1. Introduction

Kobe city, including Mt. Rokko, is located in the northwestern part of the Kansai urban region, the second-most populated urban area in Japan. Kansai is also an active industrial region, where many studies of aerosol particles have been carried out. For example, Adachi (2006: Ref. 1) analyzed dry deposition of particles in winter and Iwasaki et al. (2007: Ref. 2) analyzed morphologies and chemical compositions of aerosol particles during Asian and non-Asian dust-storm events. Both these studies used scanning electron microscopy along with energy-dispersive X-ray analysis (SEM-EDX). Furthermore, Aikawa et al. (2003: Ref. 3) showed by a bulk analysis that aerosol particles were present during fog events at Mt. Rokko. Despite the many studies conducted in this region, single aerosol particles in summer have not been analyzed, even though single-particle analyses are an important method for obtaining basic information about the morphology and chemical composition of aerosol particles. The purpose of this study was to investigate the basic characteristics of aerosol particles sampled on Mt. Rokko in summer. Here we examine individual sea-salt particles obtained on Mt. Rokko in summer 2011 by transmission electron microscopy (TEM)-EDX.

2. Methods

Aerosol samples were collected at the summit of Mt. Rokko (34°77′N, 130°20′E, 931 m above sea level), Kobe, Japan (Figure 1), daily from 31 July to 1 September 2011 (except on 17, 25, 27, and 28 August). Aerosol samples were collected by a cascade impactor (model I-1L, PIXI International Corp.) with two stages having aerodynamic 50% cut off diameter of 1.0 and 8.0 μm. We used particles collected on the 1.0-μm-diameter stage. Samples were collected for 5 minutes beginning at 15:00 JST on each day.

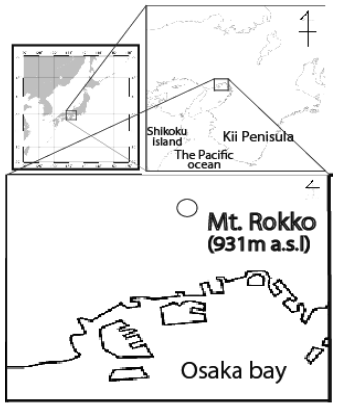

Figure 1 Location of the sampling site.

We chose two samples, one collected on 7 August and the other on 1 September, for analysis. Electron micrographs of aerosol particles were obtained by TEM (JEM-2010, JEOL Ltd.), and their chemical compositions were determined by EDS analysis (JED-2300T, JEOL Ltd.), conducted using an acceleration voltage of 200 kV and an EDX collection time of 30 s.

3. Results and discussion

Several hundred aerosol particles were captured on each grid on each of the two days, and many of them were sea-salt particles. We focused on four sea-salt particles and examined their features on electron micrographs (Figure 2) and ternary diagrams of their Na, S, and Cl contents (Figure 3).

On the ternary diagram, we also plotted the compositions of standard seawater and $NaNO_3$ and Na_2SO_4, which were generated by reacting sea-salt particles with HNO_3 and H_2SO_4, respectively, until they were completed depleted in Cl. Particles (a), (b), and (c) showed strong Cl depletion, but the Na/Cl ratio of particle (d) was similar to that of pure seawater (Figure 3). Thus, although these samples were collected at the same location and their morphologies were similar (Figure 2), their compositions differed greatly.

Many studies have investigated the modification of sea-salt particles in aerosols. For example, Li et al. (2003: Ref. 4) examined sea-salt particles collected over the North Atlantic and suggested that Cl modification occurred by chemical reactions with anthropogenic compounds such as sulfate and nitrate, and Kawakami et al. (2008: Ref. 5) suggested that the degree of modification depends on wind speed. An industrial area with a high population is situated south of our sampling site. The compositional differences among these samples may therefore reflect differences in the transport route and wind speed.

We also compared the relationship between Na and Mg in the four particles with that in seawater (Figure 4). The Na/Mg ratios of particles (b), (c), and (d) differed from the seawater ratio, whereas the ratio in particle (a) was almost the same as the seawater ratio. Thus, although Na/Cl in particle (d) was the same as that of seawater (Figure 3), its Na/Mg ratio differed. The particles of both samples were representative of aerosol particles collected at Mt. Rokko, where a wide range of Na and Mg contents is observed, possibly reflecting the influence of anthropogenic materials. Future studies are needed to understand urban atmospheric chemical processes over Kansai.

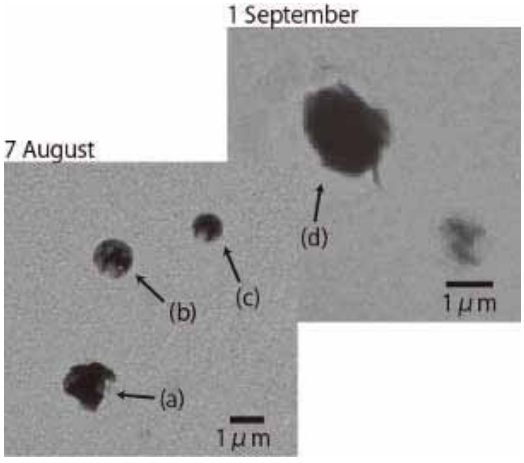

Figure 2 Photomicrographs of sea-salt particles collected on 7 August and 1 September..

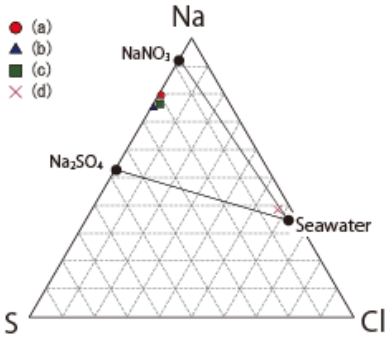

Figure 3 Ternary diagram of Na, S, and Cl. Na_2SO_4 and $NaNO_3$ were generated by reacting sea-salt particles with H_2SO_4 and HNO_3, respectively. See Figure 2 for the micrographs of particles (a), (b), (c), and (d).

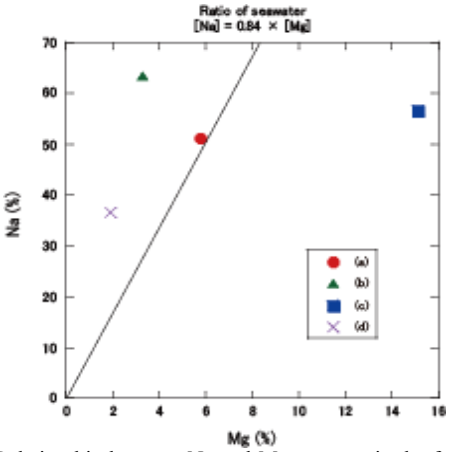

Figure 4 Relationship between Na and Mg contents in the four particles. The line on the graph shows the seawater ratio.

We thank K. Adachi (MRI), T. Hiraki (Hyogo Pref.), Y. Terakado, M. Iwasaki (Kobe Univ.), and K. Osada (Nagoya Univ.) for their help and support.

1 Adachi, K., 2006: Characterization of atmospheric dry deposition in Kobe, *Japan, Chemosphere*, **64**, 1,311-1,317.

2 Iwasaki, M., Y. Yagi and Y. Tainosho, 2007: Single particle analysis of atmospheric particulate matters collected in Kobe city at April and September, *J. Jap. Soc. Atmos. Environ*. **42**, 200-207 (in Japanese).

3 Aikawa, M., Hiraki, T., & Tamaki, M. (2006) Comparative field study on precipitation, throughfall, stemflow, fog water, and atmospheric aerosol and gases at urban and rural sites in Japan. *Science of the Total Environment,* **366**(1), 275-85. doi: 10.1016/j.scitotenv.2005.06.027.

4 Li, J., J. R. Anderson and P. R. Buseck, 2003: TEM study of aerosol particles from clean and polluted marine boundary layers over the North Atlantic. *Journal of Geophysical Research*, **108**(D6). doi: 10.1029/2002JD002106.

5 Kawakami, N., K. Osada, C. Nishita, M. Yabuki, H. Kobayashi, K. Hara and M. Shiobara, 2008: Factors controlling sea salt modification and dry deposition of nonsea-salt components to the ocean. *Journal of Geophysical Research*. **113**(D14), 1-13. doi:10.1029/2007JD

Laser post-ionization mass spectrometry of PAHs on diesel soot particles

Kenji Ohishi[1], Norihito Mayama[1,2], Kana Kitatsugu[2], Kentaro Misawa[2], Tetsuo Sakamoto[1] and Masaaki Fujii[2]

[1]Department of Electrical Engineering, Kogakuin University, 2665-1, Nakano-cho, Hachioji-City, Tokyo 192-0015, Japan
[2]Chemical Resources Laboratory, Tokyo Institute of Technology, 4259 Nagatsuta-cho, Midori-ku, Yokohama 226-8503, Japan

**Corresponding author. Tel.: & Fax: +81 42 628 4872; Email address: kt13222@ns.kogakuin.ac.jp (K. Ohishi)*

Polycyclic aromatic hydrocarbons (PAHs), which are found in diesel soot and suspended particulate matter, are well known to be harmful to human health. Pi-conjugated organic materials such as PAHs absorb photons in the ultraviolet light range. Here, we detected PAHs on diesel soot particles, chosen as suitable real environmental samples to demonstrate single-particle analysis by gallium focused ion beam time-of-flight secondary ion mass spectrometry (Ga-FIB-TOF-SIMS) and laser systems, including laser post-ionization sputtered neutral mass spectrometry. We optimized the Ga-FIB-TOF-SIMS apparatus to keep the sample at a low temperature of about 170 K to suppress the evaporation of PAHs from the sample, and for the laser post-ionization mass spectrometry, the apparatus incorporated a new optical system that allowed the focus to be adjusted by moving the laser and the lens in parallel in order for laser light to be accessible to the nearer point sputtered by FIB.

Keywords: Laser-SNMS; REMPI; Diesel soot; SPM; PAHs; Asian dust; Kosa; Single particle analyzer;

1. Introduction

Several kinds of polycyclic aromatic hydrocarbons (PAHs) are found on diesel soot particles, Asian dust "*Kosa*", and suspended particulate matter that are transported long distances. Because PAHs are well known to be harmful to human health, it is important to understand the long-range transport of Asian dust to study the internal and external mixing states of individual particles with inorganic and/or organic materials.

Our single-particle analyzer [1, 2] uses gallium focused ion beam time-of-flight secondary ion mass spectrometry (Ga-FIB-TOF-SIMS) and several laser systems. The combination of laser-induced resonance-enhanced multi-photon ionization (REMPI), laser post-ionization sputtered neutral mass spectrometry (laser-SNMS), and TOF mass spectrometry allows several highly selective and sensitive analytical techniques to be applied. To increase the sensitivity and selectivity of the analysis, sputtered neutral particles are post-ionized by irradiating them with an electron beam or photon field. Many experiments have been carried out with this system on inorganic and organic materials [3-7].

For REMPI and laser-SNMS experiments, the laser focus position, shape, and input energy are important for ionizing and detecting the materials with high sensitivity. In general, laser light is focused by a cylindrical or positive lens, but to move the focus point parallel in both vertical and horizontal directions along the optical beam axis, a system with a new type of focus lens and a movable light axis is needed to control the focus position.

In this paper, we report on optimizations of our apparatus for detection of PAHs, and we show an example of its use for detection of PAHs on diesel soot.

2. Experiment

Figure 1 shows our single-particle analyzer, which consists of a Ga-FIB-TOF-SIMS apparatus and laser systems, including a laser-SNMS system. To optimize the apparatus and suppress the evaporation of PAHs from the diesel soot sample, we modified the system so that it would keep the sample cool at about –100 °C (~170 K) by lowering the pressure in the chamber from atmospheric pressure to ultra-high vacuum pressure.

For laser post-ionization mass spectrometry, the handling of the laser light is very important. Many similar apparatuses have a simple positive lens or a cylindrical lens for focusing the laser light on the sample stage. We designed a new optical system that enabled us to move the focus point of the laser and the lens in parallel (Figure 2). We selected

laser light with a wavelength of 266 nm, and used a 266-nm pulsed laser beam timed to coincide with the FIB. Because PAHs have a pi-conjugated system, most PAH molecules are ionized by 1-color 2-photon process after they are sputtered by the FIB and have absorbed at least two photons during their exposure to the 266 nm laser light. As a result, it is possible to analyze PAHs by TOF-MS. In this study, we analyzed diesel soot particles by laser-SNMS.

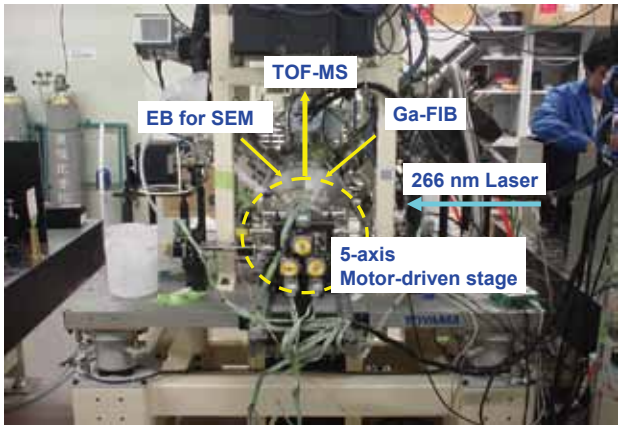

Figure 1 Instruments of time-of-fight secondary ion mass spectrometry and YAG + dye laser system. Repetition rate 30 Hz, pulse energy ~5mJ. TOF-MS: time-of-flight mass spectrometer, EB for SEM: electro beam for scanning electron microscope, Ga-FIB: gallium focused ion beam.

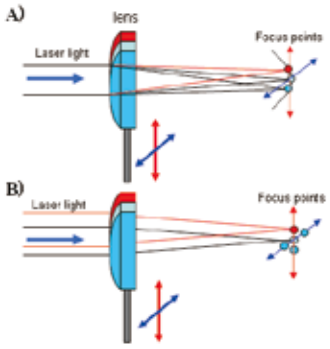

Figure 2 (Left): Diesel soot on the indium plate. The diesel soot was pressed on the flat indium plate and set in the sample stage. The sample was cooled below 170 K in the load lock chamber using liquid nitrogen. (Right): A) Old type focus shifter. The optical beam axis is fixed, and only the lens is moved. Therefore, in changing the focus horizontally and vertically, old type focus shifter moves the focal point to back and forth. B) New optical parallel axis and focus shifter. In front of the lens, the laser beam can be moved parallelly, horizontally and vertically. Also, the lens on the motor stage is simultaneously moved parallel to the laser. So this shifter keeps focal point no swingable back and forth for the area sputtered by FIB.

We chose diesel soot particles as a suitable real environmental sample to use as an example. The sample was collected from a diesel bus exhaust pipe with a diesel particulate filter (DPF). Several milligrams of diesel soot particles were pressed onto an indium metal substrate.

In the case of non-conductive materials, such as diesel soot, charge-up is caused by bombardment of the Ga-FIB; therefore, a low-energy electron gun for charge neutralization was also used to compensate for the charge-up. In addition, PAHs have a vapor pressure of several kilopascals (kPa). Injection of the PAH sample into the system at room temperature would cause the PAHs to evaporate from the sample. Therefore, to suppress the evaporation of PAHs, the sample was cooled by using liquid nitrogen under ultra-high vacuum pressure.

3. Results and discussion

Laser-SNMS analysis performed with the apparatus modified to incorporate a sample cooling system and an optical parallel axis and focus shifter successfully detected PAHs on diesel soot (Figure 3). The mass-to-charge (*m/z*) ratios of PAHs with 3 or 4 rings were detected, but not those of PAHs with 5 or more rings.

In previous other experiments, pyrene and benzopyrene were found to coexist in diesel soot, but the molar ratios of pyrene and benzopyrene drastically changed at the different emission patterns [8]. Our result shows that benzopyrene quite probably was caught in the DPF or the emission pattern of diesel engine was very low. We did not identify benzopyrene on laser-SNMS spectra obtained by several analyses of diesel exhaust soot.

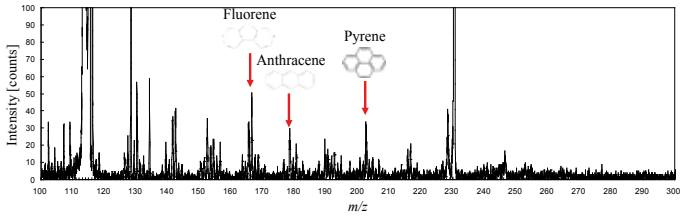

Figure 3 Laser post ionization mass spectrum of PAHs on diesel soot. The results suggest the mass-to-charge ratio values (*m/z*) is several PAHs detected in diesel soot by laser post-ionization mass spectrometry.

This research was supported by the Environment Research and Technology Development Fund (number B-1006), Ministry of the Environment, Japan.

1 Sakamoto, T., et al. 2008: *Applied Surface Science*, **255**(4), 1,617-1,620.
2 Koizumi, M., et al. 2008 : *Applied Surface Science*. **255**(4), 901-904
3 Wucher, A., J.C. Vickerman and D. Briggs (Eds.), 2001: ToF-SIMS: Surface Analysis by Mass Spectrometry, *IM Publications,* p .347.
4 Mazarov, P., A.V. Samartsev and A. Wucher, 2006: *Appl. Surf. Sci*. **252**, 6,452.
5 King, B.V., J.F. Moore, W.F. Calaway, I.V. Veryovkin and M.J. Pellin, 2006: *Appl. Surf. Sci*. **252**, 6,426.
6 Peterson, R.E., et al. 2006 : *Appl. Surf. Sci*. **252**, 7006.
7 Samartsev A.V. and A. Wucher, 2006: *Appl. Surf.* Sci. **252**, 6470.
8 Ji Yi Lee, et al. 2006 : *J. Geophys. Res.* **111**, D11303.

Analysis of black carbon particles by high-resolution TOF-SIMS

Norihito Mayama[1, 2,*], Yusuke Miura[2], Kenji Ohishi[2], Tetsuo Sakamoto[2] and Masaaki Fujii[1]

[1]Chemical Resources Laboratory, Tokyo Institute of Technology, 4259 Nagatsuta-cho, Midori-ku, Yokohama, Kanagawa 226-8503, Japan
[2]Department of Electrical Engineering, Kougakuin University, 2665-1 Nakano-machi, Hachioji, Tokyo 192-0015, Japan

Corresponding author. Tel.: +81 42 628 4872, Email address: mayama.n.aa@m.titech.ac.jp (N. Mayama)

We analyzed particles containing black carbon by time-of-flight secondary ion mass spectrometry with a high lateral resolution. After sulfate particles with a diameter of about 1 μm were sputtered by gallium primary ions (a gallium focused ion beam), solid materials with a diameter of about 100 nm were sometimes found within the particles. Since the mass spectrum for the solid material was almost the same as that of graphite, we concluded that the solids might be black carbon. Furthermore, we inferred a possible structure from the results, in which black carbon occurred at one edge of sulfates, and the sulfates were usually surrounded by organic matter.

Keywords: Black carbon; Aerosol particles; Time-of-flight secondary ion mass spectrometer; Single-particle analysis; Focused ion beam; Mass spectrum

1. Introduction

Black carbon, which is emitted by incomplete combustion of fossil fuel, biofuel, and biomass carbon, is a major contributor to global warming because in the air it absorbs solar radiation. Aerosol particles containing black carbon are typically aggregated carbonaceous spherules a few tens of nanometers in diameter that are coated with sulfates and/or organic matter. It is important to know the structure and composition of these particles for use in climate simulations [1]. Because of the small size of black carbon, transmission electron microscopy (TEM), electron energy-loss spectroscopy (TEM-EELS), and energy dispersive X-ray spectroscopy (EDX) [2] are most often used for their analysis. However, the structures of aerosol particles containing black carbon and the composition of the coating materials have yet to be clarified.

We developed a time-of-flight secondary ion mass spectroscopy (TOF-SIMS) system with high lateral resolution [3]. The apparatus can analyze single aerosol particles with the high lateral resolution of 40 nm, and a cross-section of the particle can be fabricated by using a gallium focused ion beam (FIB). Individual aerosol particles have already been analyzed with the apparatus to clarify their chemical reactions and sources [4, 5]. In this study, we used the apparatus to analyze aerosol particles containing black carbon.

2. Methods

Aerosol particles were collected at the Fukue-Jima Island, Nagasaki Prefecture, Japan, and on the Kougakuin University campus (Hachioji, Tokyo, Japan). A custom-made single stage impactor [6] was used for the sampling. The impactor collected particles less than 10 μm in diameter. Silicon wafers with an area of 4 mm^2 were used as collection substrates. Each sampling was performed for 10 minutes at a suction rate of 1.5 L/min. The silicon wafers with aerosols were introduced into the TOF-SIMS apparatus at room temperature and without any pretreatment.

All experiments described here were performed with a TOF-SIMS apparatus developed by the authors [3]. The apparatus has two beams: a gallium FIB as the primary ion beam and an electron beam (EB). The FIB was used as a machining tool to fabricate particles, to observe the particle surface, and to map the elements of the particle. A 30-keV gallium FIB was rastered to obtain the FIB-induced secondary electron image. The EB was used to search for particles to be analyzed and observe during the FIB machining. The base pressure of the apparatus was around 3.0×10^{-6} Pa.

First, aerosol particles on the silicon wafer were observed on the FIB-induced secondary electron image and the secondary electron image produced by the EB. Next, elemental mapping was performed using a pulsed FIB and TOF mass

spectrometry (MS) of an area a few tens of square micrometers in size on the silicon wafer, involving particles with a diameter of about 1 μm (128 × 128 pixels). The pulse duration was 300 ns, and 300 sweeps were performed. The FIB current was about 300 pA.

3. Results and discussion

Figure 1 shows the FIB-induced secondary electron image of a particle with a diameter of about 1 μm after ion sputtering. A solid material with a diameter of about 100 nm remained at the edge of the particles. The solid was not spherical but irregular in shape, similar to aggregated carbonaceous spherules observed by TEM [2]. This solid might be composed of black carbon.

Elemental mapping in negative analysis mode of particles with a diameter of about 1 μm before the sputtering showed an area of sulfate ions surrounded by carbon ions. In contrast, after the sputtering, an area of carbon ions was observed at one edge of the sulfates, which is consistent with the position of the solid material seen in Figure 1. However, the elemental mapping alone could not identify the carbon ions after the ion sputtering as black carbon, because the source of the carbon before and after ion sputtering was not clear.

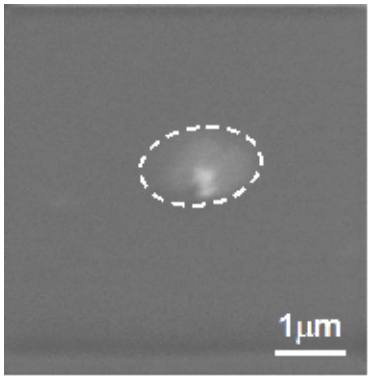

Figure 1 FIB-induced secondary electron image of particles with a diameter of about 1 μm after ion sputtering.

In the mass spectrum of the carbon area after ion sputtering (Figure 2), the carbon cluster ions C^-, C_2^-, C_3^-, C_4^-, C_5^-, and C_6^- were detected. In particular, C_3^- and C_6^- (m/z = 36 and 72, respectively) could be distinguished. The line at m/z = 48 is interpreted as C_4^- rather than SO^- because SO_2^- (m/z = 64) was not detected. The detected ions in the carbon area after ion sputtering were almost the same as those of graphite, used as a reference for elemental carbon. In addition, the solid carbon material remaining after ion sputtering was identified as black carbon. The materials in the carbon area

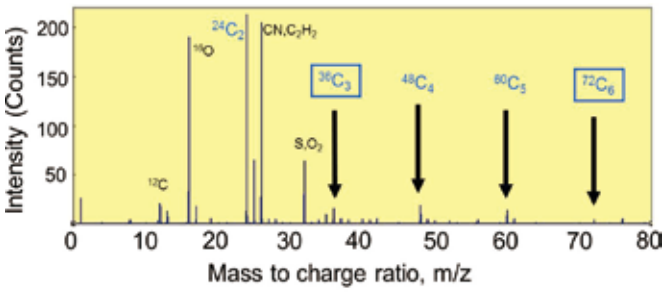

Figure 2 Mass spectrum of the carbon area of particles with a diameter of about 1 μm after ion sputtering

before ion sputtering were identified as organic matter from their mass spectra.

These results suggest that in the structure of the original aerosol particles containing black carbon. The black carbon may have been at one edge of the sulfates, and that the sulfates were usually surrounded by organic matter.

4. Summary

Aerosol particles containing black carbon were analyzed with a high lateral resolution TOF-SIMS system. After sulfate particles with a diameter of about 1 μm were sputtered by FIB, solid materials sometimes remained in the particles. On the basis of our analysis results, we concluded that the solids might be identified as black carbon. Furthermore, the aerosol particles containing black carbon might have a structure in which the black carbon is at one edge of sulfates, and the sulfates are usually surrounded by organic matter.

This work was supported by the Environment Research and Technology Development Fund (ERTDF, Ministry of the Environment, Japan, B-1006).

1 Moteki, N. and Y. Kondo 2007: Effects of mixing state on black carbon measurement by laser-induced incandescence. *Aerosol Science and Technology*, **41**: 398–417

2 Adachi, K., S. H. Chung and P. R. Buseck, 2010: Shapes of soot aerosol particles and implications for their effects on climate. *Journal of Geophysical Research*, **115**: doi: 10.1029/2009JD012868

3 Sakamoto, T., M. Koizumi, J. Kawasaki, et al. 2008: Development of a High Lateral Resolution TOF-SIMS Apparatus for Single Particle Analysis. *Applied Surface Science*, **255** (4): 1,617-1,620

4 Sakamoto, T., A. Takami, S. Hatakeyama, et al. 2012: Individual Analysis of Atmospheric Aerosol Particles at West-Japan Area using High Lateral Resolution Time-of-Flight Secondary Ion Mass Spectrometry. *Abstract of International symposium on aerosol studies explored by electron microscopy*. p.29

5 Mayama, N., E. Goto, Y. Miura, et al. 2012: Development of Source Apportionment of Individual Particle by High Resolution Time of Flight- Secondary Ion Mass Spectrometry. *Journal of the Vacuum Society Japan*, **55** (3): 104-107

6 Yamaguchi, J. and T. Sakamoto, 2008: A Portable Aerosol Sampler for Individual Particle Analysis by Means of TOF-SIMS. *Applied Surface Science*. **255** (4): 1,505-1,508

Analysis of source apportionment and chemical transformation of particles in trans-boundary air pollution using high lateral resolution imaging SIMS

*Tetsuo Sakamoto[1], Kenji Ohishi[1], Yusuke Miura[1], Masaaki Fujii[2], Kentaro Misawa[2], Norihito Mayama[2], Mikko Riese[2], Kana Kitatsugu[2], Akinori Takami[3], Satoshi Irei[3], Shiro Hatakeyama[4], Ayako Yoshino[4], Kentaro Murano[5], Takuma Mukaida[5], Hiroshi Bandow[6] and Yasuhiro Sadanaga[6]

[1]Department of Electrical Engineering, Faculty of Engineering, Kogakuin University, 2665-1 Nakano-machi, Hachioji, Tokyo 192-0015, Japan
[2]Chemical Resources Laboratory, Tokyo Institute of Technology, 4259 Nagatsutacho, Midori-ku, Yokohama, Kanagawa 226-8503, Japan
[3]Asian Environment Research Group, National Institute for Environmental Studies, 16-2 Onogawa, Tsukuba, Ibaraki 305-8506, Japan
[4]Graduate School of Agriculture, Tokyo University of Agriculture and Technology, 3-8-1 Harumicho, Fuchu, Tokyo 183-8538, Japan
[5]Department of Chemical Science and Technology, Faculty of Bioscience and Applied Chemistry, Hosei University, 3-7-2 Kajino-cho, Koganei-shi, Tokyo 184-8584, Japan
[6]Department of Applied Chemistry, Graduate School of Engineering, Osaka Prefecture University, 1-1 Gakuen-cho, Naka-ku, Sakai, Osaka 599-8531, Japan

Corresponding author. Tel.: +81 42 628 4872; Fax: +81 42 628 4872, Email address: ct13087@ns.kogakuin.ac.jp (T. Sakamoto)

Aerosol particles collected on the Fukue-Jima Island in western Japan were analyzed individually by a time-of-flight secondary ion mass spectrometry (TOF-SIUS) system with high lateral resolution. Two major coarse particle types were found in the sample from an air mass that had passed over the Korean Peninsula: one with a crystalline part, and another with a fluidic part. Examination of the first type showed that formed by the reaction of mineral dust containing $CaCO_3$ with HCl that had been produced by a decomposition reaction between sea salt and dust. The latter reaction would be enhanced in the presence of the pollutant HNO_3.

Keywords: Aerosol particles; Mixing properties of aerosols; Single particle analysis; TOF-SIMS

1. Introduction

Trans-boundary air pollution is of great interest because of its potential impacts on the environment in the downstream area. Aerosols transported from East Asia to western Japan have been studied to determine their sources and the chemical transformations that they undergo during transport. Conventionally, aerosol studies have employed chromatography and mass spectrometry to analyze particle composition. These analysis methods result in highly precise compositional data on bulk samples, but they cannot be used to analyze individual particles.

We formed a research group with the aim of combining bulk analysis with individual particle analysis. Bulk analysis was used to obtain information about overall trends in aerosol transport, and then individual particles from particular samples identified as of interest by the bulk analysis were analyzed. For individual particle analysis, a novel imaging apparatus based on time-of-flight secondary ion mass spectrometry (TOF-SIMS) was employed [1]. Here, we present the results of some individual aerosol particle analyses.

2. Methods

Aerosol particles were collected at the Fukue-Jima Island, Nagasaki prefecture, Japan, at 16:50 JST on 29 March and at 9:30 on 31, March 2010. A custom-made single-stage impactor [2] was used for the sampling. Silicon wafers 4×4 mm in size were used as collection substrates because it is easy to observe small particles on them owing to their surface smoothness. Each sampling was performed for 10 min at a pumping rate of 1.5 L/min. After the sampling, the wafers were stored in airtight boxes at room temperature

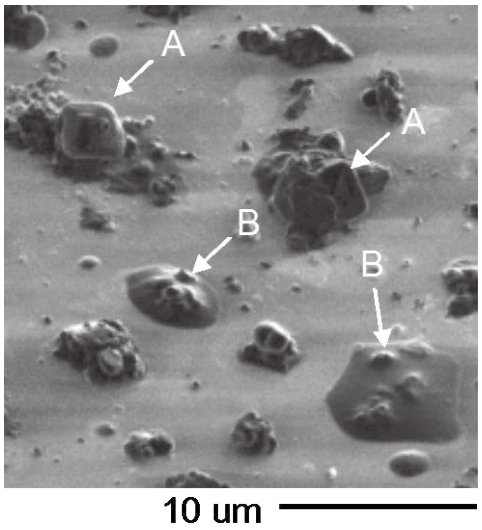

Figure 1 FIB-induced secondary electron image of aerosols collected on a Si wafer on 29 March. Particle type A is partly crystalline, and particle type B is partly fluidic.

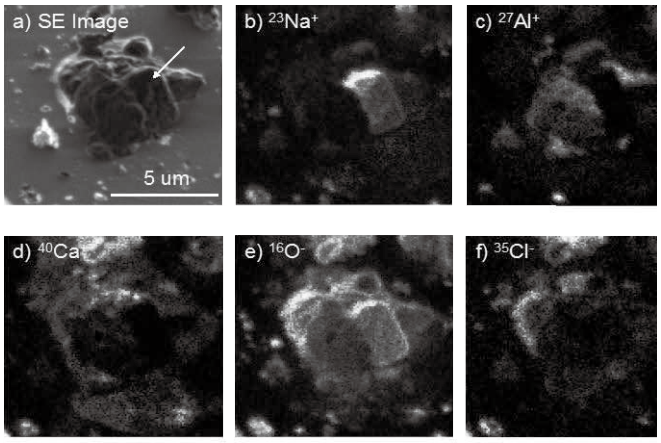

Figure 2 Secondary electron (SE) image (a) and secondary ion maps of a type A particle: (b) $^{23}Na^+$; (c) $^{27}Al^+$; (d) $^{40}Ca^+$; (e) $^{16}O^-$; (f) $^{35}Cl^-$. The arrow in (a) indicates the crystalline part.

until analysis in the laboratory.

All analyses were performed with a high-resolution TOF-SIMS apparatus. This apparatus can perform single-particle analysis with high lateral resolution, down to 40 nm. A cross section of the targeted particle is fabricated with a gallium focused ion beam (Ga-FIB) operated in DC mode at 30 keV, with a beam current of 300 to 500 pA and at an incident angle of 45° with respect to the surface normal. The Si wafers with the collected aerosols were introduced into the apparatus at room temperature and without any pretreatment. The particles were mapped at a resolution of 128 pixels × 128 pixels with a Ga-FIB pulse repetition of 200 per pixel. The typical time required for one mapping analysis was 300 s. The pressure in the specimen chamber was around 3.0×10^{-6} Pa.

3. Results and discussion

Before the individual particle analysis, the origin of each day's air mass was deduced by back-trajectory analysis using the HYSPLIT-4 method of the U.S. National Oceanic and Atmospheric Administration [3]. The air mass sampled on 29 March had passed over the Korean Peninsula, whereas that sampled on 31 March first passed over the Japanese Islands and then subsequently moved northward into the Pacific Ocean. Therefore, we expected that the particles collected on 29 March would be more affected by anthropogenic chemical species than those collected on 31 March.

In the FIB-induced secondary electron image of particles collected on 29 March (Figure 1), two major types of coarse particles were observed: type A particles were partly crystalline, and type B particles were partly fluidic.

Secondary ion maps of the major constituents of a type A particle analyzed by SIMS (Figure 2) show that the particle consisted of a crystalline part surrounded by non-crystalline components. The crystalline part (arrow in Figure 2a) consisted of Na and O, not of Na and Cl (sea salt). If the Na originated from sea salt, then the following sea salt decomposition reaction must have occurred in the air mass:

$$NaCl + HNO_3 \rightarrow NaNO_3 + HCl. \qquad (1)$$

In this reaction, HNO_3 is assumed to be emitted from industrial processes. The non-crystalline parts of the particle contained Cl and the mineral dust components Al and Ca, indicating that mineral dust had reacted with the HCl produced by the decomposition reaction.

4. Conclusion

Trans-boundary aerosol particles were individually analyzed with a state-of-the-art SIMS apparatus. An air mass that had passed over the Korean Peninsula had two major types of particles. One type contained $CaCl_2$ that originated from a reaction between mineral dust and sea salt.

This work was supported by the Environment Research and Technology Development Fund (ERTDF, Ministry of the Environment, Japan, B-1006), which is greatly appreciated.

1 Sakamoto, T., M. Koizumi, J. Kawasaki and J. Yamaguchi, 2008: *Appl. Surf. Sci*., **255**, 1,617.
2 Yamaguchi, J. and T. Sakamoto, 2005 : *Appl. Surf. Sci*. **255** (4), 1,505.
3 http://ready.arl.noaa.gov/HYSPLIT.php

Mixing state of atmospheric black carbon particles and its effect on light absorption

Hiroaki Naoe[1,*] and Kikuo Okada[1]

[1] Atmospheric Environment and Applied Meteorology Research Department, Meteorological Research Institute, 1-1 Nagamine, Tsukuba, Ibaraki 305-0052, Japan
[2] Present affiliation: Ozone Layer Monitoring Office, Japan Meteorological Agency, 1-3-4 Otemachi, Chiyoda-ku, Tokyo 100-8122, Japan

Corresponding author. Tel.: +81 3 3212 8341(ext.4212); Fax: +81 3 3211 4640, Email address: hnaoe@met.kishou.go.jp (H. Naoe)

The mixing state of light-absorbing carbonaceous particles is investigated in relation to their light-absorption properties by electron microscopy examination, analyses of black carbon (BC) on a quartz fiber filter by the thermal/optical reflectance method, and measurements made with two continuous light-absorbing photometers at a suburban site in Tsukuba, about 60 km northeast of Tokyo, Japan. The volume fraction of water-soluble material (ε) in individual particles is an important parameter for assessing particulate light absorption and/or scattering by atmospheric aerosols. The ε values in BC particles are evaluated by examining electron micrographs before and after dialysis (extraction) of water-soluble material. In BC particles with radii between 0.05 and 0.5 μm, the mass absorption coefficient (in units of $m^2 g^{-1}$) tends to increase as the average ε value increases, indicating that coatings of water-soluble material around BC particles can enhance their absorption of solar radiation. Moreover, the single scattering albedo also increases because a large amount of coating material will scatter more light.

Keywords: Aerosol particles; Elemental composition; Mixing properties of aerosols; Single particle analysis; Electron microscopy

1. Introduction

Light-absorbing carbonaceous particulate matter, often called "black carbon" (BC) or "soot," is an important constituent of atmospheric particles. Airborne BC is the most important particulate material absorbing solar radiation in the atmosphere, and it is one of major contributors to global climate forcing (IPCC, 2007). A mass absorption coefficient (MAC; in units of $m^2 g^{-1}$), which is defined as the ratio of the aerosol absorption coefficient (m^{-1}) to the mass concentration ($\mu g\ m^{-3}$) of the absorbing particles, is a crucial parameter in many applications. For BC particles with known size distribution and refractive index, MAC can be calculated by using a Mie theory. BC-containing aerosol particles can have MAC values between 3.8 and 17 $m^2 g^{-1}$ [1] or between 5 and 13 $m^2 g^{-1}$ [2], depending on the size distribution and the refractive index.

Measurements of BC concentrations or model calculations often use values on the order of 10 $m^2 g^{-1}$. Hansen (2003: Ref. 1) showed when measurements of aerosol absorption by soot absorption photometer were regressed against Aethalometer measurements of mass concentration, the resulting regression line had a slope of 10.8 $m^2 g^{-1}$. However, Bond and Bergstrom (2006: Ref. 2) recommended a MAC value of 7.5 $m^2 g^{-1}$ at or near combustion sources. To evaluate the contribution of different substances to light absorption by BC-containing particles, the mixing state of BC with other particulate matter (usually non-light-absorbing substances) must be considered [3]. Externally mixed BC particles have a lower MAC than internally mixed particles with the same chemical composition [1, 4].

To date, our understanding of light absorption obtained from measurements is insufficient because there were only a few studies to evaluate light absorption properties in BC-containing aerosol particles in relation to their mixing state. Thus, the aim of this study is to obtain information on the mixing state of BC particles by using electron microscopy and to evaluate its effect on the light absorption properties of BC-containing particles determined from observational results obtained in the suburban atmosphere of Tsukuba, Japan.

2. Methods

Ground-based aerosol measurements were performed in

the radiation observation building of the Meteorological Research Institute (MRI, 36.06°N, 140.01°E) in Tsukuba in October 2005. Naoe et al. (2009: Ref. 6) described the observational method in detail. Number-size distributions of aerosol particles were measured with a differential mobility analyzer (TSI, Model 3071A) in combination with a condensation nucleus counter (TSI, Model 3025). Aerosol particles were collected on carbon-coated nitrocellulose film in an impactor with a 0.5-mm-diameter round jet. After the collection, the particles on the film are coated with a Pt/Pd alloy at a thickness of 0.7 nm and a shadowing angle of 26.6°. Then, the shape and volume of the individual particles are assessed by using transmission electron microscopy (Hitachi, H-600 and H-6010). The system for measuring their optical properties consists of an integrating nephelometer (TSI, Model 3563), a continuous light absorbing photometer (PSAP; Radiance Research, M903), and a seven-wavelength black carbon aethalometer (Magee Scientific Company, AE-31).

Before sampling, quartz fiber filters (47 mm in diameter) for total suspended particulates were used that were punched out of a filter sheet of the same lot. For concentrated filtration, the aerosol particles were collected in an 8-mm-diameter area on the filter using a mask. Organic carbon (OC) and elemental carbon (EC) are analyzed with a DRI model 2001 carbon analyzer [7]. The IMPROVE protocol uses for the analysis and comprises the following seven steps: OC1, 120 °C; OC2, 250 °C; OC3, 450 °C; and OC4, 550 °C in a 100% He atmosphere; EC1, 550 °C; EC2, 700 °C; and EC3, 800 °C in a 2% O_2 and 98% He atmosphere.

3. Results

Figure 1 shows the relationship between MAC and the average volume fraction of water-soluble material ε in BC particles ($0 \leq \varepsilon < 1$) with radii between 0.05 and 0.5 μm in each sample. MAC is the ratio of the aerosol absorption coefficient at 565 nm, obtained from the PSAP measurements, to the BC mass concentration, measured by the thermal/optical reflectance method. MAC thus does not depend on the total particulate mass but on the mass of the only BC component. Although MAC is a function of wavelength and its properties determined at a single wavelength are insufficient for climate modeling studies, here we focus on identifying BC optical properties at a mid-visible wavelength (565 nm). For the Tsukuba aerosol collected in October 2005, the MAC values are distributed within a narrow range (10–13 $m^2\ g^{-1}$), and MAC tends to increase as the average volume fraction of water-soluble material increases. MAC (y-axis) and average ε (x-axis) are somewhat correlated ($r^2 = 0.41$; regression line, $y = 4.5x + 11.1$ (± 1.0) $m^2\ g^{-1}$). Therefore, the enhancement of MAC in our observational results is qualitatively comparable to that obtained by theoretical calculations. Since BC is fully externally mixed when $x = 0$, MAC in BC particles without water-soluble components is shown by the y-intercept to be 11.1 ± 1.0 $m^2\ g^{-1}$. Thus, this value is different from the value of 7.5 for ε = 0.0 recommended by Bond and Bergstrom (2006: Ref. 2).

Bond and Bergstrom (2006: Ref. 2) showed that MAC of BC particles ranges usually between 5 and 13 $m^2\ g^{-1}$ but that at or near combustion sources it does 6.3–8.6 $m^2\ g^{-1}$. Although a MAC of 10 $m^2\ g^{-1}$ is commonly cited, they recommended a MAC of 7.5 ± 1.2 $m^2\ g^{-1}$ for uncoated (i.e., freshly produced) aerosols and small BC particles. Our MAC value estimated from the y-intercept of the regression line is similar to the commonly cited value.

When ε is close to 1, BC particles correspond to be fully internally mixed. The estimated MAC value of 16 ± 1 $m^2\ g^{-1}$ in our result may represent the maximum of MAC that can result from the coating of BC particles.

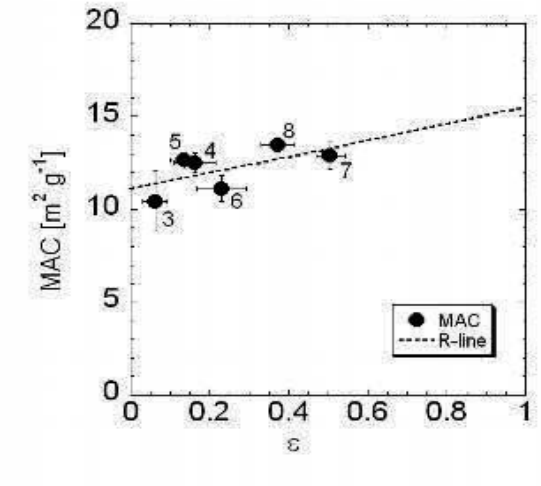

Figure 1 Mass absorption coefficient (MAC; aerosol absorption coefficient divided by BC mass concentration) versus the average volume fraction of water-soluble material (ε) in BC particles. BC mass concentrations were obtained by the thermal/optical reflectance method. The numbers close to the symbols indicate the sample IDs.

1 Horvath, H., 1993: Atmospheric light absorption - A review. *Atmos. Environ*. **27A**, 293-317.

2 Bond, T.C. and R.W. Bergstrom, 2006: Light absorption by carbonaceous particles: An investigative review. *Aerosol Sci. and Technol*. **40**, 27-67.

3 Naoe, H., and Okada K. 2001: Mixing properties of submicrometer aerosol particles in the urban atmosphere -with regard to soot particles, *Atmos. Environ*. **35**, 5765-5,772.

4 Heintzenberg, J., 1978: Light scattering parameters of internal and external mixtures of soot and non-absorbing material in atmospheric aerosols. *Proceedings of the Conference on Carbonaceous Particles in the Atmosphere*, Berkeley, CA. 278-281.

5 Hansen, A.D.A., 2003. The Aethalometer Manual. Berkeley, CA, USA: *Magee Scientific*.

6 Naoe, H., S. Hasegawa, J. Heintzenberg, K. Okada, A. Uchiyama, Y. Zaizen, E. Kobayashi and A. Yamazaki, 2009: State of mixture of atmospheric submicrometer black carbon particles and its effect on particulate light absorption. *Atmos. Environ.*, **43**, 1,296–1,301.

7 Hasegawa, S., S. Wakamatsu and K,Tanabe, 2005: Comparison of particulate carbon analysis between the thermal method and the thermal/optical method using the same ambient samples. *Journal of Japan Society for Atmospheric Environment* **40**, 181–192 (in Japanese).

Fine mineral aerosols collected in Japan during two Asian dust events: Size distributions and mixing properties

Yuji Zaizen[1]*, Hiroaki Naoe[1], Hiroshi Takahashi[1] and Kikuo Okada[1]

[1] Atmospheric Environment and Applied Meteorology Research Department, Meteorological Research Institute, 1-1 Nagamine, Tsukuba, Ibaraki 305-0052, Japan

*Corresponding author. Tel.: +81 29 856 8622; Fax: +81 29 855 7240, Email address: yzaizen@mri-jma.go.jp (Y. Zaizen)

Asian dust samples were collected from the prefrontal and postfrontal air masses of an extratropical cyclone on 20 March 2010, and the size distributions and mixing properties of the mineral aerosols were examined by transmission electron microscopy and energy-dispersive X-ray analysis. Mineral aerosols were predominant in the large size ranges (Dp > 0.5 μm) in both samples. In the smaller size range (Dp < 0.5 μm), mineral particles dominated in the postfrontal samples, but particles with abundant sulfur were predominant in the prefrontal sample. Mixing properties of the mineral particles were examined by irradiation of individual particles by intense electron beams. In the postfrontal sample, most of the fine mineral particles were externally mixed, whereas most of those in the pre-frontal sample were internally mixed with volatile aerosols. The coating thickness depended on the core size. In particular, particles smaller than 0.3 μm were thickly coated. The mode diameters of mineral aerosols and of mineral cores were both in the fine size range of both dust samples. The aging properties of prefrontal dust and the strong influence of anthropogenic pollutants were due to the slow transport of the dust in the mixing layer over coastal China and the East China Sea. In contrast, the postfrontal dust was not particularly influenced by anthropogenic aerosols, because the front separated the air mass from the anthropogenic pollution south of the front.

Keywords: Aerosol particles; Asian dust; Single particle analysis; Electron microscope

1. Introduction

Asian dust particles affect human activities and health, plants, the environment, and climate. During dust events, fine particles are not important in terms of mass. However, observations at source regions suggest that the number concentrations of fine mineral particles are comparable to or higher than those of coarse mineral particles.

Aerosols in the fine size range are generally dominated by particles formed through gas-to-particle conversion, and they are thus composed of volatile materials, namely, sulfuric acid, sulfate, nitrate, ammonium, and organic matter. The number concentrations of these accumulation mode particles are generally several orders of magnitude higher than those of coarse particles. Therefore, number concentrations of fine mineral dust are expected to be lower than those of volatile particles even during Asian dust events over Japan.

During Asian dust events, mineral dust particles are typically transported in association with extratropical cyclones from the Asian continent to Japan. Dusty air is sometimes observed to be associated with northwesterly winds after the passage of a cold front, and increased particle concentrations are associated with southerly winds before the passage of a cold front [1, 2]. Increases in the number concentration of fine particles are particularly notable in prefrontal air masses, and they are attributable to anthropogenic pollution transported from China.

On 21 March 2010, Asian dust events were observed over Japan before and after the passage of a cold front. For the present study, we collected aerosol particles at Tsukuba during these events. We examined the mixing properties of the individual particles (examining approximately 10,000 particles) by observing morphological changes of the particles after their irradiation with strong electron beams during transmission electron microscopy (TEM).

2. Methods

Aerosol samples were collected with a two-stage jet impactor with nozzle diameters of 1 and 0.5 mm at flow rate of 2 L min^{-1} onto the surface of a carbon-coated nitrocellulose (collodion) film on a reference copper grid (Graticules, Ltd., Maxtaform H7). The 50% cutoff diameters of the

0.5-mm and 1-mm impactors were evaluated as 0.66 and 0.14 μm, respectively. The sampling sites were at the Meteorological Research Institute (MRI) in Tsukuba (36.08°N, 140.12°E) and at Mt. Haruna (36.48°N, 138.87°E; elevation, 1390 m).

The samples were analyzed by TEM (Hitachi, H-600 and H-6010), scanning TEM (STEM H-6010), and energy dispersive x-rays (EDX). Individual particles were irradiated by intense electron beams to remove volatile components such as sulfate, nitrate, and organic matter. Minerals and soot in the residues remaining after removal of the volatile materials were distinguished by their morphological appearance. The volatile aerosols were distinguished by the traces remaining after the irradiation. The size (volume equivalent diameter) of volatile aerosols was evaluated by assuming a spherical cap from the disk on the collection film.

3. Results and discussion

Figure 1 shows the number-size distributions of the different types of fine aerosol particles normalized to scanning mobility particle sizer/optical particle counter data (SMPS/OPC) for the prefrontal (left) and postfrontal (right) samples collected at Tsukuba. In the prefrontal event, externally mixed volatile aerosols predominated, and externally mixed refractory aerosols (minerals, soot, and fly ash) were present in very low concentrations. The refractory materials were mostly internally mixed with volatile aerosols. Number fractions of mineral particles were lower than 1%, even including the internally mixed particles.

Most soot particles were internally mixed. In the postfrontal event, the concentration of mineral aerosols was greater than the concentrations of soot and volatile particles in the 0.2–0.4 μm size range, and most mineral particles were externally mixed. It is notable that the maximum number concentration of total aerosols with a diameter of 0.4 μm was attributable to externally mixed mineral aerosols.

A model simulation showed that the source of the prefrontal and postfrontal dust was the Badain Jaran Desert (approximately 40°N, 100°E), a result that is consistent with back-trajectory analysis results. A dust storm was observed continuously at the meteorological observatories in that area from the beginning of March 2010. Therefore, we considered that the properties of the mineral particles in the prefrontal and postfrontal events were originally similar and that they became differentiated during transport. We interpreted the fine minerals in the prefrontal air to have been originally present as externally mixed particles, which became internally mixed under the influence of anthropogenic pollutants during transport.

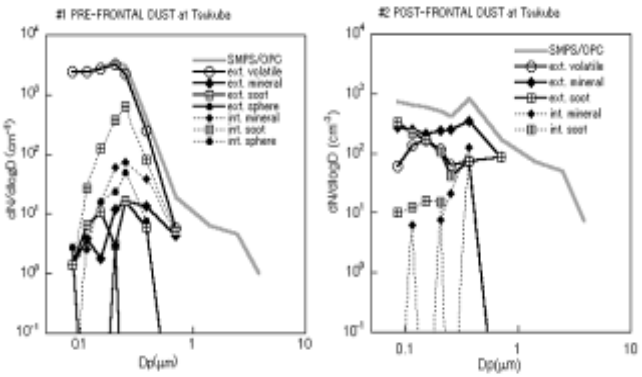

Figure 1 Size distributions of particles of different mixing types from the prefrontal (left) and postfrontal (right) events.

Bates et al. (2004: Ref. 1) observed aerosols from a research vessel in the Japan Sea near Sakhalin (approximately 50°N latitude) before and after the passage of a cold front accompanying an extratropical cyclone and reported that the prefrontal air was dominated by ammonium sulfate and organic carbon, with mineral dust particles as a minor component, whereas the postfrontal air was dominated by mineral dust particles. Zhang et al. (2005: Ref. 2) analyzed aerosol samples obtained at Qingdao, China, before and after the passage of a cold front passing over Mongolia (approximately 50°N latitude) and reported that the prefrontal dust had been highly influenced by anthropogenic pollution whereas the postfrontal dust was relatively unmodified. Moreover, some investigators have reported increased fine particle concentrations before the arrival of high concentrations of Asian dust in Japan. Taken together, these findings suggest that the effects of anthropogenic pollution on prefrontal air are generally stronger than their effects on postfrontal air.

1 Bates, T. S., P. K. Quinn, D. J. Coffman, D. S. Covert, T. Miller, J. E. Johnson, G. R. Carmichael, I. Uno, S. A. Guazzotti, D. A. Sodeman, K. A.Prather, M. Rivera, L. M. Russell and J. T. Merrill, 2004: Marine boundary layer dust and pollutant transport associated with the passage of a frontal system over eastern Asia. *Journal of Geophysical Research*, **109**, D19S19, doi: 10.1029/2003JD004094.

2 Zhang, D., Y. Iwasaka, G. Shi, J. Zang, M. Hu and C. Li, 2005: Separated status of the natural dust plume and polluted air masses in an Asian dust storm event at coastal areas of China. *Journal of Geophysical Research*. **110**, D06302, doi: 10.1029/2004JD005305.

Climatic effect of black carbon in the MRI global climate model

Taichu Y. Tanaka[1*] and MRI Earth System Modeling Group[*]

[1]Atmospheric Environment and Applied Meteorology Research Department, Meteorological Research Institute, 1-1 Nagamine, Tsukuba, Ibaraki 305-0052, Japan

Corresponding author. Tel.: +81 29 853 8621; Fax: +81 29 855 7240, Email address: yatanaka@mri-jma.go.jp (T. Y. Tanaka)

We used the global climate model MRI-CGCM3 to investigate the climatic effect of black carbon (BC) aerosols and to estimate the effectiveness of mitigation of global warming by the reduction of BC. As the first step, we conducted an idealized sensitivity study to investigate the climatic response of air temperature in the presence or absence of atmospheric BC aerosol, as well as the response with an atmospheric loading of BC 10 times that of the control experiment. We found that the atmospheric heating effect of BC was large in the tropical upper troposphere in mid-latitude regions of the Northern Hemisphere and in the Antarctic region. In addition, the surface air temperature in tropical regions, especially the Sahel, India, and Southeast Asia, was reduced by the presence of atmospheric BC. These results suggest that radiative heating of atmospheric BC modifies atmospheric stability conditions and hence the general circulation of the atmosphere and ocean.

Keywords: Black carbon; Climate change; Aerosol particles; Numerical climate model

1. Introduction

Black carbon (BC) in atmospheric aerosols is an efficient absorber of radiation, and it affects the Earth's climate by scattering and absorbing atmospheric radiation. BC is estimated to be the second-most important warming agent after carbon dioxide [1]. Moreover, when deposited on snow- or ice-covered ground, BC acts as a light-absorbing impurity and reduces the surface albedo (e.g. [2]). Because the lifetime of BC is shorter than that of other greenhouse gases (GHGs), reduction of atmospheric BC emissions may be an efficient way to mitigate global warming [1]. However, the climatic impact of BC is still uncertain because of the uncertainties in numerical climate models.

We used a global climate model developed in the Meteorological Research Institute (MRI) of the Japan Meteorological Agency to investigate the climatic effect of BC aerosols and to estimate the effectiveness of the mitigation of global warming by the reduction of BC. In section 2, we describe the MRI global climate model, and we present preliminary results of an experiment on the effect of BC aerosols in section 3.

2. Model description

2.1. MRI climate model

We used the global climate model MRI-CGCM3, which consists of an atmospheric general circulation model (MRI-AGCM3), an ocean general circulation model (MRI.COM), and a global aerosol model (MASINGAR mk-2; Model of Aerosol Species IN the Global Atmosphere) [3]. The horizontal resolution used was TL159 (approximately 1.1°) for the AGCM, 1° × 0.5° (tripolar) for the OGCM, and TL95 (approximately 1.8°) for the aerosol model. The vertical resolution of the AGCM and aerosol model was 48 vertical layers from the ground to 0.01 hPa with a terrain-following and pressure hybrid (η) coordinate system. The model components were interactively connected by a coupler library called Simple coupler (Scup, [4]). MRI-CGCM3 is a part of the MRI Earth System Model (MRI-ESM1) [5].

MASINGAR mk-2 considers five aerosol species, namely sulfate (and its precursors), BC, organic carbon (OC), sea salt, and mineral dust. The concentrations of the aerosols are passed to the AGCM and used for the calculation of atmospheric radiative transfer. Deposition fluxes of light-absorbing aerosols, namely BC and mineral dust, are also considered as snow impurities and used in the calculation of the albedo of snow and ice. Emission inventories of the Representative Concentration Pathways (RCP) emission scenario [6] are used for BC, OC, and SOx.

2.2. Experimental conditions

We performed a series of 25-year simulations for the period from 1 January 2005 to 31 December 2029, setting all GHG concentrations and BC, OC, and SOx emissions to those in 2005. The initial experimental conditions were adopted from a historical CMIP5 climate experiment

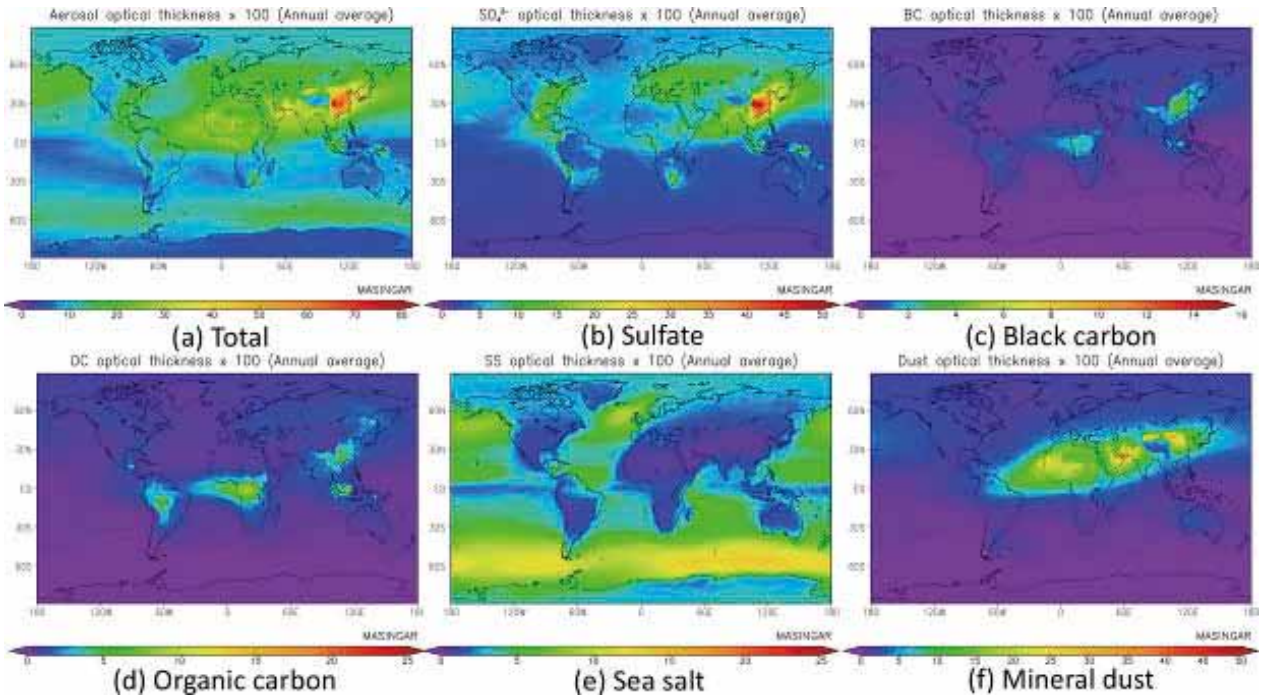

Figure 1 Annually averaged optical depth (at 550 nm) of the simulated aerosols: (a) total, (b) sulfate, (c) black carbon, (d) organic carbon, (e) sea salt, and (f) mineral dust.

conducted with MRI-CGCM3.

To elucidate the radiative effects of the BC aerosols, we conducted experiments under three sets of conditions. The default setup of the model simulation was used as the "Control" experiment. The second experiment (the "No-BC" experiment) excluded airborne BC from the radiative transfer calculation. The difference between the Control experiment and the No-BC experiment represented the effect of total elimination of BC emissions into the atmosphere. Because of uncertainties in the concentrations, mixing states, and optical properties in the BC simulation, as a sensitivity study we conducted a third experiment (the BC×10 experiment), in which the BC concentration was assumed to be 10 times the concentration in the atmosphere used for the Control radiative transfer calculation.

3. Results

3.1. Simulated optical depth of aerosols

The globally averaged annual mean optical depths of the aerosol species in the Control experiment (Figure 1) were 0.050 for sulfate, 0.003 for BC, 0.007 for OC, 0.042 for sea salt, and 0.029 for mineral dust. The horizontal distribution of the BC optical depth indicates that in the early 21st century BC loading will be highest over China, India, South-

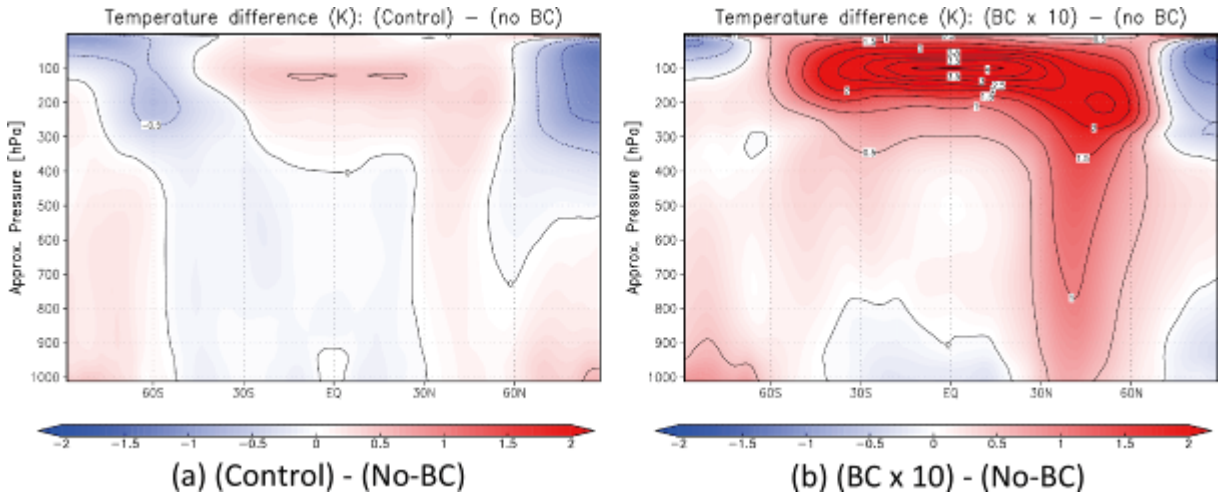

Figure 2 Annual mean zonally averaged temperature differences caused by the radiative effect of BC. Differences between the (a) Control and No-BC experiments and the (b) BCx10 and No-BC experiments.

east Asia, and the equatorial region in Africa. Most of the BC loading was in the Northern Hemisphere, and it was very low over the ocean in the Southern Hemisphere.

3.2. Zonal mean temperature differences

Zonal mean temperature differences between the Control and No-BC experiments (Figure 2a) show both positive and negative temperature anomalies, whereas those between the BC×10 and the Control experiments show positive temperature anomalies (Figure 2b) at most latitudes and altitudes.

In both experiments, a considerable positive temperature difference is present in the tropical upper troposphere, indicating BC heating there. In the middle and lower troposphere, negative temperature anomalies are seen from about 60°S to 30°N, suggesting that BC causes cooling of the lower troposphere at those latitudes.

Atmospheric heating in the presence of BC is also seen in mid-latitude regions of the Northern Hemisphere, where the BC loading is high, and positive temperature anomalies are found in the lower troposphere over the Arctic and Antarctic regions (Figure 2a), although in the upper troposphere and lower stratosphere, negative temperature anomalies are seen over the Arctic and Antarctic. However, the differences between the BC×10 and Control experiments indicate only a slight positive anomaly in the lower troposphere over the Antarctic and a slight negative anomaly over the Arctic (Figure 2b).

These results suggest that the presence of BC in the atmosphere affects large-scale atmospheric circulation. In the tropics, BC heats the upper troposphere and cools the lower troposphere, which should reinforce atmospheric stability and weaken convective transport.

3.3. Ground surface temperature differences

The annually averaged surface air temperature difference between the Control experiment and No-BC experiment (Figure 3a) suggests that with the current BC loading the surface air temperature will increase over northeastern China and Europe, where anthropogenic BC emissions are high. Also, surface air temperature in the presence of current BC loading is increased in Antarctic regions. In contrast, in low-latitude continental regions, especially the African Sahel, India, and Southeast Asia, surface air temperature differences show cooling with the current BC loading (Figure 3a). Moreover, more pronounced cooling tendencies are seen in these regions when the differences between the BC×10 and No-BC experiments are examined (Figure 3b).

In some regions, however, the current BC loading and the BC×10 loading show different tendencies when compared with the Control results. The considerable heating over the Arctic with the current BC loading (Figure 3a), compared with cooling over that region with BC×10 loading (Figure 3b), suggests that the effect of BC on surface temperatures in the Arctic region depends on the BC loading amount. In addition, the pattern of surface air temperature differences with respect to the No-BC experiment differs greatly over the ocean between the Control (Figure 3a) and BC×10 (Figure 3b) experiments. Large heating over the Antarctic in the latter experiment (Figure 3b) is attributable to a decrease in sea ice in that region. This result suggests that the surface air temperature change with the amount of BC loading is due to feedback from changes in the general circulation of the atmosphere and ocean induced by radiative heating due to the atmospheric BC loading.

3.4. Seasonal change in the global average surface temperature

The seasonal variation of the globally averaged ground surface temperature anomalies between the Control and No-BC experiments (Figure 4, blue line) suggests that globally averaged ground surface temperature from May to

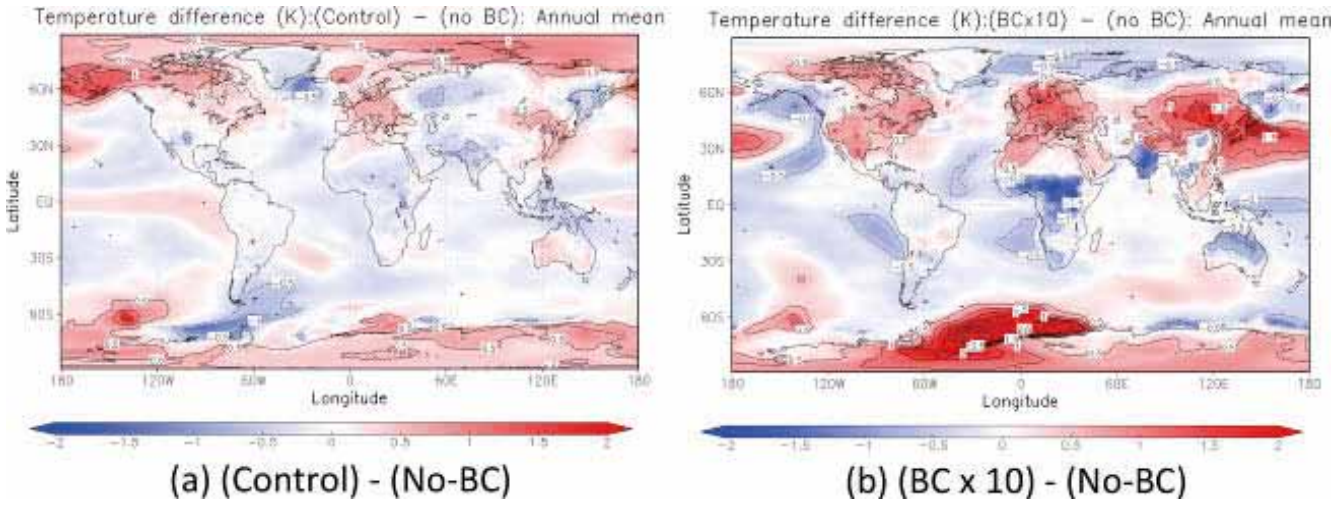

Figure 3 Annual mean surface air temperature differences due to the radiative effect of BC. Differences between the (a) Control and No-BC experiments, and the (b) BC×10 and No-BC experiments.

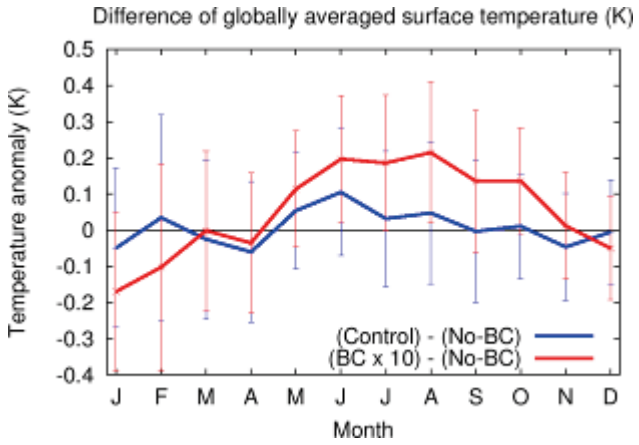

Figure 4 Seasonal variation of the globally averaged surface air temperature anomaly.

August will be slightly increased with the current atmospheric BC loading, whereas in autumn and winter, the globally averaged temperature anomalies are unremarkable. The heating due to BC in summer may reflect the large radiative heating due to BC in summer in the Northern Hemisphere, where there are large land masses and high anthropogenic BC emissions. The seasonal differences of the globally averaged surface air temperature anomalies between the BC×10 and No-BC experiments (Figure 4, red line) are greater than those between the Control and No-BC experiments; large positive anomalies (higher temperatures) are seen from May to October, and negative anomalies (lower temperatures) in January and December.

4. Summary

The global climate model MRI-CGCM3 was used to investigate the radiative effect of BC and to assess the validity of mitigating global warming by reducing atmospheric BC aerosol emission. As the first step of the assessment, we conducted an idealized sensitivity study to investigate the climatic response of air temperature in the presence or absence of atmospheric BC aerosols, and with an atmospheric BC loading 10 times higher than the current loading. The results predict a large atmospheric heating effect of BC in the tropical upper troposphere, mid-latitude regions of the Northern Hemisphere, and the Antarctic region in the early 21st century, and also suggest that surface air temperatures in tropical regions, especially the Sahel, India, and Southeast Asia, will be reduced by the presence of atmospheric BC. Therefore, radiative heating of atmospheric BC is predicted to change atmospheric stability conditions and hence the general circulation of the atmosphere and ocean. To assess regional temperature changes caused by BC reductions, more sensitivity experiments and investigations of feedback processes are needed.

This research was partly supported by the Environmental Research and Technology Development Fund (A-1101) of the Ministry of the Environment of Japan.

1 Jacobson, M.Z. 2002: Control of fossil-fuel particulate black carbon plus organic matter, possibly the most effective method of slowing global warming, *J. Geophys. Res.*, **107**, (D19), 4,410, doi: 10.1029/2001JD001376.

2 Aoki, T., K. Kuchiki, M. Niwano, Y. Kodama, M. Hosaka, and T. Tanaka, 2011: Physically based snow albedo model for calculating broadband albedos and the solar heating profile in snowpack for general circulation models, *J. Geophys. Res.*, **116**, D11114, doi: 10.1029/2010JD015507.

3 Yukimoto, S., Y. Adachi, M. Hosaka, T. Sakami, H. Yoshimura, M. Hirabara, T. Y. Tanaka, E. Shindo, H. Tsujino, M. Deushi, R. Mizuta, S. Yabu, A. Obata, H. Nakano, T. Koshiro, T. Ose, and A. Kitoh, 2012: A New Global Climate Model of the Meteorological Research Institute: MRI-CGCM3 —Model Description and Basic Performance —. *J. Meteorol. Soc. Japan*, **90A**.

4 Yoshimura, H. and S. Yukimoto, 2008: Development of a Simple Coupler (Scup) for Earth System Modeling. *Papers in Meteorology and Geophysics*, **59**, 19-29.

5 Yukimoto, S., H. Yoshimura, M. Hosaka, T. Sakami, H. Tsujino, M. Hirabara, T. Y. Tanaka, M. Deushi, A. Obata, H. Nakano, Y. Adachi, E. Shindo, S. Yabu, T. Ose and A. Kitoh, 2011: Meteorological Research Institute-Earth System Model Version 1 (MRI-ESM1) - Model Description - , *Technical Reports of the Meteorological Research Institute*, **No.64**, ISSN 0386-4049, Meteorological Research Institute, Japan.

6 Meinshausen, M., S. J. Smith, K.V. Calvin, J. S. Daniel, M. Kainuma, J.-F. Lamarque, K. Matsumoto, S.A. Montzka, S.C.B. Raper, K. Riahi, A.M. Thomson, G. J.M. Velders and D. van Vuuren, 2011: The RCP Greenhouse Gas Concentrations and their Extension from 1765 to 2300. *Climatic Change* **109**(1-2), 213-24

Model formulation and predictability of atmospheric aerosol properties and processes

Mizuo Kajino[1,*]

[1]Atmospheric Environment and Applied Meteorology Research Department, Meteorological Research Institute, 1-1 Nagamine, Tsukuba, Ibaraki 305-0052, Japan

Corresponding author. Tel.: +81 29 853 8623; Fax: +81 29 855 7240, Email address: kajino@mri-jma.go.jp (M. Kajino)

A new aerosol chemical transport model, the Regional Air Quality Model 2 (RAQM2), was developed to simulate Asian air quality. We implemented a simple version of a modal-moment aerosol dynamics model (MADMS) and achieved a completely dynamical (non-equilibrium) solution for gas-to-particle mass transfer over a wide range of aerosol diameters, from 1 nm to super μm. To consider a variety of atmospheric aerosol properties, a category approach was utilized: aerosols were distributed into four categories: Aitken mode (ATK), accumulation mode (ACM), soot aggregates (AGR), and coarse mode (COR). Condensation, evaporation, and Brownian coagulations for each category were solved dynamically. Modeled size distributions ($PM_{2.5}/PM_{10}$ and PM_1/bulk ratios) of total weight and chemical components were compared and found to be consistent with observations. At Hedo, proportions of non-sea-salt-SO_4^{2-} mixed with ATK + ACM were largest in summer, whereas H_2SO_4 gas was efficiently condensed onto AGR in cold seasons. Of the modeled NO_3^-, 98% was mixed with COR at Hedo, whereas 53.7% was mixed with sea salt at Gosan, which is upwind toward the Asian continent. This difference can be attributed to condensation of HNO_3 onto sea salt particles during transport over the ocean.

Keywords: Air quality modeling; Aerosol category approach; Non-equilibrium aerosol dynamics; Northeast Asia

1. Introduction

Atmospheric trace gases and aerosols have various detrimental effects on ecosystems and human health. Because their emission, secondary formation, transport, and deposition mechanisms are highly complex and still mainly unknown, many studies on the development and application of air quality modeling are ongoing. Recently, Jacobson and Ginnebaugh (2010: Ref. 1) developed a global-through-urban nested three-dimensional air pollution model that implements a large explicit photochemical mechanism with 4675 gases and 13,626 tropospheric and stratospheric chemical reactions. The mechanism also includes one internally mixed aerosol and three hydrometeor categories that are size and chemistry resolved (17 components and 14 size bins for aerosols; 18 components and 30 size bins for cloud/precipitation liquid, cloud/precipitation ice, cloud/precipitation graupel). On the other hand, there is still a strong demand for computationally efficient models for the purpose of long-term integration with higher grid resolutions. For example, the Community Multiscale Air Quality (CMAQ) model [2] has been extensively used, and continually updated, worldwide for more than 10 years; the current version is 4.7 [3].

Asian air quality is highly complex because Asia covers regions from the tropics to the polar zones with huge amounts of anthropogenic air pollutants and natural dust particles together with other natural species. The Regional Air Quality Model (RAQM) was developed at the Acid Deposition and Oxidant Research Center (now called the Asia Center for Air Pollution Research), which focuses on such Asian air quality problems [4, 5]. RAQM has been used for various air pollution studies in Asia, such as studies on high-oxidant, massive dust transport, and volcanic sulfur events, and it has been substantially modified by means of comparisons and evaluation with extensive and long-term monitoring data [4, 5] and with other models ([6] and references therein). However, an aerosol dynamics module was not implemented in RAQM, and thermodynamic equilibrium was assumed for gas–aerosol partitioning of semi-volatile inorganic components such as sulfate, nitrate, and ammonium.

To simulate the evolutionary processes of aerosol microscale properties such as chemical composition, size distribution, and mixing state, we implemented a simple ver-

sion of a new modal-moment aerosol dynamics model [7-9] that enables the non-equilibrium calculation of gas-to-particle mass transfer for a wide range of aerosol diameters from 1 nm to super μm. We also implemented six important parameterizations relating to aerosol dynamics: (1) new particle formation, (2) cloud condensation nuclei activation, (3) ice nuclei activation, (4) an explicit grid-scale cloud microphysical module, (5) dry deposition, and (6) sub-grid-scale convection and scavenging. This new model is called RAQM2. In this report, only the general findings of the study are summarized. A detailed description of the model and further details of our findings are presented by Kajino et al. (2012a: Ref. 10, 2012b: Ref. 11).

2. Methods

The model framework is illustrated in Figure 1. The U.S. National Center for Environmental Prediction (NCEP) 6 h, 1° final operational global analysis data set ds083.2 (http://rda.ucar.edu/datasets/ds083.2/), the Japan Meteorological Agency (JMA) Climate Data Assimilation System data set (JCDAS, 6 h, 1.25°, http://jra.kishou.go.jp/JRA-25/AboutJCDAS_en.html), or the JMA Meso Regional Objective Analysis (MANAL) data set (3 h, 5 km) are used for the initial and boundary conditions of the global and regional meteorological model simulations and also for the analysis nudging method. The Advanced Research Weather Research and Forecasting (WRF) model or the JMA nonhydrostatic model (NHM) are used to simulate the regional-scale meteorological field. In this study, WRF was selected as the regional model and it was driven by NCEP ds083.2.

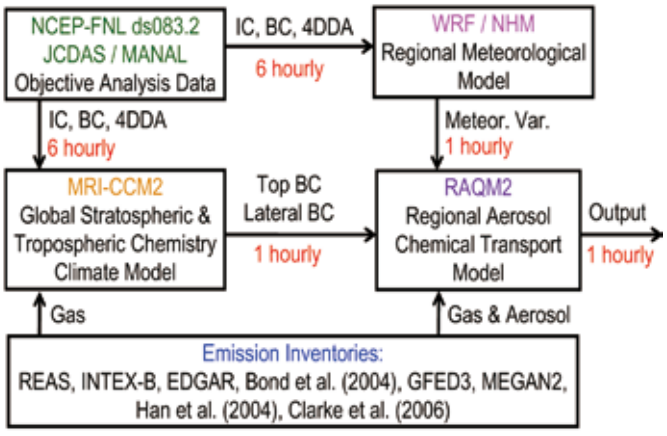

Figure 1 Framework of the RAQM2 system

The model domain, common to both WRF and RAQM2, is illustrated in Figure 2, which also shows locations of observation sites of the Acid Deposition Monitoring Network in East Asia (EANET). The horizontal grid resolution is 60 km with a Lambert conformal map projection; vertically there are 28 layers from the ground to 100 hPa for WRF, and 13 layers from the ground to 10 km for RAQM2, with terrain-following coordinates. The output time interval of the WRF was set to 1 h, and thus the input/output time interval for RAQM2 was also 1 h.

We used EANET monitoring data (Guidelines for acid deposition monitoring in East Asia, available at http://www.eanet.cc/product.html) for model evaluation. The EANET stations monitor 1- or 2-week accumulated concentrations of gaseous species and aerosol components using the filter pack (FP) method (Technical documents for the filter pack method in East Asia; http://www.eanet.cc/product.html). These stations monitor hourly concentrations of air pollutants and meteorological data such as wind speed, wind direction, temperature, relative humidity, and solar radiation.

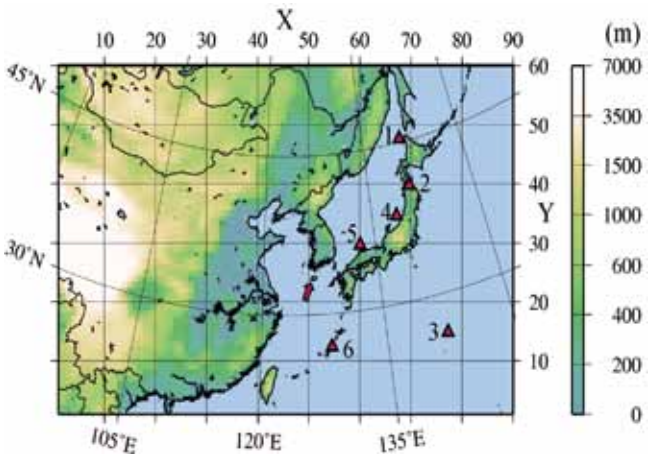

Figure 2 Model domain showing terrestrial elevation (m) and six Japanese EANET sites (1, Rishiri; 2, Tappi; 3, Ogasawara; 4, Sado; 5, Oki; 6, Hedo). The arrow indicates the Gosan site on Jeju Island, Korea.

Six EANET stations located on small islands or on isolated capes in the downwind region in Japan were selected for the model evaluation (Figure 2, red triangles). These stations have no nearby large anthropogenic emission sources and lack the complexity of local orographically induced winds. Therefore, air pollutant transport events mostly coincided with synoptic-scale disturbances at these stations and are generally well reproduced by regional-scale models. On the other hand, because the stations are very close to ocean surfaces, regional-scale simulations of ocean-originated species such as sea salt often do not agree well with the observations. Thus, we often obtain a better agreement for sea salt-originated components at inland or mountainous stations.

3. Results and discussion

Statistical analyses by Kajino et al. (2012a: Ref. 10). showed that the model reproduced the regional-scale transport and transformation of the major inorganic anthro-

pogenic and natural air constituents within factors of 2 to 5.

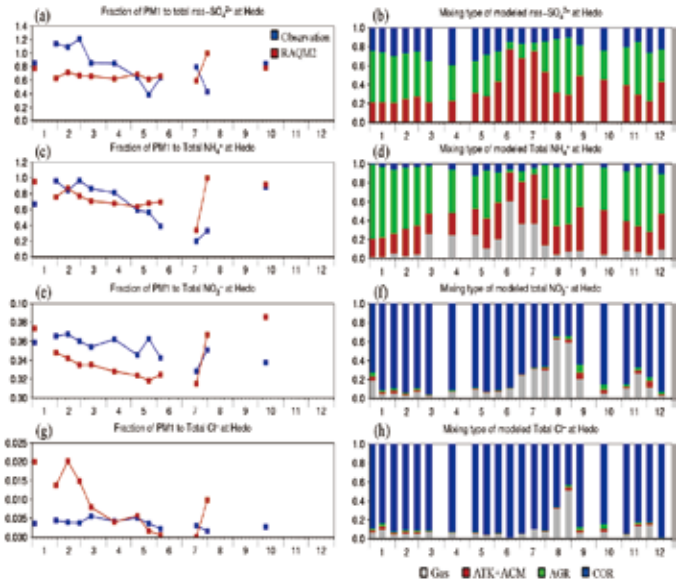

Figure 3 Biweekly mean PM_1 to total (gas plus aerosol) concentration ratios (left) and modeled fractions of the gas phase (gray) and aerosol categories ATK+ACM (red), AGR (green), and COR (blue) (right) at Hedo: (a), (b) nss-SO_4^{2-}; (c), (d) T-NH_4^+; (e), (f) T-NO_3^-; and (g), (h) T-Cl^-.

Figure 3 summarizes the major findings of the study at Hedo. The observed values are depicted only when the available hourly aerosol mass spectrometer data exceeded 50% during each biweekly FP sampling period (more than 140 hourly data during two weeks). The observed median PM_1 to bulk non-sea-salt (nss)-SO_4^{2-} ratio was 0.85. The ratio exceeded 1.0 in some cases, so it may be within the uncertainties of the analysis (Figure 3a). The modeled ratio was also large because approximately 80% of the nss-SO_4^{2-} was mixed with submicron particles, such as ATK, ACM, and AGR (Figure 3b). The modeled median ratio was 0.66, smaller than the observed ratio, indicating that the modeled size distribution of nss-SO_4^{2-} may have been larger than the observed distribution, or the proportions mixed with larger COR particles might have been overestimated. The features of the NH_4^+ ratio were similar to those of the nss-SO_4^{2-} ratio because nss-SO_4^{2-} is a major counterpart of NH_4^+. The proportion of total NH_4^+ (T-NH_4^+) in the gas phase, as NH_3, ranged from 20% to 60% in summer, because the temperature was high enough for NH_4NO_3 to evaporate and/or because the amount of nss-SO_4^{2-} was not enough to take up NH_3 gas and fix it to the aerosol phase as ammonium sulfate. Because the modeled nss-SO_4^{2-} and NH_4^+ were both underestimated, improvement of nss-SO_4^{2-} could also result in improvement of NH_4^+.

The mixing type of NO_3^- at Hedo was interesting in comparison with that at Gosan, Jeju Island, Korea. The observed and modeled median PM_1 to total NO_3^- (T-NO_3^-) ratios were 0.054 and 0.035, respectively, more than one order of magnitude smaller than those of nss-SO_4^{2-} and NH_4^+. This result means that the observed and modeled T-NO_3^- partitioned into the gas phase or internally mixed with aerosols larger than PM_1 were close to each other, at 94.6% and 96.5%, respectively. Kajino and Kondo [9] conducted a similar analysis of the $PM_{2.5}/PM_{10}$ ratios of chemical components at Gosan and calculated that on average 53.7% of the modeled NO_3^- was internally mixed with sea-salt particles in March 2005. This value was consistent with observations; the mean modeled and observed $PM_{2.5}/PM_{10}$ ratios of NO_3^- were both 0.66. In the current simulation, 98% of the NO_3^- was internally mixed with COR, based on the annual average at Hedo (Figure 3f).

During long-range transport, HNO_3 gas is produced via photochemical oxidation of NO_x. The mass transfer coefficients for each aerosol category are nearly proportional to their total surface area for atmospheric aerosol size ranges (free-molecular regime). Over the continent, more than 90% of the NO_3^- was mixed with submicron particles as NH_4NO_3. In contrast, over the ocean, toward downwind regions of the continent, HNO_3 gas produced during transport is more efficiently condensed onto sea-salt particles, because the proportions of sea-salt surface area become large.

Gosan is located approximately 700 km upwind of Hedo, in the direction of the Asian continent. The spatial distributions of the mixing types of NO_3^- showed that more than 90% of the NO_3^- could be internally mixed with sea salt over regions further downwind such as Hedo, whereas approximately 50% was mixed with sea salt over the Yellow Sea, where Gosan is located (Figure 6l of [9]).

Kajino et al. (2012b: Ref. 11) also evaluated model system performance regarding the major inorganic components of rain and snow precipitation measured at EANET stations. Statistical analysis showed that the model system successfully reproduced the regional-scale emission, transport, transformation, and wet deposition processes of major inorganic components of both anthropogenic and natural species, such as nss-SO_4^{2-}, NH_4^+, NO_3^-, Na^+ and nss-Ca^{2+}. Interestingly, however, we found that only modeled Na^+ in precipitation at near-coast stations was significantly underestimated (by a factor of up to 30), which suggests that the contribution of short-lived, super-large sea-salt droplets (SLSD; D = ~10–100 μm) was substantial in precipitation samples at near-coast stations in Japan (150–700 m from the coast). SLSD can be transported horizontally from the coast about 1–10 km, which means that the horizontal representativeness of the wet deposition of sea-salt-originated components such as Na^+ and Cl^- is limited to that transport distance. However, SLSD are not collected when aerosols are sampled by the FP method, because SLSD settle rapidly and they do not enter the air intake with the low pumping flow rate of 1 L min^{-1}. Therefore, the horizontal representativeness of Na^+ and Cl^- concentrations in air concentrations can be adequately large as the traveling distance of the coarse

mode particles (>100 km).

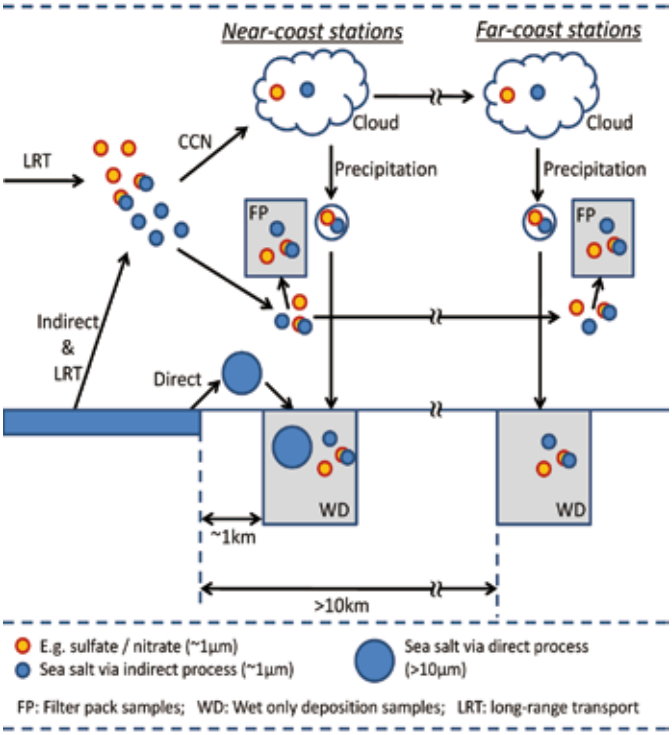

Figure 4 Schematic illustration showing the possible effects of super-large sea-salt droplets (SLSD) on wet deposition samples at near-coast stations.

These processes are summarized in Figure 4. The outcome of our study gives an important perspective on pH values of precipitation at Japanese EANET stations. Seawater pH is about 8, much higher than the pH of precipitation (~5). Thus, the pH of precipitation at near-coast stations might be increased by contamination with SLSD. However, a simple calculation suggests that the effect of SLSD on precipitation pH is very low, about 0.014 pH units on average if the SLSD fraction of sea salt in precipitation is assumed to be 90%.

4. Conclusion

A new aerosol chemical transport model, the Regional Air Quality Model 2 (RAQM2), was developed to simulate Asian air quality. A regional-scale simulation (Δx = 60 km) was performed for the entire year of 2006 covering the northeast Asian region. Statistical analyses showed that the model successfully reproduced the regional-scale transport, transformation, and wet deposition of the major inorganic anthropogenic and natural air constituents.

The modeled mixing types of the chemical components were found to be interesting, but the results were not compared with direct measurements of the mixing state. These results should be evaluated in the future by comparing them with measurements of soot mixing states made by volatility tandem differential mobility analyzer, single particle soot photometer, or transmission electron microscopy analyses. The aerosol mixing type is a key parameter influencing the light-scattering and absorbing properties of the aerosol. Further investigations are needed that compare our results with aerosol optical thickness or single scattering albedo observations for accurate assessment of aerosol–radiation interaction processes.

This research was supported by the Fundamental Research Budget of the Meteorological Research Institute of Japan, "Studies on Atmospheric Aerosol Properties and Processes". The study was partly supported by the Environmental Research and Technology Development Fund (Project No.B-0905 and A-1101) of the Ministry of the Environment of Japan. Aerosol mass spectrometer data for Hedo were provided by Dr. A. Takami at the National Institute for Environmental Studies and Prof. S. Hatakeyama at the Tokyo University of Agriculture and Technology.

1 Jacobson, M. Z. and D. L. Ginnebaugh, 2010: Global-through-urban nested three-dimensional simulation of air pollution with a 13,600-reaction photochemical mechanism. *J. Geophys. Res.*, **115**, D14304.

2 Byun, D. and K. L. Schere, 2006: Review of the governing equations, computational algorithms, and other components of the Models-3 Community Multiscale Air Quality (CMAQ) Modeling System, *Applied Mechanics Reviews*. **59**, 51-77.

3 Foley, K. M., S. J. Roselle, et al. 2010: Incremental testing of the Community Multiscale Air Quality (CMAQ) modeling system version 4.7, *Geosci. Model Dev.*, **3**, 205-226.

4 An, J., H. Ueda, et al. 2002: Simulations of monthly mean nitrate concentrations in precipitation. *Atmos. Environ.*, **36**, 4,159-4,171.

5 Han, Z., 2007: A regional air quality model: evaluation and simulation of O_3 and relevant gaseous species in East Asia during spring 2001, *Environ. Modell. Softw*. **22**, 1,328-1,336.

6 Carmichael, G. R., T. Sakurai, et al. 2008: MICS-Asia II: the model intercomparison study for Asia phase II methodology and overview of findings, *Atmos. Environ.*, **42**, 3,468-3,490.

7 Kajino, M., 2011: MADMS: Modal Aerosol Dynamics model for multiple modes and fractal shapes in free-molecular and near-continuum regimes. *J. Aerosol Sci.*, **42**, 224-248.

8 Kajino, M. 2011: Development of an efficient but accurate new dynamics model to predict a variety of atmospheric aerosol properties and their elemental processes, *Earozoru Kenkyu*. **26** (4) 296-306 (in Japanese).

9 Kajino, M., Y. Kondo, 2011: EMTACS: Development and regional-scale simulation of a size, chemical, mixing type, and soot shape resolved atmospheric particle model. *J. Geophys. Res.*, **116**, D02303, doi: 10.1029/2010JD015030.

10 Kajino, M., Y. Inomata, et al. 2012a: Development of an aerosol chemical transport model RAQM2 and predictions of Northeast Asian aerosol mass, size, chemistry, and mixing type. *Atmos. Chem. Phys. Discuss.*, **12**, 13,405-13,456, doi: 10.5194/acpd-12-13405-2012.

11 Kajino, M., M. Deushi, et al. 2012b: Modeling rain and snow precipitation quality over Northeast Asia using MRI-PM/c and implications of super large sea salt droplets effects at near-coast stations. Geosci. *Model Dev. Discuss*. **5**, 1,341-1,379, doi: 10.5194/gmdd-5-1,341-2,012.

Aerosol-related services of the Japan Meteorological Agency

Hiroki Shiozuru[1*], Nozumu Ohkawara[1], Kensuke Ishii[1] and Akinori Ogi[1]

[1]Aerosol Observation Section, Atmospheric Environment Division, Global Environment and Marine Department, Japan Meteorological Agency, 1-3-4 Otemachi, Chiyoda, Tokyo 100-8122, Japan

**Corresponding author. Tel.: & Fax: +81 3 3212 8341 (ext.4762); Email address: shiozuru@met.kisho.go.jp (H. Shiozuru)*

The Atmospheric Environment Division, Japan Meteorological Agency (JMA), is in charge of monitoring global/regional aerosols and issuing information about them. Our main products are as follows:

1) Measurement data of aerosol optical depth (AOD) by sun photometer

We operate three observational sites to measure AOD: Ryori in northern Japan since 1988; Minamitorishima in the northwestern Pacific since 1995; and Yonagunijima in the southwestern islands since 1998. In 2002, the measurement instrument at Ryori was upgraded to a precision filter radiometer and in 2007 the instruments at Minamitorishima and Yonagunijima were upgraded. Monthly mean AOD at those stations are published in the "Annual Report on Atmospheric and Marine Environment Monitoring."

2) *Kosa* (aeolian dust) information

In spring, Japan is frequently affected by *Kosa* from the Eurasian continent. We present the current and expected risk of K*osa* to the public by providing information about visibility at meteorological observation stations and forecasts of dust concentrations through the JMA website. The dust forecasts are derived by using the MASINGAR numerical dust forecast model, which was developed at the Meteorological Research Institute/JMA to study global atmospheric aerosols and related trace species.

3) Satellite aerosol monitoring products

The Meteorological Satellite Center of JMA retrieves aerosol products from the visible and infrared channels of the Geostationary Meteorological Satellite (MTSAT). The aerosol optical thickness is determined for the area from 52°N to 17°N and 114°E to 150°E. We also monitor aerosols using products derived from Earth Observation Satellites such as Aqua and CALIPSO.

4) Global Aerosol Optical Depth climatology for the numerical weather prediction (NWP) model

We processed AOD data derived from MODIS on Terra (2000–2005) and AOD data from MODIS on Terra and Aqua (2000–2008) to create a global monthly AOD climatology. This product is used in the JMA's operational global NWP model to improve the radiation-aerosol interaction.

Keywords: Aerosol optical depth; *Kosa* (Asian dust) forecasts; Retrieved satellite products; Japan Meteorological Agency

気象研究所技術報告一覧表

第１号　バックグラウンド大気汚染の測定法の開発（地球規模大気汚染特別研究班，1978）
Development of Monitoring Techniques for Global Background Air Pollution. (MRI Special Research Group on Global Atmospheric Pollution, 1978)

第２号　主要活火山の地殻変動並びに地熱状態の調査研究（地震火山研究部，1979）
Investigation of Ground Movement and Geothermal State of Main Active Volcanoes in Japan. (Seismology and Volcanology Research Division, 1979)

第３号　筑波研究学園都市に新設された気象観測用鉄塔施設（花房龍男・藤谷徳之助・伴野　登・魚津　博，1979）
On the Meteorological Tower and Its Observational System at Tsukuba Science City. (T. Hanafusa, T. Fujitani, N. Banno, and H. Uozu, 1979)

第４号　海底地震常時観測システムの開発（地震火山研究部，1980）
Permanent Ocean－Bottom Seismograph Observation System. (Seismology and Volcanology Research Division, 1980)

第５号　本州南方海域水温図－400m（又は 500m）深と 1,000m 深－（1934－1943 年及び 1954－1980 年）（海洋研究部，1981）
Horizontal Distribution of Temperature in 400m (or 500m) and 1,000m Depth in Sea South of Honshu, Japan and Western －North Pacific Ocean from 1934 to 1943 and from 1954 to 1980. (Oceanographical Research Division, 1981)

第６号　成層圏オゾンの破壊につながる大気成分及び紫外日射の観測（高層物理研究部，1982）
Observations of the Atmospheric Constituents Related to the Stratospheric ozon Depletion and the Ultraviolet Radiation. (Upper Atmosphere Physics Research Division, 1982)

第７号　83 型強震計の開発（地震火山研究部，1983）
Strong－Motion Seismograph Model 83 for the Japan Meteorological Agency Network. (Seismology and Volcanology Research Division, 1983)

第８号　大気中における雪片の融解現象に関する研究（物理気象研究部，1984）
The Study of Melting of Snowflakes in the Atmosphere. (Physical Meteorology Research Division, 1984)

第９号　御前崎南方沖における海底水圧観測（地震火山研究部・海洋研究部，1984）
Bottom Pressure Observation South off Omaezaki, Central Honsyu. (Seismology and Volcanology Research Division and Oceanographical Research Division, 1984)

第 10 号　日本付近の低気圧の統計（予報研究部，1984）
Statistics on Cyclones around Japan. (Forecast Research Division, 1984)

第 11 号　局地風と大気汚染質の輸送に関する研究（応用気象研究部，1984）
Observations and Numerical Experiments on Local Circulation and Medium－Range Transport of Air Pollutions. (Applied Meteorology Research Division, 1984)

第 12 号　火山活動監視手法に関する研究（地震火山研究部，1984）
Investigation on the Techniques for Volcanic Activity Surveillance. (Seismology and Volcanology Research Division, 1984)

第 13 号　気象研究所大気大循環モデルーⅠ（MRI・GCMーⅠ）（予報研究部，1984）
A Description of the MRI Atmospheric General Circulation Model (The MRI・GCMーⅠ). (Forecast Research Division, 1984)

第 14 号　台風の構造の変化と移動に関する研究－台風 7916 の一生－（台風研究部，1985）
A Study on the Changes of the Three - Dimensional Structure and the Movement Speed of the Typhoon through its Life Time. (Typhoon Research Division, 1985)

第 15 号　波浪推算モデル MRI と MRIーⅡの相互比較研究－計算結果図集－（海洋気象研究部，1985）
An Intercomparison Study between the Wave Models MRI and MRIーⅡ －A Compilation of Results－ (Oceanographical Research Division, 1985)

第 16 号　地震予知に関する実験的及び理論的研究（地震火山研究部，1985）
Study on Earthquake Prediction by Geophysical Method. (Seismology and Volcanology Research Division, 1985)

第 17 号　北半球地上月平均気温偏差図（予報研究部，1986）
Maps of Monthly Mean Surface Temperature Anomalies over the Northern Hemisphere for 1891－1981. (Forecast Research Division, 1986)

第 18 号　中層大気の研究（高層物理研究部・気象衛星研究部・予報研究部・地磁気観測所，1986）
Studies of the Middle Atmosphere. (Upper Atmosphere Physics Research Division, Meteorological Satellite Research Division, Forecast Research Division, MRI and the Magnetic Observatory, 1986)

第 19 号　ドップラーレーダによる気象・海象の研究（気象衛星研究部・台風研究部・予報研究部・応用気象研究部・海洋研究部，1986）
Studies on Meteorological and Sea Surface Phenomena by Doppler Radar. (Meteorological Satellite Research Division, Typhoon Research Division, Forecast Research Division, Applied Meteorology Research Division, and Oceanographical Research Division, 1986)

第 20 号　気象研究所対流圏大気大循環モデル（MRI・GCMーⅠ）による 12 年間分の積分（予報研究部，1986）
Mean Statistics of the Tropospheric MRI・GCMーⅠbased on 12－year Integration. (Forecast Research Division, 1986)

第 21 号　宇宙線中間子強度 1983－1986（高層物理研究部，1987）
Multi－Directional Cosmic Ray Meson Intensity 1983－1986. (Upper Atmosphere Physics Research Division, 1987)

第 22 号　静止気象衛星「ひまわり」画像の噴火噴煙データに基づく噴火活動の解析に関する研究（地震火山研究部，1987）
Study on Analysis of Volcanic Eruptions based on Eruption Cloud Image Data obtained by the Geostationary Meteorological satellite (GMS). (Seismology and Volcanology Research Division, 1987)

第 23 号　オホーツク海海洋気候図（篠原吉雄・四竈信行，1988）
Marine Climatological Atlas of the sea of Okhotsk. (Y. Shinohara and N. Shikama, 1988)

第 24 号　海洋大循環モデルを用いた風の応力異常に対する太平洋の応答実験（海洋研究部，1989）
Response Experiment of Pacific Ocean to Anomalous Wind Stress with Ocean General Circulation Model. (Oceanographical Research Division, 1989)

第 25 号　太平洋における海洋諸要素の季節平均分布（海洋研究部，1989）
Seasonal Mean Distribution of Sea Properties in the Pacific. (Oceanographical Research Division, 1989)

第 26 号　地震前兆現象のデータベース（地震火山研究部，1990）
Database of Earthquake Precursors. (Seismology and Volcanology Research Division, 1990)

第 27 号　沖縄地方における梅雨期の降水システムの特性（台風研究部，1991）
Characteristics of Precipitation Systems During the Baiu Season in the Okinawa Area. (Typhoon Research Division, 1991)

第 28 号　気象研究所・予報研究部で開発された非静水圧モデル（猪川元興・斉藤和雄，1991）
Description of a Nonhydrostatic Model Developed at the Forecast Research Department of the MRI. (M. Ikawa and K. Saito, 1991)

第 29 号　雲の放射過程に関する総合的研究（気候研究部・物理気象研究部・応用気象研究部・気象衛星・観測システム研究部・台風研究部，1992）
A Synthetic Study on Cloud－Radiation Processes. (Climate Research Department, Physical Meteorology Research Department, Applied Meteorology Research Department, Meteorological Satellite and Observation System Research Department, and Typhoon Research Department, 1992)

第 30 号　大気と海洋・地表とのエネルギー交換過程に関する研究（三上正男・遠藤昌宏・新野　宏・山崎孝治，1992）
Studies of Energy Exchange Processes between the Ocean－Ground Surface and Atmosphere. (M. Mikami, M. Endoh, H. Niino, and K. Yamazaki, 1992)

第 31 号　降水日の出現頻度からみた日本の季節推移－30 年間の日降水量資料に基づく統計－（秋山孝子，1993）
Seasonal Transition in Japan, as Revealed by Appearance Frequency of Precipitating-Days. －Statistics of Daily Precipitation Data During 30 Years－(T. Akiyama, 1993)

第 32 号　直下型地震予知に関する観測的研究（地震火山研究部，1994）
Observational Study on the Prediction of Disastrous Intraplate Earthquakes. (Seismology and Volcanology Research Department, 1994)

第 33 号　各種気象観測機器による比較観測（気象衛星・観測システム研究部，1994）
Intercomparisons of Meteorological Observation Instruments. (Meteorological Satellite and Observation System Research Department, 1994)

第 34 号　硫黄酸化物の長距離輸送モデルと東アジア地域への適用（応用気象研究部，1995）
The Long－Range Transport Model of Sulfur Oxides and Its Application to the East Asian Region. (Applied Meteorology Research Department, 1995)

第 35 号　ウインドプロファイラーによる気象の観測法の研究（気象衛星・観測システム研究部，1995）
Studies on Wind Profiler Techniques for the Measurements of Winds. (Meteorological Satellite and Observation System Research Department, 1995)

第 36 号　降水・落下塵中の人工放射性核種の分析法及びその地球化学的研究（地球化学研究部，1996）
Geochemical Studies and Analytical Methods of Anthropogenic Radionuclides in Fallout Samples. (Geochemical Research Department, 1996)

第 37 号　大気と海洋の地球化学的研究（1995 年及び 1996 年）（地球化学研究部，1998）
Geochemical Study of the Atmosphere and Ocean in 1995 and 1996. (Geochemical Research Department, 1998)

第 38 号　鉛直２次元非線形問題（金久博忠，1999）
Vertically 2-dmensional Nonlinear Problem (H. Kanehisa, 1999)

第 39 号　客観的予報技術の研究（予報研究部，2000）
Study on the Objective Forecasting Techniques（Forecast Research Department, 2000）

第 40 号　南関東地域における応力場と地震活動予測に関する研究（地震火山研究部，2000）
Study on Stress Field and Forecast of Seismic Activity in the Kanto Region（Seismology and Volcanology Research Department, 2000）

第 41 号　電量滴定法による海水中の全炭酸濃度の高精度分析および大気中の二酸化炭素と海水中の全炭酸の放射性炭素同位体比の測定（石井雅男・吉川久幸・松枝秀和，2000）
Coulometric Precise Analysis of Total Inorganic Carbon in Seawater and Measurements of Radiocarbon for the Carbon Dioxide in the Atmosphere and for the Total Inorganic Carbon in Seawater（I.Masao, H.Y.Inoue and H.Matsueda, 2000）

第 42 号　気象研究所／数値予報課統一非静力学モデル（斉藤和雄・加藤輝之・永戸久喜・室井ちあし，2001）
Documentation of the Meteorological Research Institute / Numerical Prediction Division Unified Nonhydrostatic Model (Kazuo Saito, Teruyuki Kato, Hisaki Eito and Chiashi Muroi，2001)

第 43 号　大気および海水中のクロロフルオロカーボン類の精密測定と気象研究所クロロフルオロカーボン類標準ガスの確立（時枝隆之・井上(吉川)久幸，2004）
Precise measurements of atmospheric and oceanic chlorofluorocarbons and MRI chlorofluorocarbons calibration scale

(Takayuki Tokieda and Hisayuki Y. Inoue，2004)

第 44 号　PostScript コードを生成する描画ツール"PLOTPS"マニュアル（加藤輝之，2004）
Documentation of "PLOTPS": Outputting Tools for PostScript Code (Teruyuki Kato，2004)

第 45 号　気象庁及び気象研究所における二酸化炭素の長期観測に使用された標準ガスのスケールとその安定性の再評価に関する調査・研究（松枝秀和・須田一人・西岡佐喜子・平野礼朗・澤　庸介・坪井一寛・堤　之智・神谷ひとみ・根本和宏・長井秀樹・吉田雅司・岩野園城・山本　治・森下秀昭・鎌田匡俊・和田　晃，2004）
Re-evaluation for scale and stability of CO_2 standard gases used as long-term observations at the Japan Meteorological Agency and the Meteorological Research Institute (Hidekazu Matsueda, Kazuto Suda, Sakiko Nishioka, Toshirou Hirano, Yousuke, Sawa, Kazuhiro Tuboi, Tsutumi, Hitomi Kamiya, Kazuhiro Nemoto, Hideki Nagai, Masashi Yoshida, Sonoki Iwano, Osamu Yamamoto, Hideaki Morishita, Kamata, Akira Wada，2004)

第 46 号　地震発生過程の詳細なモデリングによる東海地震発生の推定精度向上に関する研究（地震火山研究部, 2005）
A Study to Improve Accuracy of Forecasting the Tokai Earthquake by Modeling the Generation Processes (Seismology and Volcanology Research Department, 2005)

第 47 号　気象研究所共用海洋モデル（MRI.COM）解説（海洋研究部, 2005）
Meteorological Research Institute Community Ocean Model (MRI.COM) Manual (Oceanographical Research Department, 2005)

第 48 号　日本海降雪雲の降水機構と人工調節の可能性に関する研究（物理気象研究部・予報研究部, 2005）
Study of Precipitation Mechanisms in Snow Clouds over the Sea of Japan and Feasibility of Their Modification by Seeding (Physical Meteorology Research Department, Forecast Research Department, 2005)

第 49 号　2004 年日本上陸台風の概要と環境場（台風研究部, 2006）
Summary of Landfalling Typhoons in Japan, 2004 (Typhoon Research Department, 2006)

第 50 号　栄養塩測定用海水組成標準の 2003 年国際共同実験報告（青山道夫, 2006）
2003 Intercomparison Exercise for Reference Material for Nutrients in Seawater in a Seawater Matrix (Michio Aoyama, 2006)

第 51 号　大気および海水中の超微量六フッ化硫黄(SF_6)の測定手法の高度化と SF_6 標準ガスの長期安定性の評価（時枝隆之、石井雅男、斉藤 秀、緑川 貴, 2007）
Highly developed precise analysis of atmospheric and oceanic sulfur hexafluoride (SF_6) and evaluation of SF_6 standard gas stability (Takayuki Tokieda, Masao Ishii, Shu Saito and Takashi Midorikawa, 2007)

第 52 号　地球温暖化による東北地方の気候変化に関する研究（仙台管区気象台, 環境・応用気象研究部, 2008）
Study of Climate Change over Tohoku District due to Global Warming (Sendai District Meteorological Observatory, Atmospheric Environment and Applied Meteorology Research Department, 2008)

第 53 号　火山活動評価手法の開発研究（地震火山研究部, 2008）
Studies on Evaluation Method of Volcanic Activity (Seismology and Volcanology Research Department, 2008)

第 54 号　日本における活性炭冷却捕集およびガスクロ分離による気体計数システムによる ^{85}Kr の測定システムの構築および 1995 年から 2006 年の測定結果（青山道夫, 藤井憲治, 廣瀬勝己, 五十嵐康人, 磯貝啓介, 新田 済, Hartmut Sartorius, Clemens Schlosser, Wolfgang Weiss, 2008）
Establishment of a cold charcoal trap-gas chromatography-gas counting system for ^{85}Kr measurements in Japan and results from 1995 to 2006 (Michio Aoyama, Kenji Fujii, Katsumi Hirose, Yasuhito Igarashi, Keisuke Isogai, Wataru Nitta, Hartmut Sartorius, Clemens Schlosser, Wolfgang Weiss, 2008)

第 55 号　長期係留による 4 種類の流速計観測結果の比較（中野俊也, 石崎 廣, 四竈信行, 2008）
Comparison of Data from Four Current Meters Obtained by Long-Term Deep-Sea Moorings (Toshiya Nakano, Hiroshi Ishizaki and Nobuyuki Shikama, 2008)

第 56 号　CMIP3 マルチモデルアンサンブル平均を利用した将来の海面水温・海氷分布の推定（水田 亮, 足立恭将, 行本誠史, 楠 昌司, 2008）
Estimation of the Future Distribution of Sea Surface Temperature and Sea Ice Using the CMIP3 Multi-model Ensemble Mean (Ryo Mizuta, Yukimasa Adachi, Seiji Yukimoto and Shoji Kusunoki, 2008)

第 57 号　閉流路中のフローセルを用いた分光光度法自動分析装置による海水の高精度 pH_T 測定（斉藤 秀, 石井雅男, 緑川 貴, 井上（吉川）久幸, 2008）
Precise Spectrophotometric Measurement of Seawater pH_T with an Automated Apparatus using a Flow Cell in a Closed Circuit（Shu Saito, Masao Ishii, Takashi Midorikawa and Hisayuki Y. Inoue, 2008）

第58号　栄養塩測定用海水組成標準の2006年国際共同実験報告（青山道夫,J. Barwell-Clarke, S. Becker, M. Blum, Braga E.S., S. C. Coverly, E. Czobik, I. Dahllöf, M. Dai, G. O Donnell, C. Engelke, Gwo-Ching Gong, Gi-Hoon Hong, D. J. Hydes, Ming-Ming Jin, 葛西広海, R. Kerouel, 清本容子, M. Knockaert, N. Kress, K. A. Krogslund, 熊谷正光, S. Leterme, Yarong Li, 増田真次, 宮尾 孝, T. Moutin, 村田昌彦, 永井直樹, G. Nausch, A. Nybakk, M. K. Ngirchechol, 小川浩史, J. van Ooijen, 太田秀和, J. Pan, C. Payne, O. Pierre-Duplessix, M. Pujo-Pay, T. Raabe, 齊藤一浩, 佐藤憲一郎, C. Schmidt, M. Schuett, T. M. Shammon, J. Sun, T. Tanhua, L. White, E.M.S. Woodward, P. Worsfold, P. Yeats, 芳村 毅, A. Youénou, Jia-Zhong Zhang, 2008）
2006 Inter-laboratory Comparison Study for Reference Material for Nutrients in Seawater（M. Aoyama, J. Barwell-Clarke, S. Becker, M. Blum, Braga E. S., S. C. Coverly, E. Czobik, I. Dahllöf, M. H. Dai, G. O. Donnell, C. Engelke, G. C. Gong, Gi-Hoon Hong, D. J. Hydes, M. M. Jin, H. Kasai, R. Kerouel, Y. Kiyomono, M. Knockaert, N. Kress, K. A. Krogslund, M. Kumagai, S. Leterme, Yarong Li, S. Masuda, T. Miyao, T. Moutin, A. Murata, N. Nagai, G. Nausch, M. K. Ngirchechol, A. Nybakk, H. Ogawa, J. van Ooijen, H. Ota, J. M. Pan, C. Payne, O. Pierre-Duplessix, M. Pujo-Pay, T. Raabe, K. Saito, K. Sato, C. Schmidt, M. Schuett, T. M. Shammon, J. Sun, T. Tanhua, L. White, E.M.S. Woodward, P. Worsfold, P. Yeats, T.

Yoshimura, A. Youénou, J. Z. Zhang, 2008）

第 59 号　気象研究所共用海洋モデル(MRI.COM)第 3 版解説（辻野博之, 本井達夫, 石川一郎, 平原幹俊, 中野英之, 山中吾郎, 安田珠幾, 石崎廣（気象研究所海洋研究部）, 2010）

Reference manual for the Meteorological Research Institute Community Ocean Model (MRI.COM) Version 3（Hiroyuki Tsujino, Tatsuo Motoi, Ichiro Ishikawa, Mikitoshi Hirabara, Hideyuki Nakano, Goro Yamanaka, Tamaki Yasuda, and Hiroshi Ishizaki (Oceanographic Research Department), 2010）

第 60 号　栄養塩測定用海水組成標準の 2008 年国際共同実験報告（青山道夫, Carol Anstey, Janet Barwell-Clarke, François Baurand, Susan Becker, Marguerite Blum, Stephen C. Coverly, Edward Czobik, Florence D’amico, Ingela Dahllöf, Minhan Dai, Judy Dobson, Magali Duval, Clemens Engelke, Gwo-Ching Gong, Olivier Grosso, 平山篤史, 井上博敬, 石田雄三, David J. Hydes, 葛西広海, Roger Kerouel, Marc Knockaert, Nurit Kress, Katherine A. Krogslund, 熊谷正光, Sophie C. Leterme, Claire Mahaffey, 光田均, Pascal Morin, Thierry Moutin, Dominique Munaron, 村田昌彦, Günther Nausch, 小川浩史, Jan van Ooijen, Jianming Pan, Georges Paradis, Chris Payne, Olivier Pierre-Duplessix, Gary Prove, Patrick Raimbault, Malcolm Rose, 齊藤一浩, 斉藤宏明, 佐藤憲一郎, Cristopher Schmidt, Monika Schütt, Theresa M. Shammon, Solveig Olafsdottir, Jun Sun, Toste Tanhua, Sieglinde Weigelt-Krenz, Linda White, E. Malcolm. S. Woodward, Paul Worsfold, 芳村毅, Agnès Youénou, Jia-Zhong Zhang, 2010）

2008 Inter-laboratory Comparison Study of a Reference Material for Nutrients in Seawater（青山道夫, Carol Anstey, Janet Barwell-Clarke, François Baurand, Susan Becker, Marguerite Blum, Stephen C. Coverly, Edward Czobik, Florence D’amico, Ingela Dahllöf, Minhan Dai, Judy Dobson, Magali Duval, Clemens Engelke, Gwo-Ching Gong, Olivier Grosso, 平山篤史, 井上博敬, 石田雄三, David J. Hydes, 葛西広海, Roger Kerouel, Marc Knockaert, Nurit Kress, Katherine A. Krogslund, 熊谷正光, Sophie C. Leterme, Claire Mahaffey, 光田均, Pascal Morin, Thierry Moutin, Dominique Munaron, 村田昌彦, Günther Nausch, 小川浩史, Jan van Ooijen, Jianming Pan, Georges Paradis, Chris Payne, Olivier Pierre-Duplessix, Gary Prove, Patrick Raimbault, Malcolm Rose, 齊藤一浩, 斉藤宏明, 佐藤憲一郎, Cristopher Schmidt, Monika Schütt, Theresa M. Shammon, Solveig Olafsdottir, Jun Sun, Toste Tanhua, Sieglinde Weigelt-Krenz, Linda White, E. Malcolm. S. Woodward, Paul Worsfold, 芳村毅, Agnès Youénou, Jia-Zhong Zhang, 2010）

第 61 号　強雨をもたらす線状降水帯の形成機構等の解明及び降水強度・移動速度の予測に関する研究（大阪管区気象台・彦根地方気象台・京都地方気象台・奈良地方気象台・和歌山地方気象台・神戸海洋気象台・松江地方気象台・鳥取地方気象台・舞鶴海洋気象台・広島地方気象台・徳島地方気象台・予報研究部, 2010）

Studies on formation process of line-shaped rainfall systems and predictability of rainfall intensity and moving speed（Osaka District Meteorological Observatory, Hikone Local Meteorological Observatory, Kyoto Local Meteorological Observatory, Nara Local Meteorological Observatory, Wakayama Local Meteorological Observatory, Kobe Marine Observatory, Matsue Local Meteorological Observatory, Tottori Local Meteorological Observatory, Maizuru Marine Observatory, Hiroshima Local Meteorological Observatory, Tokushima Local Meteorological Observatory AND Forecast Research Department, 2010）

第 62 号　WWRP 北京オリンピック 2008 予報実証/研究開発プロジェクト（齊藤和雄, 國井勝, 原昌弘, 瀬古弘, 原旅人, 山口宗彦, 三好建正, 黄偉健, 2010）

WWRP Beijing Olympics 2008 Forecast Demonstration/Research and Development Project (B08FDP/RDP)（Kazuo Saito, Masaru Kunii, Masahiro Hara, Hiromu Seko, Tabito Hara, Munehiko Yamaguchi, Takemasa Miyoshi and Wai-kin Wong, 2010）

第 63 号　東海地震の予測精度向上及び東南海・南海地震の発生準備過程の研究（地震火山研究部, 2011）

Improvement in prediction accuracy for the Tokai earthquake and research of the preparation process of the Tonankai and the Nankai earthquakes (Seismology and Volcanology Research Department, 2011)

第 64 号　気象研究所地球システムモデル第 1 版（MRI-ESM1）―モデルの記述―（行本誠史, 吉村裕正, 保坂征宏, 坂見智法, 辻野博之, 平原幹俊, 田中泰宙, 出牛真, 小畑淳, 中野英之, 足立恭将, 新藤永樹, 籔将吉, 尾瀬智昭, 鬼頭昭雄, 2011）

Meteorological Research Institute-Earth System Model Version 1 (MRI-ESM1) — Model Description — (Seiji Yukimoto, Hiromasa Yoshimura, Masahiro Hosaka, Tomonori Sakami, Hiroyuki Tsujino, Mikitoshi Hirabara, Taichu Y. Tanaka, Makoto Deushi, Atsushi Obata, Hideyuki Nakano, Yukimasa Adachi, Eiki Shindo, Shoukichi Yabu, Tomoaki Ose and Akio Kitoh, 2011)

第 65 号　東南アジア地域の気象災害軽減国際共同研究（斉藤和雄, 黒田徹, 林修吾, 瀬古弘, 國井勝, 小司禎教, 上野充, 川畑拓矢, 余田成男, 大塚成徳, Nurjanna Joko Trilaksono, 許智揚, 古関俊也, Le Duc, Kieu Thi Xin, 黄偉健、Krushna Chandra Gouda, 2011）

International Research for Prevention and Mitigation of Meteorological Disasters in Southeast Asia (Kazuo Saito, Tohru Kuroda, Syugo Hayashi, Hiromu Seko, Masaru Kunii, Yoshinori Shoji, Mitsuru Ueno, Takuya Kawabata, Shigeo Yoden, Shigenori Otsuka, Nurjanna Joko Trilaksono, Tieh-Yong Koh, Syunya Koseki, Le Duc, Kieu Thi Xin, Wai-Kin Wong and Krushna Chandra Gouda, 2011)

第 66 号　太平洋における大気－海洋間二酸化炭素フラックス推定手法（杉本裕之, 平石直孝, 石井雅男, 緑川貴, 2012）

A method for estimating the sea-air CO2 flux in the Pacific Ocean (Hiroyuki Sugimoto, Naotaka Hiraishi, Masao Ishii and Takashi Midorikawa, 2012)

第 67 号　太平洋における大気－海洋間二酸化炭素フラックス推定手法（坪井一寛, 松枝秀和, 澤庸介, 丹羽洋介, 中村雅道, 久保池大輔, 岩坪昇平, 齊藤和幸, 花宮義和, 辻健太郎, 大森英裕, 西秀紘, 2012）

Development of a flask sampling and its high-precision measuring system for greenhouse gases observations using a cargo aircraft C-130H (Kazuhiro Tsuboi, Hidekazu Matsueda, Yousuke Sawa, Yosuke Niwa Masamichi Nakamura, Daisuke

Kuboike, Shohei Iwatsubo, Kazuyuki Saito Yoshikazu Hanamiya, Kentaro Tsuji, Hidehiro Ohmori, Hidehiro Nishi, 2012)